2011

Research Experience for Undergraduates Program, 2011

University of Arkansas, Fayetteville. Dept. of Chemistry and Biochemistry

Research Experience for Undergraduates 2011

Department of Chemistry and Biochemistry
University of Arkansas

David W. Paul – Julie Stenken
Program Co-Directors

Supported by the National Science Foundation

Table of Contents

Research Experience for Undergraduates
University of Arkansas

The University of Arkansas Department of Chemistry and Biochemistry hosted a National Science Foundation sponsored Research Experience for Undergraduates (REU) summer program for the 23rd year. The department first hosted an REU in 1959. The 10-week summer program, funded by the National Science Foundation, allowed students an opportunity to gain hands-on experience in a chosen research area while introducing them to careers in scientific research in areas including analytical chemistry and sensor technology, biochemistry and protein dynamics, inorganic chemistry and nanotechnology, organic chemistry, and physical and theoretical chemistry.

Undergraduate chemistry majors, who were sophomores or juniors in fall 2010, applied to the program, which took place at the University of Arkansas, Fayetteville.

Outside the lab, students met each week to hear presentations from campus experts about topics ranging from how to get into graduate school and test-taking skills to ethics, and how to make a poster presentation. A number of social activities took place throughout the summer to give students a chance to interact.

Selected students received a scholarship to pay for room and board and an allowance to attend a regional or national chemical conference in the 2011-2012 academic year. Students involved in the program were enrolled as students at the U of A and received one hour of research credit. The program was conducted from May 22, 2011 to July 28, 2011.

Tony Jude Award

Mississippi native Edward Evans, Jr. was the recipient of the Tony Jude Award for his summer research. He is a student at Wabash College in Indiana. The Tony Judy Award was created in 2002 to recognize a student for outstanding research. It is awarded in memory of a former REU student who returned to the University of Arkansas and obtained a doctorate degree.

Ed, under the direction of Professor Paul Adams, presented a poster entitled "Expression and Purification of Cdc42 and PBD46, an Important Ras-Protein Complex."

He is pictured below with Program Co-Director Professor David Paul.

2011 REU Participants

Terry Anderson
Philander Smith College
Hometown: Wichita, Kansas
Mentors: Julie Stenken and Frank Hahn

Jasmine Brown
Philander Smith College
Hometown: Jacksonville
Mentor: Colin Heyes

Ryan Christman
Ohio Northern University
Hometown: Archbold, Ohio
Mentor: Nan Zheng

Edward Evans
Wabash College
Hometown: Gulfport, Miss.
Mentor: Paul Adams

Elaine Haas
Spring Hill College
Hometown: Memphis, Tenn.
Mentor: Ingrid Fritsch

Jonathan Janzen
Northeastern State University
Hometown: Tahlequah, Okla.
Mentor: Jingyi Chen

Ja'Qualane Scales
Philander Smith College
Hometown: Little Rock, Ark.
Mentor: Paul Adams

Sweta Shrestha
Cameron University
Hometown: Kathmandu, Nepal
Mentors: Jingyi Chen and Julie Stenken

Jin Sun Woo
Mount Holyoke College
Hometown: Tenafly, N.J.
Mentor: Bob Gawley

Patience Wright
Spring Hill College
Hometown: Hartselle, Ala.
Mentor: Bill Durham

Faculty Project List

Paul Adams *Assistant Professor*	Biophysical Characterization of Proteins Associated with Signal Transduction
Neil Allison *Associate Professor and Vice-Chair*	Synthesis and Chemistry of Potential Organometallic Anticancer Drugs
Jingyi Chen *Assistant Professor*	Chemical synthesis of Platinum-based nanostructures as electrocatalysts for fuel cell application or Synthesis and surface modification of cage-like nanoparticles for drug delivery
Dan Davis *Professor*	Protein-Protein Interactions in Photosynthesis: Structure-Function Relationships in Electron Transfer Proteins
Ingrid Fritsch *Professor*	Microelectrochemical detection and microfluidics for lab-on-a-chip applications: protein, DNA, and microorganism analysis
Denise Greathouse *Research Assistant Professor*	Characterization of structure and peptide-lipid interactions of membrane active antimicrobial peptides
Bob Gawley *Distinguished Professor*	Synthetic and mechanistic organ(ometall)ic chemistry
Colin Heyes *Assistant Professor*	Development of Nanocrystals for Biophysical Applications
Roger Koeppe *University Professor*	Biophysical Studies of Single-Span Transmembrane Proteins and Membrane Channel Gating
T.K.S. Kumar *Associate Professor*	Structure, dynamics, folding and interactions of proteins
Matt McIntosh *Professor*	Total Synthesis of Biomedically Significant Complex Natural Products
Frank Millett *Distinguished Professor*	Biological Electron Transfer
David Paul *Associate Professor*	Development of Chemical Sensors for Clinical and Environmental Applications
Peter Pulay *Distinguished Professor*	Ab initio Calculation of the Vibrational and NMR Spectra of Protein Models
Joshua Sakon *Associate Professor*	Structure and function of drug-targets

Derek Sears *University Professor*	For an expanded REU program in Space Science visit: http://spacecenter.uark.edu/97.htm
Julie Stenken *Professor*	Measurement of Chemical Communication (Signaling) molecules, e.g., cytokines, neuropeptides, etc, Biosensors or In Vivo Chemical Analysis
Wes Stites *Professor*	Exploring the influence of the denatured state upon protein stability, or Isolation, characterization, and impact upon blood clotting of human thrombomodulin in disease.
Z. Ryan Tian *Associate Professor*	Syntheses and applications of ordered and complex nanostructures
Charles Wilkins *Distinguished Professor*	Matrix-assisted Laser Desorption Fourier Transform Mass Spectrometry for Whole-Cell Bacteria and Polymer Analysis
Nan Zheng *Assistant Professor*	Natural product synthesis, method development, and organometallics

UNIVERSITY OF ARKANSAS

NSF – CHEMISTRY – REU - SUMMER 2011

NIH – CHEMISTRY/ENGINEERING - INBRE

Activities and Events

Sunday, May 22

1:00 p.m. – 4:00 p.m. **Arrival, Check-In & Registration**
Maple Hill East (front desk: (479)718-2590)

4:30 p.m. – 5:30 p.m. **Housing Orientation**
Maple Hill South Classroom, Room 143

6:00 p.m. – 7:30 p.m. **Welcome Dinner**
University House, Whole Hog Barbeque

Monday, May 23

7:00 a.m. – 8:00 a.m. **Breakfast**
Quad Dining Room

8:15 a.m. Meet in quad lobby to go to university together

8:30 a.m. – 9:45 a.m. **Group Photo**
Front of Library

9:45 a.m. – 11:45 a.m. **Campus Logistics** (Concurrent Sessions)

RED **Session I: 9:45-10:30 a.m. Session II: 10:45-11:30 a.m. (Carver, MEEG, SPAC, Food Sci)**
YELLOW **Session II: 9:45-10:30 a.m. Session I: 10:45-11:30 a.m. (CHEM, Phys, MicroEP, CeMB)**

Session I: **ID Cards Issued, UARK email account setup**
Arkansas Union
Parking and Transit available: $22.65 per parking tag. License plate number and your vehicle registration are required for purchasing a tag. May park in lot 40 Sunday for unloading. Must move car to lot 41 (near Reid Hall) or 37 (corner of Garland and Cleveland) before Monday morning. Tag needs to be displayed by Tuesday to avoid ticketing.

Session II: **Library Orientation**
University of Arkansas Mullins Library, Room 102

12:00 p.m. - 1:00 p.m. **Opening Luncheon**
Place: Student Union Ballroom
Speaker: Dr. Donald Pederson, Vice Chancellor, Professor of Physics

1:00 p.m. – 2:30 p.m.	**Campus Tour** Meet in Ballroom with campus ambassadors
2:30 p.m. – 4:30 p.m.	**Departmental Logistics** **Place:** Chemistry Building Room 105 **Meet your Mentor:** Refreshments will be served **Get Keys, Take Photos**
Tuesday, May 24	
8:00 a.m. – 10:00 a.m.	**Safety Briefing:** Bill Durham, Department Chair CHEM 105
11:00 a.m. – 12:00 p.m.	**CHEMISTRY Library Tour** **Place:** MULLINS 102, moving to CHEM Library **Librarian:** Luti Salisbury
12:00 noon	**Go to Your Lab and Get Started!**
Wednesday, May 25	
8:00 a.m.	**Report to your lab**
5:30 p.m. – 7:00 p.m.	**Dinner & Dialogue** **Place:** Donald W. Reynolds Center, Seminar Room A **Speaker:** Dr. Rosemary Ruff **Topic:** Research and Ethics
Friday, May 27 **1:00 p.m.**	**REU/INBRE Group Meeting** CHEM 105 Speaker: Julie Stenken Topic: From REU student to Endowed Chair: Lessons in Seeking and Taking all Opportunities

Saturday, May 28– Monday May 30 Free for Memorial Day Weekend

Wednesday, June 1 **5:30 p.m. – 7:00 p.m.**	**Dinner & Dialogue** **Place:** Arkansas Union Ballroom **Speaker:** Marcelo Schubach **Topic:** Science Careers
Thursday, June 2 **6:00 p.m. – 9:00 p.m**.	**Evening Entertainment** **Host:** Chemistry **Location:** Devil's Den State Park (bring swim suit!)
Friday, June 3 **1:00 p.m.**	**REU/INBRE Group Meeting** CHEM 105 **Speaker**: Jingyi Chen

Title: Engineering multifunctional nanomaterials for biomedical applications

Wednesday, June 8
5:30 p.m. – 7:00 p.m.

Dinner & Dialogue
Location: Alumni House
Speaker: Brady and Grady Wright
Topic: Branding Yourself

Thursday, June 9
6:00 p.m. – 9:00 p.m.

Evening Entertainment
Host: MicroEP and SPAC
Location: The Gardens

Friday, June 10
1:00 p.m.

REU/INBRE Group Meeting
CHEM 105
Speaker: Jack Lay
Title: Rapid Characterization of Lipids by MALDI MS

Wednesday, June 15
5:30 p.m. – 7:00 p.m.

Dinner & Dialogue
Place: Donald W. Reynolds Center, Seminar Room A
Speaker: Graduate Student Panel
Topic: Q & A Session

Thursday, June 16
6:00 p.m. – 9:00 p.m.

Evening Entertainment
Host: Carver
Location: Lokomotion

Friday, June 17
1:00 p.m.

REU/INBRE Group Meeting
CHEM 105
Speaker: Dr. Colin Heyes
Title:

Monday, June 20

Canoe Trip

Wednesday, June 22
5:30 p.m. – 7:00 p.m.

Dinner & Dialogue
Place: Donald W. Reynolds Center, Seminar Room A
Speaker: Dr. Lynn Meade
Topic: How to Give an Effective Presentation

Thursday, June 23
6:00 p.m. – 9:00 p.m.

Evening Entertainment
Host: CeMB
Location: Razorback Malco Theater

Friday, June 24
1:00 p.m.

REU/INBRE Group Meeting
CHEM 105
Speaker: T.K.S. Kumar

Topic: Molecular interactions that are crucial for cell growth and differentiation

Saturday, June 25 **Practice GRE and GMAT test offered**
10 a.m. **Location:** MEEG Auditorium - Testing is FREE
Participation requires pre-registration

Mon-Tues, June 27-28 **NCTR Tour**
Jefferson, AR
Overnight stay in Little Rock, Dinner w/ INBRE students

Wednesday, June 29 **Dinner & Dialogue**
5:30 p.m. – 7:00 p.m. **Place:** Donald W. Reynolds Center, Seminar Room A
Speaker: Alfred Dowe & Vicky Hartwell
Topic: Applying to Graduate School & Funding your Graduate Degree

Thursday, June 30 **Evening Entertainment**
Host: Mechanical Engn.
Location: Ozark Lanes

Friday, July 1 **REU/INBRE Group Meeting**
1:00 p.m. CHEM 105
Half-way Progress Report Presentation
Progress Reports Due

Saturday, July 2 – Monday, July 4 **Free for Independence Day Weekend**
You **must** return to Fayetteville by 8:00 a.m., July 5

Friday, July 8 **INBRE student presentations**
10:30 a.m. Access Grid – Mullins Library

1:00 p.m. **REU/INBRE Group Meeting**
CHEM 105
Speaker: Bob Gawley
Topic: Why did Alice say to Kitty: "Perhaps looking glass milk isn't good to drink?" A guided tour from Lineland to Spaceland.

Wednesday, July 13 **Final Carver Presentations**
3:00p.m. – 7:00 p.m. Willard J. Walker Hall - All are invited

Friday, July 15 **INBRE student presentations**
11:00 a.m. Access Grid – Mullins Library

1:00 p.m. **REU/INBRE Group Meeting**
CHEM 105

	Speaker: Ingrid Fritsch Topic: From Research to Commercialization
Friday, July 22	**INBRE student presentations**
10:30 a.m.	Fayetteville Students presenting - Access Grid – Mullins Library
1:00 p.m.	**REU/INBRE Group Meeting** Chem 105 David Paul - How to Make a Poster
Thursday, July 28	**Meeting in Miniature, Lunch Served**
10:00 a.m.	CHEM 105
Friday, July 29	**End of Program**
5:00 p.m.	Final reports due / Dorm check-out
Saturday, July 30	**End of Program**
By 11:00 a.m.	Get out of the Dorm, last check-out

Phospholipid Analyses Utilizing GC-MS

Terry Anderson, Philander Smith College
Little Rock, Arkansas

Abstract

Phospholipids such as Phosphatidylcholine, are some of the most abundant lipids found in nature. These lipids are able to be analyzed by using the GC-MS, although the method for analysis is not as efficient. In this study a more efficient process of analysis for phospholipids was developed with possible application to tissue analysis. Utilizing an esterfication process to transform the lipids from a non-volatile state to a volatile state for GC-MS analysis. The phospholipids Phosphatidylcholine & Phosphatidylinositol were found to form FAMES better with a basic catalyst such as $NaOCH_3$. Whereas a phospholipd such as Sphingomyelin was able to use an acidic catalyst such as BF_3 to create FAMES. When standard samples were run with multiple test a Relative Standard Deviation (RSD) of below 1%. When a beef tissue sample underwent lipid extraction the sample was used in the developed protocols. The tissue lipids were identified and resulted in an RSD parallel to the standard lipids used in the experiment.

Introduction

A GC-MS is two part Instrument, A) a Gas Chromatograph (GC) for separating volatile compounds; and B) a Mass Spectrometer (MS) for analyzing the mass-to-charge ratio of the substances exiting the GC.

The purpose of this research was the development of proper analytical methods and their applications to tissue samples to properly profile the phospholipids. The only way to profile lipids in a GC-MS is an esterfication process which is necessary to make the lipid more volatile, or as a Fatty Acid Methyl Ester (FAMES) to move through the GC-MS column. A tissue extraction process has to be performed to obtain the lipids. Then esterfication process must be done on the extract.

The lipids that were used in this project: Phosphatidylcholine(PC), Phosphatidylnostiol(PI), are of the glycreophospholipids lipid classification, and Sphingomyelin(SM) of the sphingolipids lipid classification, are some of the most abundant lipids that are found in nature.

Phosphatidylcholine (PC):

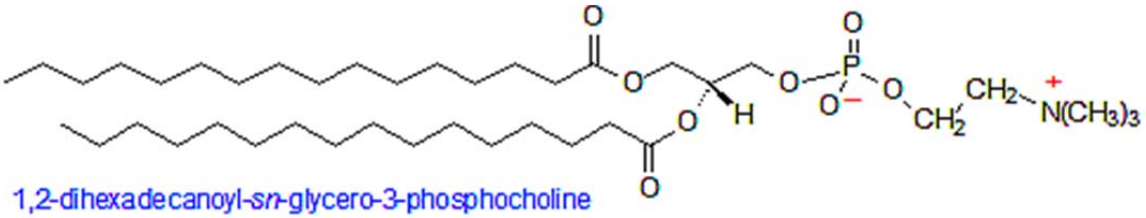

1,2-dihexadecanoyl-*sn*-glycero-3-phosphocholine

Phosphotidylinositol (PI):

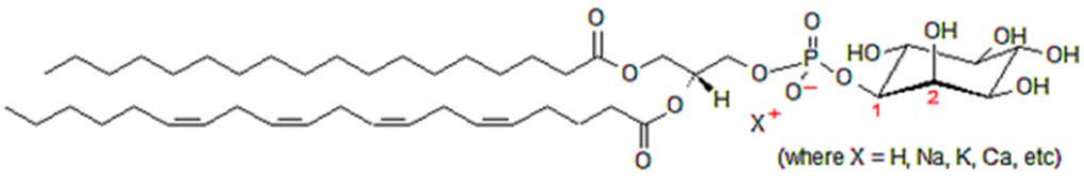

1-octadecanoyl, 2-(5Z,8Z,11Z,*14Z*-eicosatetraenoyl)-*sn*-glycero-3-phospho-(1'-*myo*-inositol)

Sphingomyelin (SM):

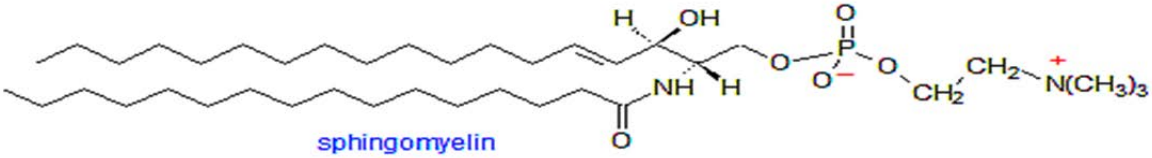

GC-MS Lipid Standard Fatty Acid Methyl Ester's (FAMES) Preparation:

Weigh 2mg of standard lipid sample into a 16 X 125 mm Pyrex screw cap culture tube. Next, add 2 ml of BCl3-methanol 12% (w/w)*. Then heat the test tube in a hot water bath for 5-10† min, at 60 C. Afterwards remove the test tube from heat and allow to cool for 10 min, before adding 1 ml of Distilled water and 1 ml of Hexane. Agitate the mixture, then allow the layers to partition apart. Remove the top organic layer and dry the layer in a separate vial of anhydrous sodium sulfate. Allow layers to form again, remove the top layer, noting only to remove the top liquid layer, no solid particles. Place this layer into a GC vial for storage at -20°C.

GC-MS Lipid Standard Mixture Fatty Acid Methyl Ester's (FAMES) Preparation:

Weigh .25mg of PC & SM sample, and 25 ul of PI in to a 16 X 125 mm Pyrex screw cap culture tube. Next add, 2 ml of BCl_3-methanol 12% (w/w)*. Then heat the test tube in a hot water bath for 1.5hrs, at 60 C. Afterwards remove the test tube from heat and allow to cool for 10 min, before adding 1 ml of Distilled water and 1 ml of Hexane. Agitate the mixture, then allow the layers to partition apart. Remove the top organic layer and dry the layer in a separate vial of anhydrous sodium sulfate. Allow layers to form again, remove the top layer, noting only to remove the top liquid layer, no solid particles. Place this layer into a GC vial for storage at -20 C.

GC-MS Tissue Lipid Extraction & FAMES Preparation:

Take freeze-dried tissue sample and grind it in a blender for 10-15s at room temperature. Next .5g of the tissue sample is placed into a 16 X 125 mm Pyrex screw cap culture tube. Next, 680 ul of Chloroform and 340 ul MeOH (in a 2:1 vol/vol) are added to the sample. Following this, 2 ml of BCl_3-methanol 12% (w/w)*. Then heat the test tube in a hot water bath for 1.5 hrs, at 60 C with vigorous handshaking for every 5's, every 20 min. Afterwards remove the test tube from heat and allow to cool for 10 min, before adding 2 ml of saturated $NaHCO_3$ and 3 ml of

Hexane. Vortex the mixture, then centrifuge the mixture for 30 sec. Remove the hexane layer and dry the layer in a separate vial of anhydrous sodium sulfate and Potassium Carbonate (10:1 wt/wt). Allow layers to form again, remove the top layer, noting only to remove the top liquid layer, no solid particles. Place this layer into a GC vial for storage at -20°C.

GC-MS Temperature Gradient Method

Utilizing a Varian 320 Triple Quadrupole GC-MS the machine was set at an initial temperature of 140°C, with a 5 min. hold. The temperature was then set at an increasing rate of 4°C/min to 240°C with a 15 min hold.

Results & Discussions

FAMES Catalyst Comparison:

When the catalyst BF_3 was used in FAME procedure unique results followed regarding the type of lipid that was used in the process. Gylcerophospolipids such as Phosphatidylcholine (PC) (*Fig. 2-1*) when used with the BF_3 procedure produced minimal FAMES with a decrease in signal to noise ratio, and a reduced ion count. When utilizing $NaOCH_3$ in the FAME procedure the exact opposite occurs with a minimal amount of noise present in the GC-MS run. Ion counts for the sample also increase dramatically when the base catalyst is used. The finding also applies to Phosphatidylinositol (PI) lipid (*Fig. 2-2*) .

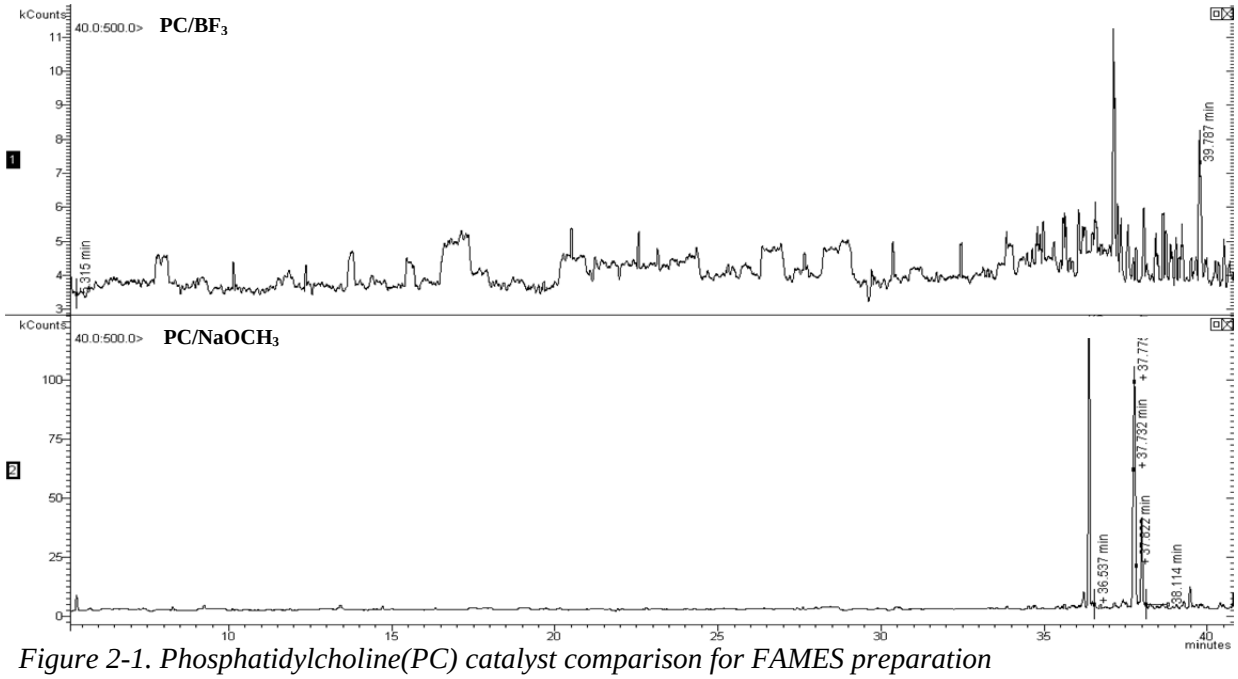

Figure 2-1. Phosphatidylcholine(PC) catalyst comparison for FAMES preparation

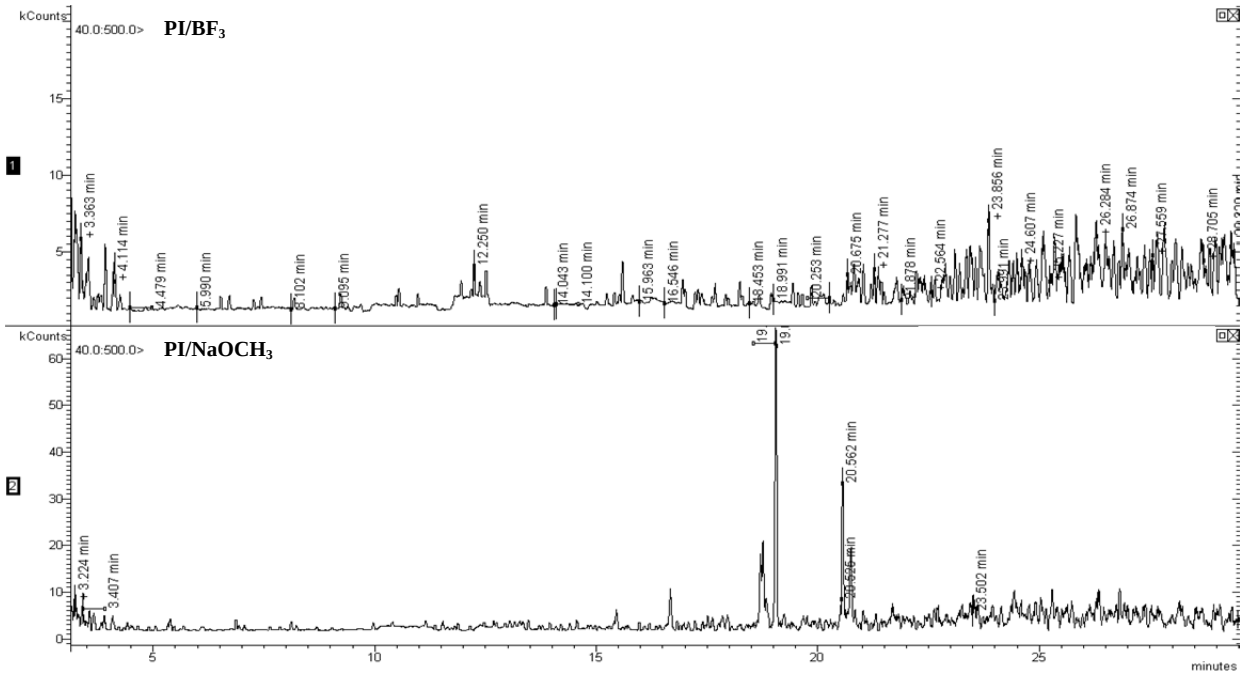

Figure 2-2. Phosphatidylinositol(PC) catalyst comparison for FAMES preparation.

Although this is not the case for the sphingolipids lipid type, such as Sphingomyelin (SM) (*Fig. 2-3)* which has a better FAME creation with BF_3 than with $NaOCH_3$. Because of this all lipids were used with their respective catalyst to obtain the best results.

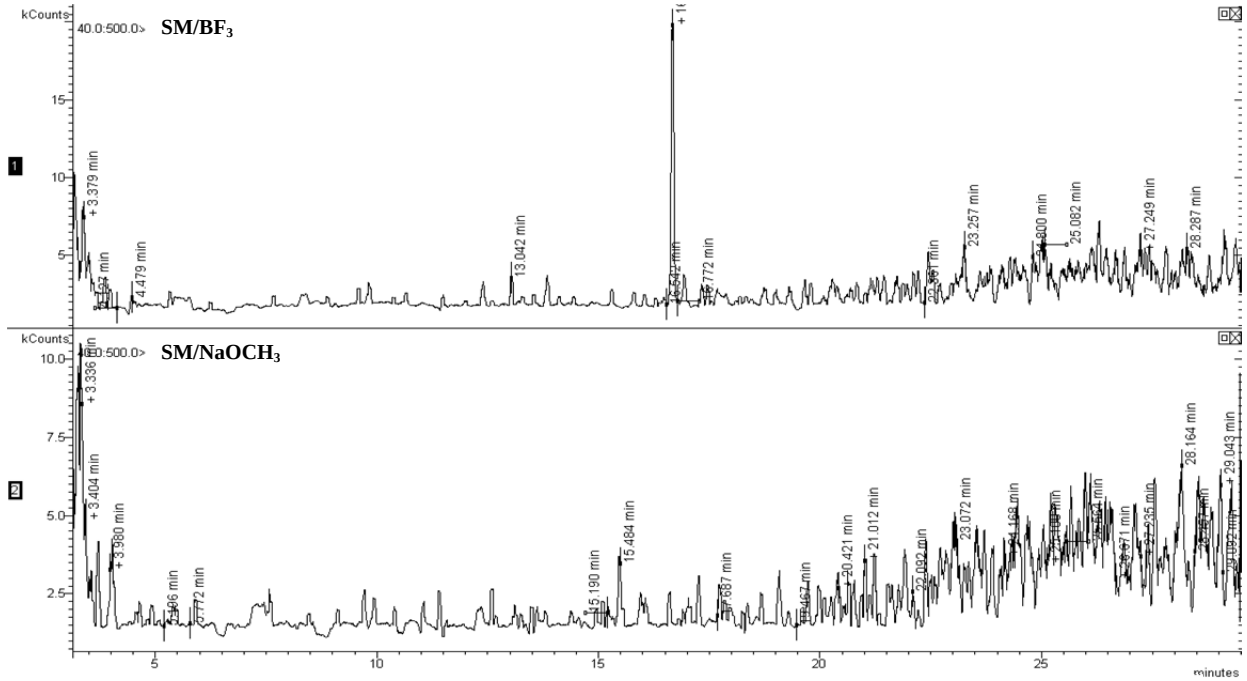

Figure 2-3. Sphingomyelin(SM) catalyst comparison for FAMES preparation.

Lipid Standard FAMES Identification:

The FAMES of the standard lipid were identified based off of the possible methyl ester that created from the fatty acids of the lipid. For PC & PI two major FAMES were identified (*Table 1-1,2)* in correspondence to the structure provided. Multiple test runs under the same conditions were run with all lipid standards. This resulted in a relative standard deviation (RSD) at the retention time of each respective lipid to be below 1%. The standard lipid SM, on the other hand only had one major FAME that was identified (*Table 1-3).* This lipid was also run under the same conditions multiple times, and also resulted in an RSD of below 1%.

PC FAMES Identification Table

Average Retention Time (min)	Systematic Name	Formula	m/z	Shorthand Designation	RSD of Retention Time
19.426 ± 0.0067	Hexadecanoic Acid, 15-methyl, methyl ester	$C_{17}H_{36}O_2$	272.2715	16:1	0.03%
23.553 ± 0.0085	15-Octadecanoic Acid, methyl ester	$C_{19}H_{36}O_2$	296.2715	18:1	0.04%

Table 1-1. Phosphatidylcholine(PC) FAME ID Table.

PI FAMES Identification Table

Average Retention Time (min)	Systematic Name	Formula	m/z	Shorthand Designation	RSD of Retention Time
23.398 ± 0.0070	11,14-Eicosadienoic Acid, methyl ester	$C_{21}H_{38}O_2$	322.5315	20:2	0.03%
24.147 ± 0.0067	Octadecanoic Acid, methyl ester	$C_{19}H_{38}O_2$	298.2872	18:0	0.03%

Table 1-2. Phosphatidylinositol(PI) FAME ID Table.

SM FAMES Identification Table

Average Retention Time (min)	Systematic Name	Formula	m/z	Shorthand Designation	RSD of Retention Time
19.4247± 0.0071	Hexadecanoic Acid, methyl ester	$C_{17}H_{34}O_2$	270.2559	16:0	0.04%

Table 1-3. Sphingomyelin(SM) FAME ID Table.

Lipid Standard Mixture FAMES Identification:

When the lipid standards were used in a combination that underwent the FAMES creation process, as previously done singularly each FAME was identified based off of the carbon length and retention time placement *(Table 2-1, 2).* Only two FAMES per catalyst were identifiable: SM & PC with the BF_3 catalyst; and PC & PI with the $NaOCH_3$ catalyst. This is unique in the fact that it can show a potential interaction between the lipids that had not previously been seen before.

Mixture with BF_3

Average Retention Time (min)	Systematic Name	Formula	m/z	Shorthand Designation	RSD	Phospholipid Source
19.415 ± 0.0060	Hexadecanoic Acid, methyl ester	$C_{17}H_{34}O_2$	270.2559	16:0	0.03%	SM
23.552 ± 0.0148	15-Octadecanoic Acid, methyl ester	$C_{19}H_{36}O_2$	296.2715	18:1	0.06%	PC

Table 2-1. Mixture with BF_3 FAME ID Table.

Mixture with $NaOCH_3$

Average Retention Time (min)	Systematic Name	Formula	m/z	Shorthand Designation	RSD	Phospholipid Source
19.432 ± 0.0218	Hexadecanoic Acid, 15-methyl ester	$C_{17}H_{36}O_2$	272.2715	16:1	0.11 %	PC
24.145 ± 0.0014	Octadecanoic acid, Methyl Ester	$C_{19}H_{38}O_2$	298.2872	18:0	0.01 %	PI

Table 2-2. Mixture with $NaOCH_3$ FAME ID Table.

Beef Tissue:

Using Ground Beef tissue, the lipid extraction process succeeded in removing the lipids from tissue for FAME esterfication. Utilizing both catalyst on the extracted lipids FAMES were created for analysis by GC-MS. Many FAMES were found to be present with in the test sample, but due to the retention time placement, and carbon length of particular FAMES a comparison to the lipid standards was done. With the BF_3 sample a maximum of two FAMES were identified to have possible come from SM & PC (*Table 3*-1), with other FAMES from other lipids being found present with in the sample, but with no standard to identify these particular FAMES. This was not the case with the tissue lipid extracts with $NaOCH_3$, where a majority of the FAMES that were identified as being PC with only one peak being identified as PI, none as SM(*Table 3-2*). Although just as the BF_3 sample there were other FAMES from lipids that were present within the sample tested that could not be identified due to a standard not being available to compare the retention time and carbon length.

Tissue with BF_3

Average Retention Time (min)	Systematic Name	Formula	m/z	Shorthand Designation	RSD	RSD	Phospholipid Source
19.413 ± 0.0072	Hexadecanoic Acid, methyl ester	$C_{17}H_{34}O_2$	270.2559	16:0	0.04%	0.04 %	SM
20.620 ± 0.0092	Dodecane, 1,1-dimethyl-	$C_{14}H_{30}O_2$	230.2246		0.04%	0.04 %	Other lipid
23.543 ± 0.0010	16- Octadecanoic acid, methyl ester	$C_{19}H_{36}O_2$	296.2715	18:1	0.004%	0.004 %	PC
24.145 ± 0.0050	Undecanoic acid, methyl ester	$C_{12}H_{24}O_2$	200.1776	11:0	0.02%	0.02 %	Other lipid
25.204 ± 0.0052	4,5 Bis-dimethoxymethyl-octanedioic acid, dimethyl ester	$C_{16}H_{30}O_8$	350.1941		0.02%	0.02 %	Other lipid

Table 3-1. Tissue with BF_3 FAME ID Table.

Tissue with $NaOCH_3$

Average Retention Time (min)	Systematic Name	Formula	m/z	Shorthand Designation	RSD	RSD	Phospholipid Source
14.302 ± 0.0065	Methyl Tetradecanoate	$C_{15}H_{30}O_2$	242.2246	14:0	0.05%	0.05	Other lipid
18.890 ± 0.0095	Unknown				0.05%	0.05 %	Other lipid
19.418 ± 0.0065	Hexadecanoic acid, methyl ester	$C_{17}H_{34}O_2$	270.2559	16:0	0.03%	0.03 %	PC
23.516 ±0.0551	9-Octadecanoic acid (Z)-, methyl ester (C19:1)	$C_{19}H_{36}O_2$	296.2715	18:1	0.23%	0.23 %	PC
24.142 ± 0.0044	Octadecanoic acid, methyl ester	$C_{19}H_{38}O_2$	298.2872	18:0	0.02%	0.02 %	PI

Table 3-2. Tissue with $NaOCH_3$ FAME ID Table.

Conclusion

In conclusion, the GC-MS data showed that the FAME synthesis procedure worked in creating methyl esters, for GC-MS analysis. The $NaOCH_3$ catalyst being the better catalyst when trying to analyze, PC & PI, whereas BF_3 is the better catalyst when trying to analyze SM with the

GC-MS, to obtain the least amount of noise within the chromatogram. The lipid extraction from the beef tissue was successful, with the $NaOCH_3$ showing more lipids FAMES for identification from standard comparison, than BF_3. Due to the fact that the Relative Standard Deviation (RSD) was below 1%, all tests were run with multiple runs having a little to no difference in retention time placement.

Acknowledgments

I would like to acknowledge the following people for helping with this research project. I have learned many things from you all this summer and hope to carry all of this information with me for a long time to come:

Beth Emerson
Dr. Jennifer Gidden
Dr. Frank Hahn
Dr. Jack Lay
Dr. Julie Stenken
Dr. Rohana Liyanage
I would also like to acknowledge the National Science Foundation CHE-0851505/REU and the University of Arkansas for giving me the opportunity to participate in this summer enriching experience.

References

Arnhold, J., K. Arnold, B. Fuchs, J. Lebig, M. Muller, M. Petkovic, J. Schiller, H. Spalteholz, R. Sub, O. Zchornig. "Matrix-assisted Laser Desorption and Ionization time-of-flight (MALDI-TOF) mass spectrometry in Lipid and Phospholipid research". Progress in Lipid Research (2004): 449-488.

Busboom, J. R., C. T. Gaskins, M. L. Nelson, and J. V. OFallon. "A direct method for fatty acid methyl ester synthesis: Application to wet meat tissues, oils, and feedstuffs". Journal of Animal Science.(2007)

Folch, Jordi, M. Lees, and G. H. Sloane Stanley. "A Simple Method For The Isolation and Purification Of Total Lipides From Animal Tissues". McLean Hospital Research Laboratories, Waverley, and the Department of Biological Chemistry, Harvard Medical School, Boston, Massachusetts. (1965)

Jackson, Shelly N., Amina S. Woods. "Direct profiling of tissue lipids by MALDI-TOF". Journal of Chromatography B. (2008)

Sigma-Aldrich. "Fatty Acid/FAME Application Guide: Analysis of food for nutritional needs". Sigma-Aldrich, Supelco Analytical. (2008): 5-6

Fluorescence Labeling of cpSRP43 to Monitor the Protein Structure by Single Molecule FRET

Jasmine Brown, Philander Smith College
Little Rock, Arkansas

Abstract

Various studies have been conducted to determine the structural changes of chloroplast protein signal recognition particle 43 (cpSRP43) upon its interaction with chloroplast protein signal recognition particle 54 (cpSRP54). These two proteins form a heterodimer which transport the light harvesting chlorophyll binding proteins to the thylakoid membrane to be used in photosynthesis. In this research, several methods were used to optimize the fluorescence labeling of cpSRP43 with the dyes alexa488 and alexa546. We used ensemble and single molecule Förster resonance energy transfer (FRET) to determine the structural changes during the interaction between cpSRP43 and cpSRP54. We were successful in establishing a labeling protocol that increased the concentration of FRET labeled proteins and used single molecule FRET (smFRET) to show structural heterogenity.

Introduction

Plants are efficient in converting sunlight into chemical energy which is essential for every form of life. There are various proteins in the chloroplast that are responsible for generating chemical energy. In our research, we are interested in the cpSRP43 and cpSRP54 proteins. cpSRP are chloroplast protein signal recognition particles that are used to transport light harvesting chlorophyll a and b binding proteins to the thylakoid membrane (LHCP) (Stengel, Holdermann, Cain, Robinson, Wild, & Sinning, 2008). cpSRP is formed by a combination of chromodomains and ankyrin domains (Stengel, Holdermann, Cain, Robinson, Wild, & Sinning, 2008) (see figure 1). The cpSRP43 has four ankyrin sequential repeats that are involved in protein-protein interactions and complex formation (Cain, Holdermann, Sinning, Johnson, & Robinson, 2011).

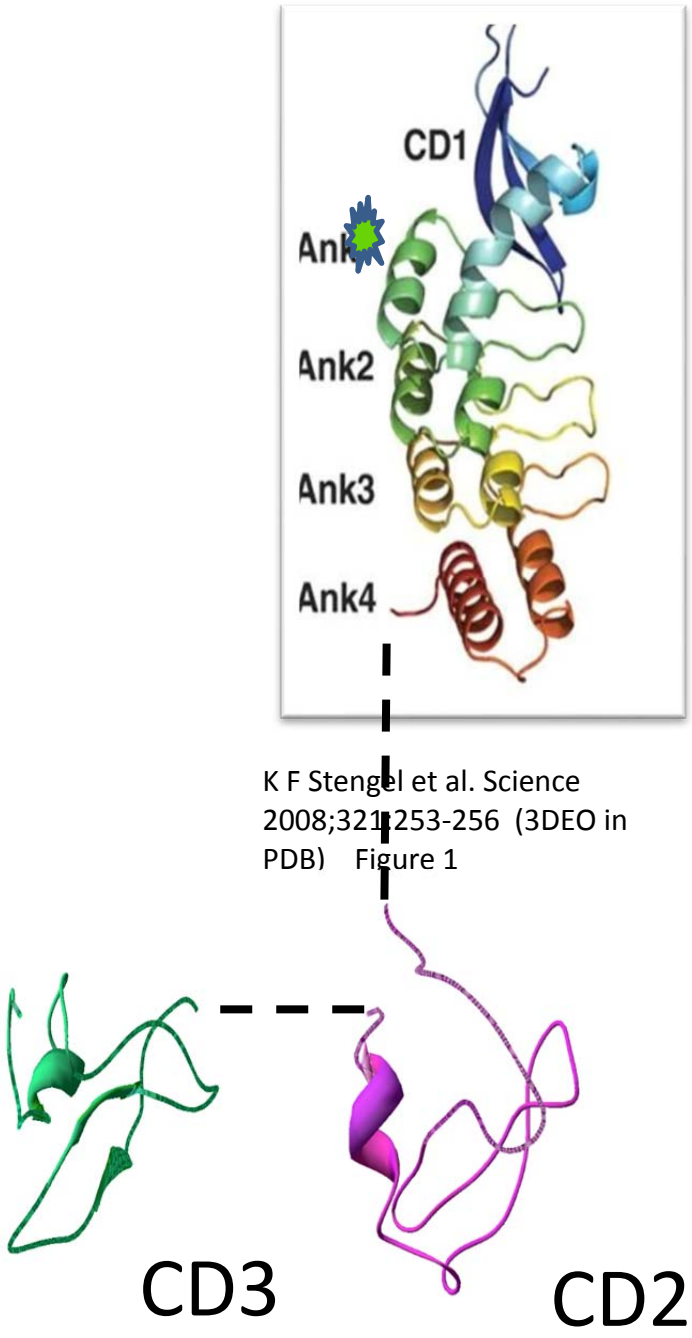

K F Stengel et al. Science 2008;321:253-256 (3DEO in PDB) Figure 1

There are two chromodomains CD2 and CD3 which are located at the C-terminal of the protein (Cain, Holdermann, Sinning, Johnson, & Robinson, 2011).There is one chromodomain CD1 that is located at the N-terminal (Cain, Holdermann, Sinning, Johnson, & Robinson, 2011). cpSRP43 is also reported to serve as a chaperone that reverses the aggregation of its substrates' proteins (Jaru-Ampornpan, et al., 2010). The actual structure of cpSRP43 and cpSRP54 is unknown although structures of the individual CD1-Ank4, CD2 and CD3 have been deposited in the protein data bank as 3DEO, IX3P, and IX3Q, respectively. The SRP in cpSRP is a signal recognition particle, cyto-plasmic ribonucleoprotein that mediates GTP dependent co-translational targeting of proteins to the endoplasmic reticulum (Schuenemann, et al., 1998). The concentration of cpSRP43 controls the partitioning of cpSRP54 between co-translational and post-translational mode of targeting proteins in the chloroplast (Kathir, et al., 2008). The LHCPs of the thylakoid membrane are part of a hydrophobic family of proteins involved in photosynthesis (Schuenemann, et al., 1998). LHCPs are part of the photosystem I and II and are synthesized in cytosol (Cain, Holdermann, Sinning, Johnson, & Robinson, 2011).

The objectives for this research were to examine the structural changes of cpSRP43 upon interaction with cpSRP54 to gain an understanding of how the cpSRP43 and cpSRP54 heterodimer binds to LHCP to transport it to the thylakoid membrane to be used in photosynthesis. By understanding the transport mechanism our goal is to hopefully have an

impact on the development of efficient solar energy devices. We would like to understand how plants are capable of efficiently producing chemical energy from sunlight in particles how they transport and insert the photosynthetic proteins. In this project, two mutant proteins were used in the experiments. For one of the proteins, we labeled the ankyrin 2 and chromodomain 3 and is referred to as protein 1 (P1). The other protein we labeled ankyrin 2 and chromodomains 2 and is referred to as protein 2 (P2).

Experimental Procedures

Materials used for this research includes alexa488 maleimide (donor dye), alexa546 maleimide (acceptor dye), HKM buffer (Hepes, Potassium chloride, Magnesium chloride), PBS buffer (Phosphate Buffered Saline), nano-pure water, Econo-column, Bio-gel P-6DG gel, urea, cpSRP43, cpSRP54, and TCEP (Tris (2-carboxyethyl) phosphine). The equipment that was used included the Ultraviolet visible spectrophotometer, fluorescence spectrometer, and the Fluorescence microscope. The ultraviolet visible spectrophotometer measures the absorbance so that the concentration of the donor and acceptor dyes relative to the protein concentration can be determined to quantify the labeling efficiency. The fluorescence spectrometer is used to measure the average fluorescence resonance energy transfer (FRET) for the sample (Skoog, Holler, & Crouch, 2007). The fluorescence microscope is used to measure the single molecule FRET. There were a series of experiments that were performed in order to optimize the labeled protein that was used to determine single molecule Förster resonance energy transfer.

Protein Unfolding. The cpSRP43 was unfolded using urea concentration ranging from 0 molar to 8 molar. By conducting the unfolding experiments, the data revealed which urea concentration could be used to unfold the protein so that the two cysteines can be exposed to the fluorescent dyes for attachment. The urea was diluted in HKM buffer making an 8.6M stock urea solution. It was added to a solution that contained the protein and HKM buffer. The stock concentration of the protein was 4mM. The table below shows the how much of each solution was added to each sample (Table 1). Unfolding was monitored by the fluorescence spectroscopy (see later).

Sample	Stock protein (mL)	Stock Urea Concentration (mL)	HKM Buffer (mL)	Final Protein Concentration (nM)	Final Urea Concentration (M)
1	2.5	0	97.5	100	0
2	2.5	12.5	85	100	1.08
3	2.5	25	72.5	100	2.16
4	2.5	37.5	60	100	3.24
5	2.5	50	47.5	100	4.32
6	2.5	62.5	35	100	5.40
7	2.5	75	22.5	100	6.48
8	2.5	87.5	10	100	7.56

Table 1

Labeling cpSRP43 proteins. Proteins 1 and 2 were labeled with thiol reactive ATTO labels (maleimides). The fluorescent dyes that were used were alexa488 and alexa546 (Invitrogen). For this experiment, the materials HKM buffer, urea, and TCEP were used. We

added 10 micro liters of 10x PBS buffer, 5 micro liters of TCEP reagent, and 47.5 micro liters of nano-pure water to an eppendorf tube. TCEP is used to ensure the thiol remains as its reduced (SH) form. After the solution has been mixed, the protein is added to the solution. After allowing the solution to react for ten minutes, we added the 2.5 micro liters of 1mM alexa546 and 5 micro liters of 1mM alexa488. The mixture was covered with aluminum foil to protect it from any source of light in the room and allowed to react overnight. This method was repeated several times with different dye concentrations, time elapsed between adding the alexa546 and alexa488, and the addition of urea to unfold the protein to increase labeling. The maleimide chemistry (figure 2) and labeling protocol (table 2) is shown in the figures below.

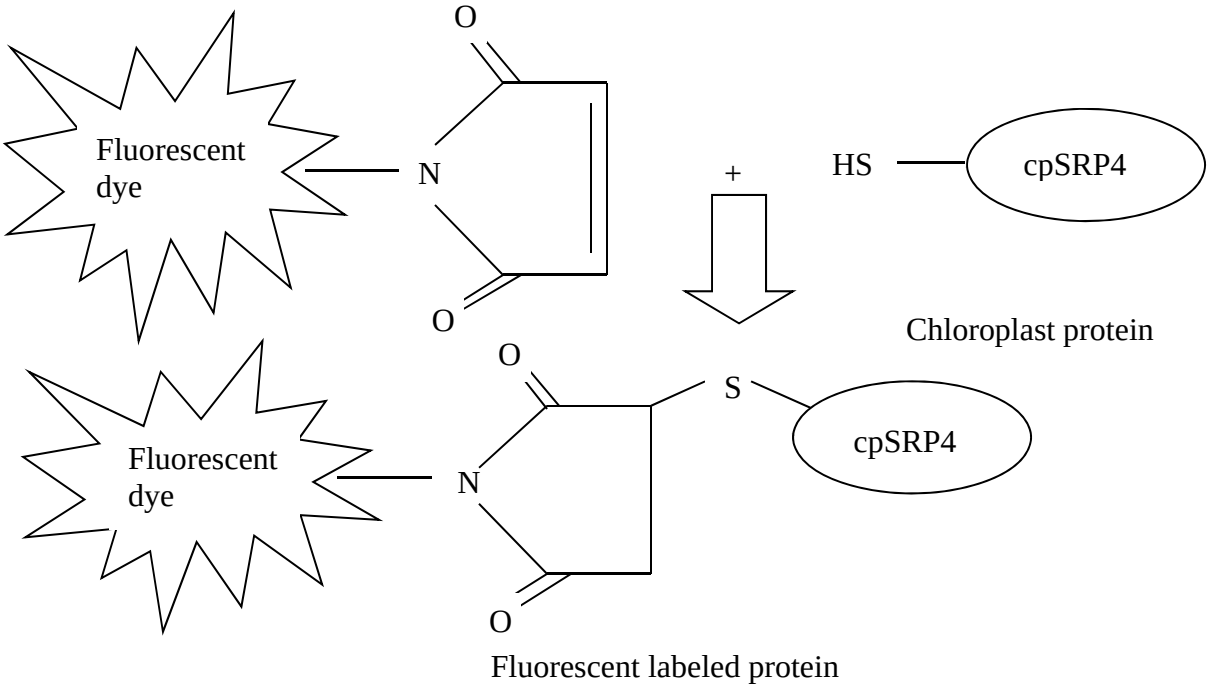

Figure 2

Components	Method 1	Method 2	Method 3	Method 4
Alexa546 Concentration	1 mM	3 mM	3 mM	3 mM
Alexa488 Concentration	1 mM	1 mM	3 mM	3 mM
Add Urea	No	No	No	Yes
Time Elapsed Between adding Alexa546 and Alexa488	0 hours	2 and 6 hours	1 hour	1 hour

Table 2

Gel filtration. A gel column is used to separate proteins, peptides, and oligonucleotides based on size (Gel Filtration Chromatography, 2011). The smaller molecules are trapped in the gel while the larger molecules move quickly through the column (Gel Filtration Chromatography, 2011). We used HKM buffer, Bio-gel, and Econo-column. The Bio-gel was packed into a glass econo-column using the eluent, HKM buffer. The sample was added to the top of the Bio-gel and eluted down the column. The sample separated into two distinct bands. The first band contained the labeled proteins while the second band contained the excess dyes. Fractions were collected from the column as the sample was filtered through the gel. The first band was collected in an eppendorf tube and separated from the excess fluorescent dye band. The formation of the bands formed during size elusion chromotagraphy is shown in figure 3.

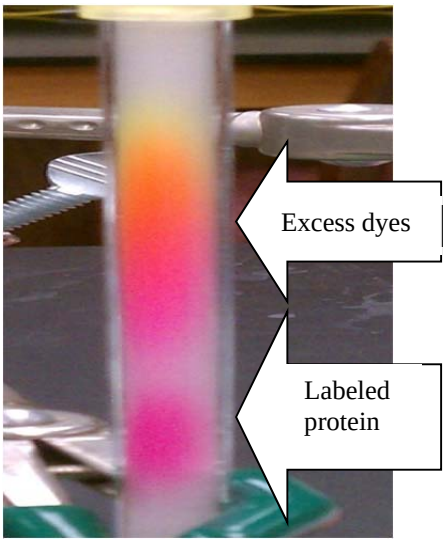

Figure 3

Fluorescence and absorbance spectra. The fluorescence and absorbance is measured and recorded for each fraction using the fluorescence spectrometer (Perkin Elmer LS-50) and ultraviolet visible spectrophotometer (Hitachi U3900H), respectively. The HKM buffer was used

as the baseline when the absorbance was measured. The parameters for measuring the absorbance included start at 800 nanometers, end at 200 nanometers, and a speed of 600 nanometers per second. The absorbances were recorded at 280 nm for the protein, 499 nm for the donor dye, 558 nm for the acceptor dye, and 700 nm for the background. From these absorbances, the labeling ratio was calculated.

To calculate the labeling ratio we used the following equation:

$$A = \varepsilon bc$$

A is the absorption that is measured at wavelengths 280 nm for the protein, 499 nm for the donor dye, and 561 nm for the acceptor dye. The epsilon is the extinction coefficient for each species. The epsilon value for the protein at 280 nm is unknown but estimated to be about 20,000$M^{-1}cm^{-1}$. For the donor at 499 nm, the epsilon value is 71,000$M^{-1}cm^{-1}$. For the acceptor at 561 nm, the epsilon value is equal to 104,000$M^{-1}cm^{-1}$. B is the length of the cuvette, 1 cm.

To calculate the labeling ratio, we collected the absorption values for the wavelengths. The absorption values at 280nm, 499nm, and 561 nm are corrected using the background absorption value from the wavelength of 700 nm due to spectral overlap. The alexa488 absorption is corrected by subtracting 15% of the alexa546 absorption at 561 nm. Protein absorption is corrected by subtracting 14% of alexa546 absorption at 558 nm and 12% of alexa488 absorption at 499 nm.

The fluorescence spectrometer was used to measure the protein, donor fluorescence, and acceptor dye fluorescence for the sample. It is used to calculate the average FRET for a sample using the following equation.

$$E = \frac{I_A}{I_A + \gamma I_D}$$

The fluorimeter can also be used to determine the protein unfolding monitoring the tryptophan fluorescence. The parameters for the tryptophan fluorescence included start at 300 nm, end at 500 nm, excitation at 280 nm, scan speed at 200 nm per second, excitation slit at 10 nm, and the emission slit at 10 nm. The donor dye parameters included start at 505 nm, end at 700 nm, excitation at 485 nm, scan speed at 300 nm per second, excitation slit at 10 nm, and emission slit at 10 nm. The acceptor dye parameters included start at 560 nm, end at 700 nm, excitation at 540 nm, scan speed at 300 nm per second, excitation slit at 10 nm, and emission at 10 nm.

Single molecule Förster Resonance Energy Transfer. The equipment used was the fluorescence microscope. Single molecule FRET (smFRET) is used to measure fluorescence intensity of the donor and acceptor fluorescence of a single molecule. The FRET is sensitive to the distance between the dyes and therefore, protein structure. And can be used to determine if there are any structural changes in the single proteins. The sample has to be diluted a hundred times so that the fluorescence of one molecule can be detected. The laser intensity is 610.83 arbtitrary units which equals about 30 mW and ten traces are collected in two minute intervals. The FRET efficiency of each molecule is calculated using the equation:

$$E = \frac{I_A}{I_A + \gamma I_D}$$

E stands for FRET efficiency value (Kuzmenkina, Heyes, & Nienhaus, 2005). I_A and I_D are the acceptor and donor fluorescence intensities (Kuzmenkina, Heyes, & Nienhaus, 2005). The gamma is used to correct the different detection efficiencies and the quantum yields of the two dyes (Kuzmenkina, Heyes, & Nienhaus, 2005) and has a value of 0.5.

Results and Discussion

Protein unfolding. With the collected data, we were able to identify that the protein unfolded at urea concentrations of about 3M so that any buried cysteine residues will be exposed to the dyes at urea concentration greater than 3M. Figure 4 (left) shows that as urea is added to the protein, the wavelength of tryptophan emission shifts from 345 nm to 356 as the protein unfolds. Using the graph on the left, we composed a graph that shows the unfolding curve.

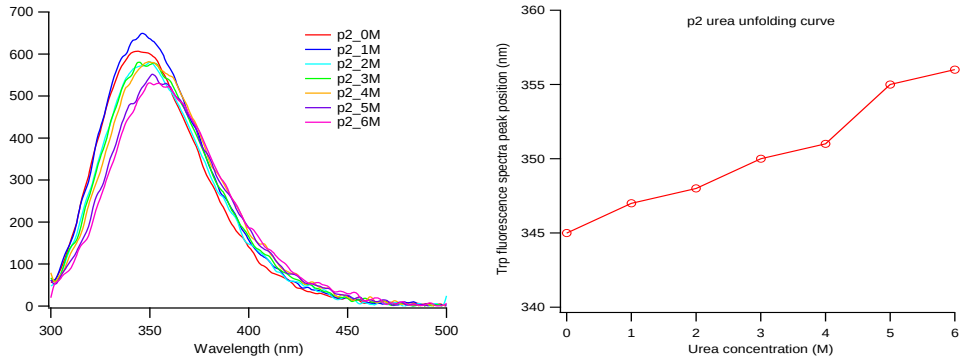

Figure 4

Protein labeling and gel filtration. The methods were consistently modified in order to decrease the number of donor only labeled proteins and to increase the number of the FRET labeled proteins. After collecting fractions from the gel filtration, we determined that fraction three contained the proteins that were attached to the dyes. There are eight possible outcomes when labeling proteins with fluorescent dyes. The protein can be single labeled with just one donor dye or one acceptor dye. The protein can also be double labeled with two of the same dyes attached the cysteines on one protein. The other possibility is the FRET labeled protein which has one of each dye attached to the cysteine groups located on the protein. The graph below (figure 5 left) is the absorbance spectrum that was obtained from the UV visible spectrophotometer after gel filtration. The absorbance spectra shows the peaks of the labeled proteins at the wavelengths 280 nm, 499 nm, and 561 nm which is located between eluted volumes 1 and 2. The peak at elute volume 3 mL shows the absorbance peak for the acceptor dye at wavelength 561 nm. The peak located between 4 and 5 shows the absorbance peak of the alexa488 at the wavelength 499 nm. This data shows the data from method 4. The graph to the right (figure 5 right) shows the absorbance peaks from protein 1 fraction 3 that were used to determine the labeling ratio which is shown in the table 3. The peaks in this graph also represent the wavelengths at 280 nm, 499 nm, and 561 nm for the fraction that contained the labeled protein.

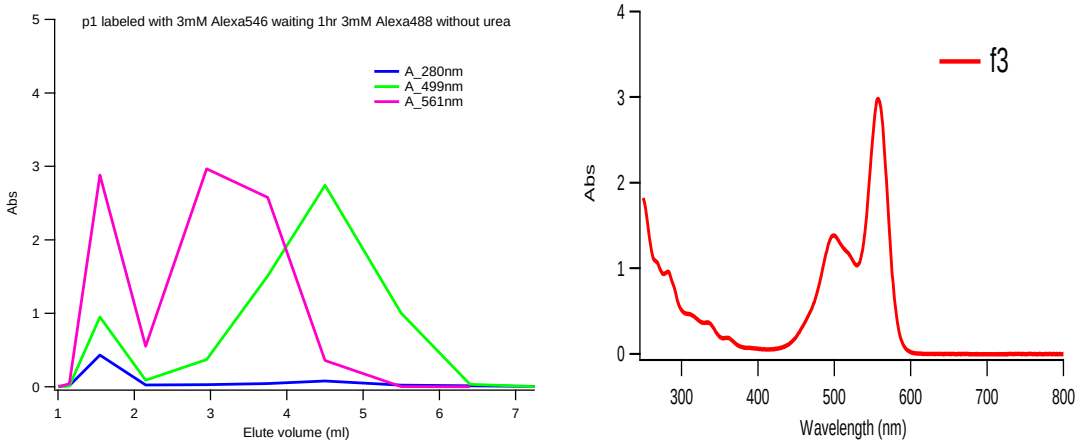

Figure 5

	Method 1	Method 2	Method 3	Method 4
Labeling ratios	1 : 0.3 : 0.6	1 : 0.06 : 0.9	1 : 0.6 : 1.3	1 : 0.56 : 1.2

Table 3

The labeling ratio is a comparison of the protein concentration to the concentration of donor and acceptor labels. The labeling ratio in methods 1 and 2 were too low in value to note any significant changes that occurred by modifying the labeling protocol. In method 1, the dye concentrations were the same and they added simultaneously. The concentration of donor only labeled and acceptor only labeled proteins were relatively low because the dye concentrations were competing to attach to the cysteine group. There was also a low level of FRET labeled proteins (see later). By tripling the alexa546 concentration compared to the alexa488 concentration and increasing the time elapsed between adding the dyes in method 2, the concentration of acceptor labeled increased and the concentration of donor labeled proteins decreased. In method 3, dye concentrations were the same and the time elapsed between adding the dyes was decreased to an hour. There was a significant increase in the concentration of both donor and acceptor labeled suggesting more FRET labeled protein. In an effort to decrease the donor-only labeled protein, urea was added to the aqueous solution before adding the dyes in method 4. This slightly decreased the donor only labeled protein.

Fluorescence Spectroscopy to measure average FRET. By increasing the alexa546 concentration to 3 mM and waiting for an hour before adding 1.5 mL of 3mM alexa488, we increased the concentration of proteins that were labeled with both fluorescent dyes. The dotted lines represent the direct excitation of the acceptor with 485 nm light in both of the graphs below that show the average FRET for the labeled sample. By measuring the FRET efficiency of each protein (P1 and P2) before and after adding cpSRP54 we found that the FRET efficiency increased for P2 but not for P1 upon addition of cpSRP54 (table 3).

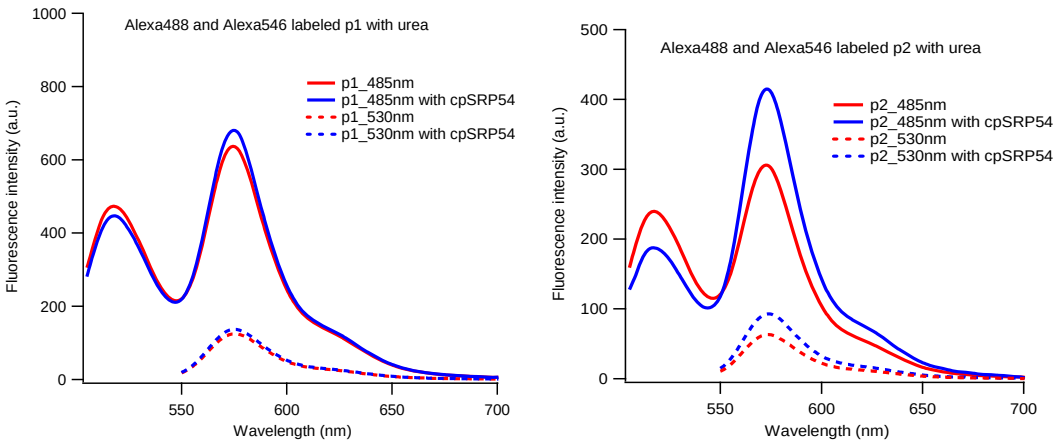

Figure 6

	Without urea		With urea	
	Without cpSRP54	With cpSRP54	Without cpSRP54	With cpSRP54
P1	0.46	0.47	0.56	0.59
P2	0.42	0.51	0.54	0.67

Table 4

Single molecule FRET. Figure 7 shows the single molecule burst data of the single proteins labeled with the alexa488 and alexa546 dyes obtained from the fluorescence microscope. The peaks that are above the horizontal axis at zero represent the intensity of the donor dye alexa488 (red). The peaks that below the horizontal axis at zero represent the intensity of the acceptor dye alexa546 (blue).

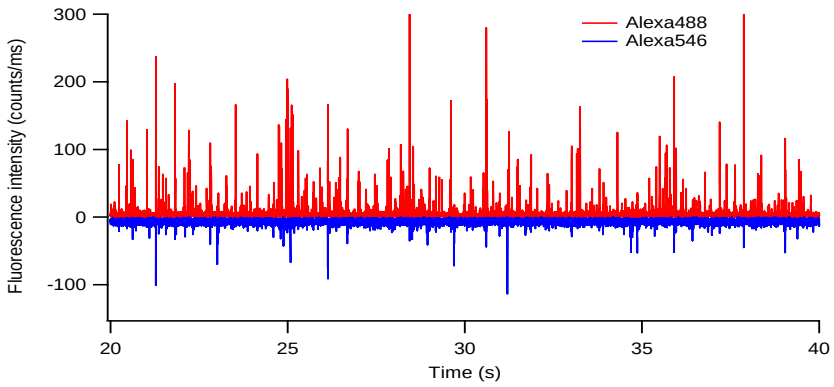

Figure 7

These intensities from each burst (single molecule) can then be substituted into the FRET efficiency equation below

$$E = \frac{I_A}{I_A + \gamma I_D}$$

The proteins labeled only with acceptor do not have any significance in the FRET histograms because the lasers that are used during the smFRET do not excite the acceptor dyes. The donor only labeled proteins are detected in the FRET histogram as a peak centered at zero FRET.

The graphs below show the data that was obtained from the single molecule FRET measurements for method 3 without urea (figure 8) and method 4 with Urea (Figure 9). The first peak (in green) represents the donor-only labeled protein. The data shows that the addition of cpSRP54 increased the FRET efficiency for peak 4 (high FRET) in both protein 1 and protein 2, although to a much lower extent in protein 1. Peaks 2, 3, and 4 in the histogram suggests that at least three distinct states of cpSRP43 are present, which can only be observed in the smFRET experiment.

The data showed that the ensemble fluorescence and smFRET are consistent in measuring the average FRET of the two protein samples. That is to say that the average FRET efficiency for P1 and P2 are similar, but that the average FRET efficiency for P2 increases with the addition of cpSRP54, whereas it increases only slightly for P1

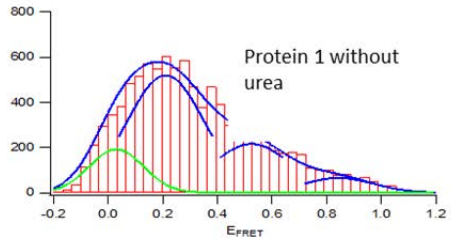

	E	Area	% Area
Peak1	0.03	48	15%
Peak2	0.21	184	56%
Peak3	0.52	76	23%
peak4	0.84	21	6%

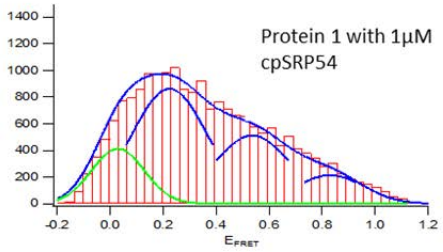

	E	Area	% Area
Peak1	0.03	103	16%
Peak2	0.22	306	46%
Peak3	0.54	182	28%
peak4	0.83	68	10%

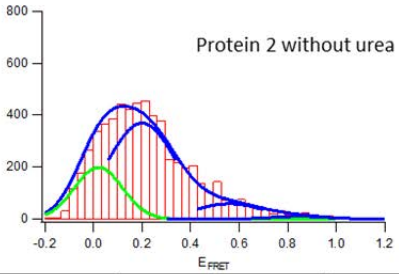

	E	Area	% Area
Peak1	0.02	49	24%
Peak2	0.2	131	64%
Peak3	0.56	21	10%
peak4	0.85	3	2%

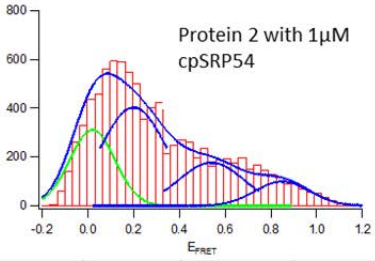

	E	Area	% Area
Peak1	0.02	77	24%
Peak2	0.2	143	46%
Peak3	0.54	63	20%
peak4	0.85	30	10%

Figure 8

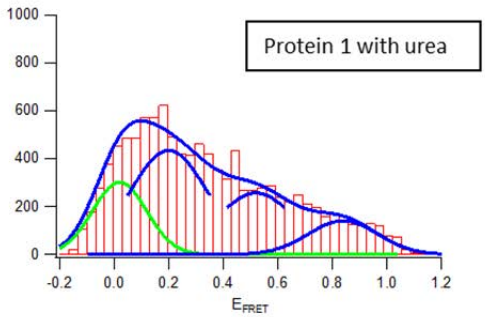

	E	Area	% Area
Peak1	0.02	75	21%
Peak2	0.2	154	42%
Peak3	0.52	91	25%
peak4	0.84	45	12%

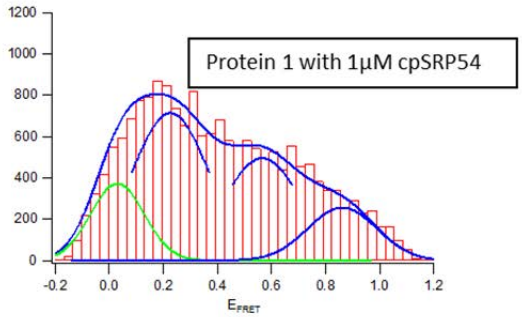

	E	Area	% Area
Peak1	0.03	92	15%
Peak2	0.23	253	42%
Peak3	0.57	176	29%
peak4	0.86	82	14%

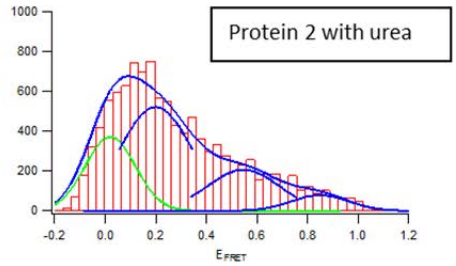

	E	Area	%Area
Peak1	0.02	92	25%
Peak2	0.2	185	50%
Peak3	0.55	73	20%
peak4	0.85	22	5%

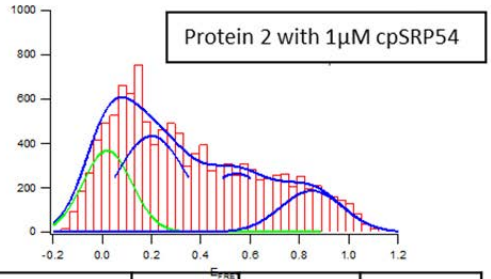

	E	Area	% Area
Peak1	0.02	91	23%
Peak2	0.2	154	39%
Peak3	0.54	93	23%
peak4	0.85	59	15%

Figure 9

Comparing figure 8 and 9 shows that the addition of the urea during the labeling reaction increased in the amount of FRET-labeled proteins, and decreased the donor-only labeled proteins, which was a major objective of this project. This reduction in the donor-only peak allows for less interference (and therefore more confidence) in determining the FRET efficiencies and populations of the different protein states. Furthermore, since the difference between the FRET efficiency in protein 1 and protein 2 upon addition of cpSRP54 was identical from both labeling methods (3 and 4), this shows that using urea for labeling did not permanently affect the protein structure but did help in reducing the donor-only peak.

Conclusion

Urea concentrations above 3M unfolds the protein and exposes both of the cysteines on the protein to the fluorescent dyes more so than the cysteines in the folded protein. By modifying the labeling protocol to add urea when the donor dye is added, the concentration of FRET labeled proteins increased, and the concentration of donor-only proteins decreases. Since both proteins P1 and P2 were improved by adding urea, and the cysteine group that is common between P1 and P2 is in the Ank2 domain, this suggests it is this ankyrin 2 cysteine that is difficult to label, possibly the cysteine residue is not exposed to the solvent when the protein is folded. This result highlights the importance of optimizing the labeling protocol for efficient labeling of cpSRP43 for FRET studies.

The smFRET data showed that there are various states of cpSRP43. The population of these states changed as cpSRP54 was added – the higher FRET state was more prevalent when cpSRP54 was present. The differences in the smFRET histograms between Ank2-CD2 and Ank2-CD3 labeled proteins upon the addition of cpSRP54 suggest that cpSRP54 interacts differently with CD2 than CD3. The reasons for these differences are not yet clear, but will be the focus of continued studies. For example, future goals will be to investigate the labeling of a mutant where the cysteines are placed in CD2 and CD3 and deleted from Ank2. The optimization of the labeling protocols described in this report will be invaluable in obtaining high FRET labeling efficiencies and reducing donor-only peaks for future cpSRP43 mutants.

Acknowledgements

Thanks National Science Foundation CHE-0851505/REU, Prof. Colin Heyes, and Dr. Feng Gao.

References

Cain, P., Holdermann, I., Sinning, I., Johnson, A., & Robinson, C. (2011) Binding of chloroplast signal recognition particle to a thylakoid membrane protein substrate in aqueous solution and delination of the cpSRP43 substrate interaction domain. *Biochemistry Journal*, 149-155.

Gel Filtration Chromatography (2011) Retrieved June 1, 2011, from Sigma Aldrich.

Jaru-Ampornpan, P., Shen, K., Lam, V., Ali, M., Doniach, S., Jia, T., et al. (2010) ATP-independent reversal of a membrane protein aggregate by a chloroplast SRP subunit. *Nature Structural and Molecular Biology*, 696-703.

Kathir, K., Rajalingam, D., Sivaraja, V., Kight, A., Goforth, R., Yu, C. et al. (2008) Assembly of Chloroplast Signal Recognition Particle involves Structural Rearrangement in cpSRP43. *NIH Public Access*, 49-60.

Kuzmenkina, E.K., Heyes, C., & Nienhaus, G.U. (2005) Single-molecule Forster Resonance energy transfer study of protein dynamics under denaturing conditions. *PNAS*, 15471-15476.

Schuenemann, D., Gupta, S., Persello-Cartieaux, F., Klimyuk, V., Jones, J., Nussaume, L., et al. (1998) A novel signal recognition particle targets light-harvesting proteins to thylakoid membranes. *Proceedings of National Academy of Sciences*, 10312-10316.

Skoog, D., Holler, F.J., & Crouch, S. (2007) *Principals of Instrumental Analysis*. Belmont, CA: Thomson Brooks/Cole.

Stengel, K.F., Holdemann, I., Cain, P., Robinson, C., Wild, K., & Sinning, I. (2008) Structural Basis for Specific Substrate Recognition by the Chloroplast Signal Recognition Particle Protein cpSRP43. *Science*, 253-256.

Synthesis and Characterization of a Ru-Pd Bimetallic Complex

Ryan Christman, Ohio Northern University
Ada, Ohio

Abstract

Despite its recent implication as the active catalyst in direct arylation via C-H functionalization, little is known about the properties and reactivity of Pd(III). To address this lack of knowledge, Dr. Zheng devised a bimetallic ruthenium-palladium model to study Pd(III). This paper details the synthesis of one of the ligands for this complex.

Introduction

The area of green, or sustainable, chemistry has become a major research focus as scientists try to make improvements for humans and our environment. Direct arylation via C-H functionalization is a specific area within green chemistry that has many advantages over current synthesis methods. By performing chemistry directly on carbon-hydrogen bonds, the need for pre-functionalized groups is eliminated. This allows for developing more efficient synthetic methods, eliminating waste and saving time and money.

Transition metals are often required to functionalize inert C-H bonds, the most common being ruthenium, rhodium, and palladium. A Pd(II)-Pd(IV) redox cycle is typically invoked as the accepted mechanism involving palladium as the catalyst for C-H functionalization. Recently though, Pd(III) has been shown to be the active catalyst in direct arylation reactions by Ritter and Sanford.[3,6] While the reactivity of palladium in its second and fourth oxidation states is well understood, palladium in its third oxidation state, only recently being recognized in organometallic reactions, has not been studied extensively. Unlike Pd(IV), which has a monomeric octahedral geometry, Pd(III) adopts a dimeric octahedral geometry.[7] Reductive elimination, the final step in Pd-catalyzed direct arylation, could be greatly affected by this geometry difference between Pd(III) and Pd(IV).

In order to address this lack of knowledge, Dr. Zheng devised a bimetallic ruthenium-palladium model to specifically study palladium in its third oxidation state. Since the electron transfer between Ru(II) and Ru(III) is strictly a one-electron process, only the desired Pd(III) complex is expected to be formed. The mononuclear Pd(III) complex is expected to be an unstable and short-lived species. Also, preparation of Pd(III) is usually accomplished by oxidation of Pd(II) with an external oxidant that is usually incorporated into the final product. Discovery of a milder and innocent oxidant would be a major help in broadening the application of Pd(III)-catalyzed direct arylation. By using complex **1.11** as a model, we hope to be able to study Pd(III) and address these issues. Through flash photolysis, Ru(II) is easily oxidized to

Ru(III) in the presence of viologen. Then Ru(III) should oxidize Pd(II) to Pd(III), while itself is reduced to Ru(II). This electron transfer process involving the Ru(II) to Ru(III) metal center has been extensively used to study electron transfer reactions in biological systems by Durham.[4]

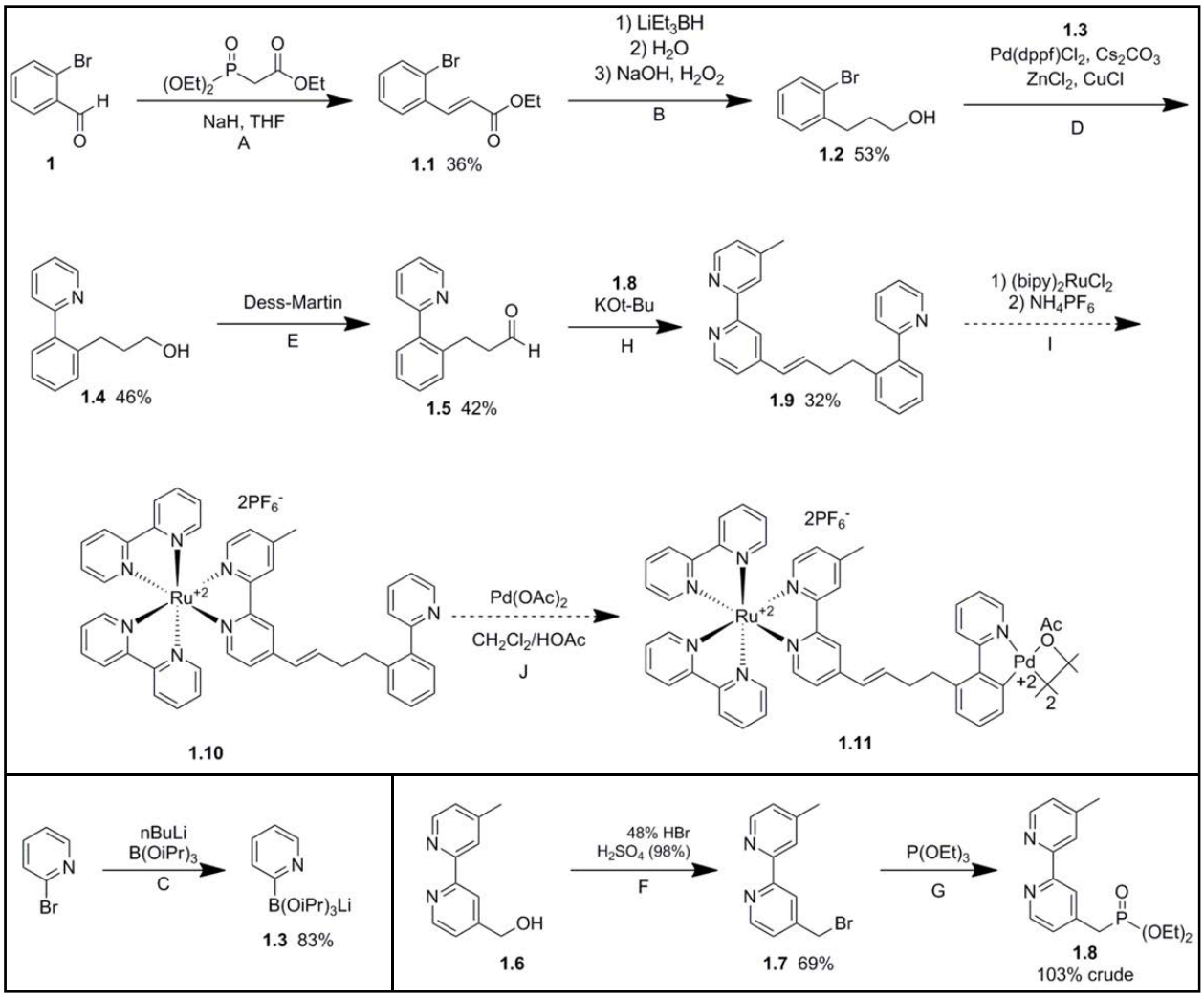

Figure 1. Synthesis Scheme for Ru-Pd complex

Experimental Procedures

All reactions were carried out under an inert atmosphere, mostly nitrogen. Purification was done using flash chromatography or distillation and products were characterized by NMR.

A) **1.1**: Triethyl phosphonoacetate (20.1 mL) was added to NaH (4.34 g) in THF (97 mL) at 0°C. Let warm to room temperature and stir for 30 minutes. Dissolve 2-bromobenzaldehyde (7.9 mL) in THF (97 mL) in a separate flask. Add the solution of 2-bromobenzaldehyde to triethyl phosphonacetate mixture at 0°C. Stir for 20 minutes at 0°C, then let warm to room temperature and stir for 1 hour. Cool to room temperature and add neat triethyl phosphonoacetate (4 mL), then NaH (0.872 g). Stir at 0°C for 20 minutes, then let warm to room temperature and stir for 1 hour. Quench it with saturated NH_4Cl (12 mL) and H_2O (10 mL).

Extract aqueous layer with EtOAc (2×10 mL). Washed with H_2O (10 mL) and brine (10 mL). Concentrate and distill off excess triethyl phosphonoacetate by high vacuum. Yield: 6.20 g (36%). ^{1}H NMR: CH_3, 1.34 (t); CH_2, 4.29 (q); CH, 6.39 (d); aromatic, 7.19-7.10; CH, 8.05(d).

B) **1.2**: Make slurry of $LiAlH_4$ (1.24 g) in THF (63 mL). Dissolve **1.1** (2.80 g) in THF (63 mL). Place $LiAlH_4$ slurry in an ice/methanol bath and add **1.1** via syringe. Stir for 1 hour in bath. Warm to room temperature and stir for 1 hour. Add H_2O (1.3 mL), NaOH (1 mL), and H_2O (3.6 mL). Filter through celite with EtOAc and concentrate. Yield: 1.92 g (82%). ^{1}H NMR: CH_2, 1.89(quintet); CH_2, 2.81(t); CH_2, 3.69(t); aromatic, 7.05-7.58.

C) **1.3**: Add 2-bromopyridine (2.2 mL) and triisopropyl borate (5.8 mL) to 4:1 mixture of toluene (90 mL) and THF (23 mL). Cool to -78°C and added 16 mL of *n*-BuLi over 30 minutes via syringe pump. Stir at -78°C for 30 minutes, then let warm to room temperature. Concentrate and dry under vacuum at 110°C for 4 hours. Yield: 5.10 g (83%).

D) **1.4**: Add **1.3** (3.24 g), $Pd(dppf)Cl_2$ (0.145 g), and $CsCO_3$ (2.57 g) to a schlenk flask with a side arm. In glove box, add $ZnCl_2$ (.539 g) and CuCl (.034 g) to the flask. Dissolve **1.2** (.848 g) in DMF (40 mL) and transfer to the flask. Degas the flask via freeze, pump, thaw for three cycles. Stir at 110°C for 19 hours (closed system). Filter through celite with EtOAc and concentrate. Yield: 0.442 g (53%). ^{1}H NMR: CH_2, 1.96(quintet); CH_2, 2.85(t); CH_2, 3.52(t); aromatic, 7.20-8.69.

E) **1.5**: Added Dess-Martin Periodinane (1.44 g) to a flask. Dissolve **1.4** in CH_2Cl_2 (16 mL) and transfer to the flask. Stir at room temperature for 48 hours. Dilute with EtOAc (30 mL) and partition with 1:1 saturated $Na_2S_2O_3$: saturated $NaHCO_3$ (30 mL). Extract with EtOAc (2×15 mL). Wash with H_2O (15 mL) and brine (15 mL) and concentrate. Yield: .183 g (42%). ^{1}H NMR: CH_2, 2.70(t); CH_2, 3.04(t); aromatic, 7.17-8.69; CH, 9.69(s).

F) **1.7**: Mix **1.6** (.401 g) in 48% HBr (8 mL) and concentrated (98%) H_2SO_4 (0.8 mL). Reflux for 3 hours. Neutralize with saturated Na_2CHO_3 and filter. Dissolve product in EtOAc and washed with brine. Dry over Na_2SO_4 and concentrate. Immediately start next step. Crude Yield: .365 g (69%)

G) **1.8**: Added neat triethyl phosphite (1.5 mL) to crude **1.7**. Stir at 80°C for 6 hours. Distill excess triethyl phosphite. Crude Yield: .460 g (103%). ^{1}H NMR: CH_3, 1.27(t); CH3, 2.43(s); CH_2, 3.22(d); CH_2, 4.09(quintet); aromatic, 7.11-8.59.

H) **1.9**: Add KO^{t}Bu (.0818 g) to THF (0.5 mL) in glove box. Dissolve **1.8** in THF (0.5 mL). Transfer **1.8** to KO^{t}Bu at 0°C and wash with THF (0.5 ml). Stir at 0°C for 30 minutes. Dissolved **1.5** (.051 g) in THF (0.5 mL). Transfer **1.5** to the flask with **1.8** and wash with THF (0.5 mL). Warm to room temperature and stir for 3 hours. Quench with H_2O (4 drops). Filter with EtOAc. Partition with H_2O (added 1 mL of Hexanes for better partition). Wash with H_2O (5 mL). Extract with EtOAc (3×5 mL). Wash with brine (5 mL) and concentrate. Crude Yield: .0478g (53%). ^{1}H NMR: CH_3, 2..43(s); CH_2, 2.56(q); CH_2, 2.84(t); CH, 6.19(q); CH, 6.29(d); aromatic, 6.94-8.78.

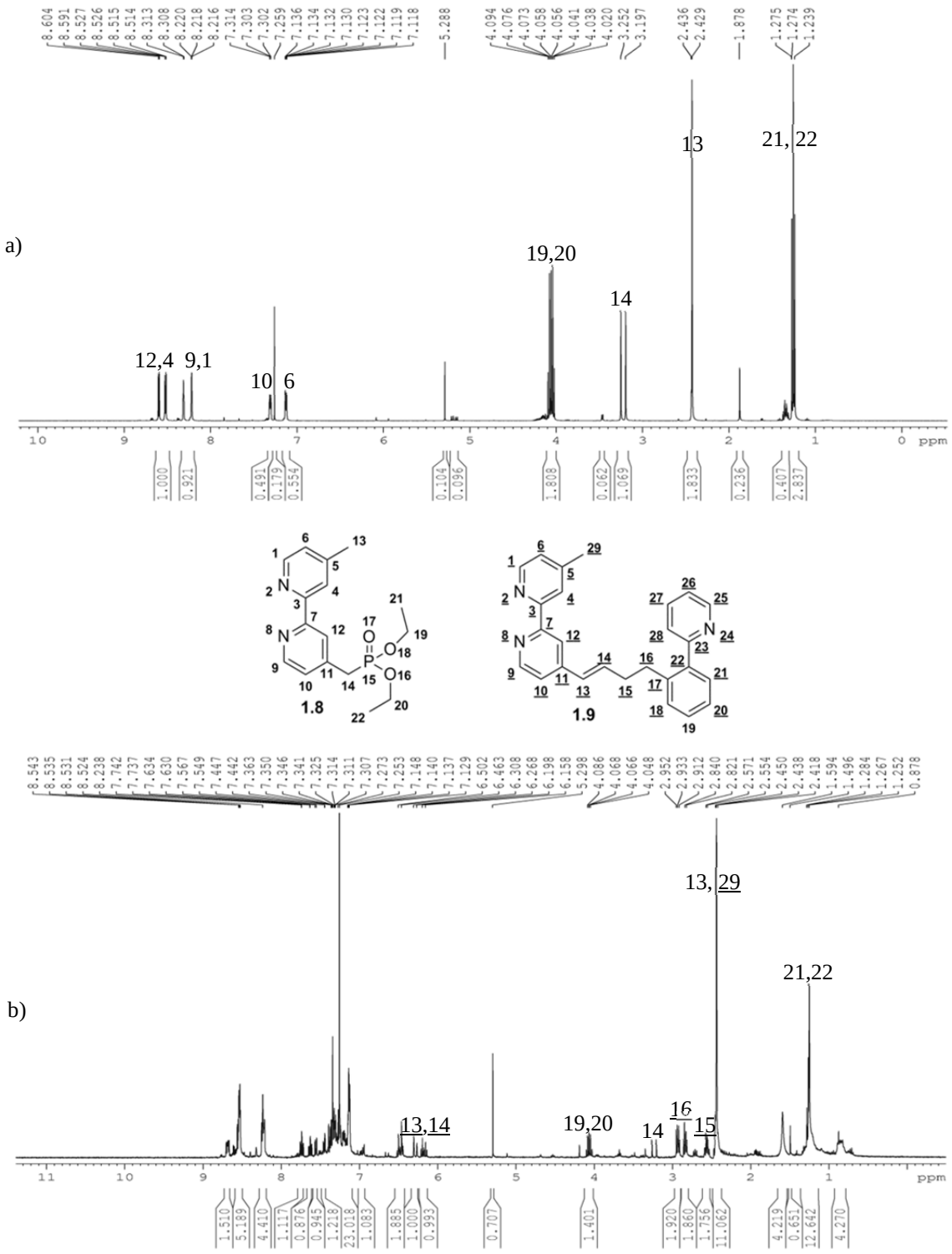

Figure 2. a) ^{1}H NMR of **1.8** b) ^{1}H NMR of **1.9** with leftover starting material **1.8**

Results and Discussion

Problems with the original synthetic scheme prevented us from completing the synthesis of complex **1.11**, and we were able to get as far as synthesizing **1.9**. The first problem was with the Suzuki Miyaura Cross-Coupling. Initial attempts using $Pd_2(dba)_3$ and diphenylphosphine oxide as the catalyst resulted in no reaction. Upon switching to the catalyst system composed of $Pd(dppf)Cl_2$, $ZnCl_2$, and CuCl, **1.4** was obtained in 38% yield on the first attempt, and 53% on the second attempt. Oxidation of **1.4** to aldehyde **1.5** also presented problems, as the Swern Oxidation yielded only 32%. Dess-Martin Oxidation yielded a slightly improved 42%. Synthesis of **1.8** worked well, with an overall yield of 72%. Problems again arose with the Horner-Wadsworth-Emmons Olefination as original attempts using KHMDS as a base yielded mostly one of the starting materials, phosphonate **1.8** while the other starting material, aldehyde **1.5** decomposed. When KO^tBu was used instead, we were able to synthesize **1.9**, but attempts to purify it from starting material **1.8** using flash chromatography were unsuccessful, as Figure 2 demonstrates.

Conclusion

Synthesis of ligand **1.9** was successful. The problem with purification of **1.9** could be easily fixed by using a slight excess of aldehyde **1.5** compared to phosphonoacetate **1.8**, as **1.5** should be easily separated using flash chromatography. As both the ruthenium and palladium metal centers have been extensively studied, we anticipate that steps I and J should be uneventful, leading to the synthesis of bimetallic complex **1.11**.

Acknowledgments

Thank you to Dr. Nan Zheng for allowing me to work on this project, and for his guidance and support in the lab. I also thank the University of Arkansas REU program and the NSF REU/CHE-0851505 for their support, and Mack Clements, Soumitra Maity, and Spencer Shinabery for their guidance in the lab.

References

1. Bateman, L. M.; McGlacken, G. P. Recent advances in aryl–aryl bond formation by direct arylation. **Chem. Soc. Rev. 2009**, **38**, 2447-2464.
2. Benitez, D.; Goddard, W. A.; Powers, D. C.; Tkatchouk, E.; Ritter, T. Bimetallic Reductive Elimination from Dinuclear Pd(III) Complexes. *J. Am. Chem. Soc.* **2010**, 132, 14092–14103.
3. Deprez, N. R.; Sanford M. S. Synthetic and Mechanistic Studies of Pd-Catalyzed C-H Arylation with Diaryliodonium Salts: Evidence for a Bimetallic High Oxidation State Pd Intermediate. *J. Am. Chem. Soc.* **2009**, 131, 11234–11241.
4. Durham, B.; Geren, L.; Hahm, S.; Millett, F. Photoinduced Electron Transfer between Cytochrome c Peroxidase and Yeast Cytochrome c Labeled at Cys 102 with (4-Bromomethyl-4'-methylbipyridine)[bis(bipyridine)]ruthenium. *Biochemistry.* **1991,** 30**,** 9450-9457.

5. Geibel, M. A. L.; Klein, J. E. M. N.; Powers, D. C.; Ritter, T. Bimetallic Palladium Catalysis: Direct Observation of Pd(III)-Pd(III) Intermediates. *J. Am. Chem. Soc.* **2009**, 131, 17050–17051.
6. Powers, D. C.;Ritter, T. Bimetallic Pd(III) complexes in palladium-catalysed carbon–heteroatom bond formation. *Nat. Chem.* **2009**, 1, 302-309.
7. Engle, K. M.; Mei, T.-S.; Wang, X.; Yu, J.-Q. Bystanding F+ Oxidants Enable Selective Reductive Elimination from High-Valent Metals in Catalysis. *Angew. Chem. Int. Ed.* **2011**, *50*, 1478-1491.

Expression and Purification of Cdc42 and PBD46, a Cancer-Causing Combination

Edward Evans Jr., Wabash College
Crawfordsville, Indiana

Abstract

The Ras superfamily consists of low molecular weight G-proteins that are heavily involved in cellular signaling, leading to various downstream responses. Like other Ras proteins, Cdc42 (cell division cycle 42) acts as a molecular switch interchanging from its active (GTP-bound) and inactive (GDP-bound) state through the utilization of GAP (GTPase-activating proteins) and GEF (guanine nucleotide exchange factors) effectors (See Figure 1). It has been shown that Cdc42 signaling pathways play a major role in cell proliferation and differentiation leading to tumor growth. PBD46 is an effector of Cdc42 proven to inhibit GTP hydrolysis, stabilizing the Ras protein in its active state. PBD46, as well as many other effectors, bind to the Switch I region (amino acids 28-40) of Cdc42. By site-directed mutagenesis, threonine of position 35 was replaced with alanine forming a Cdc42 mutant. With the use of affinity column chromatography, Cdc42(wild type), Cdc42(T35A), and PBD46 were expressed and purified for future tests of the Switch I binding interface.

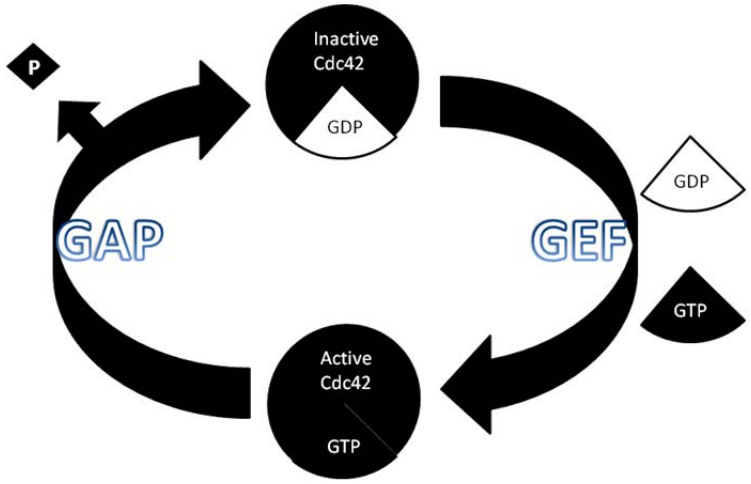

Figure 1. The Cdc42 cycle. Cdc42 interchanges from active and inactive states. Other proteins of the Ras superfamily behave similarly.

Introduction

Cell division cycle 42 (Cdc42) is a member of the Rho subfamily of small GTPases. Typical of Rho proteins, members of this family are heavily involved in cellular activity via signal transduction resulting in downstream responses. Most notably, these responses lead to cell proliferation, morphogenesis, and cytoskeletal changes. Cdc42 functions as a molecular switch, cycling between inactive (GDP-bound) and active (GTP-bound) state. This interchange is influenced by guanine nucleotide-exchange factors (GEFs), which replace GDP with GTP on

Cdc42, and GTPase-activating proteins (GAPs), which promote GTP hydrolysis to its inactive form. In its inactive state, Cdc42 is not effectively performing signal transduction; however, when bound to GTP, Cdc42 can bind to various other effectors, causing downstream signaling.

P21 Binding Domain (PBD46) is a 46-amino acid derivative of a p21 activating kinase (PAK). It has been shown that Cdc42 has a high affinity for PAKs. Particularly, PBD46 inhibits the GTP hydrolysis of Cdc42, keeping the protein in its active state and enabling the downstream signaling that leads to the formation of tumors. Therefore, producing the Cdc42-PBD46 complex allows a means to investigate Rho proteins' effect on cancer.

Furthermore, it has been found that PBD46 binds to Cdc42 in its Switch I region, amino acids 28-40 (See Figure 2). It has been documented that threonine is consistently 35th in Rho-related proteins, indicating that this amino acid is critical for proper function of Cdc42. The threonine was mutated to alanine to determine differences in the binding interfaces of Cdc42(wild type) and Cdc42(T35A). This will help determine the purpose of threonine's consistency in Ras proteins. Proper expression and purification of Cdc42(WT), T35A, and PBD46 will enable future tests to compare and contrast the wild type and mutant's binding capabilities.

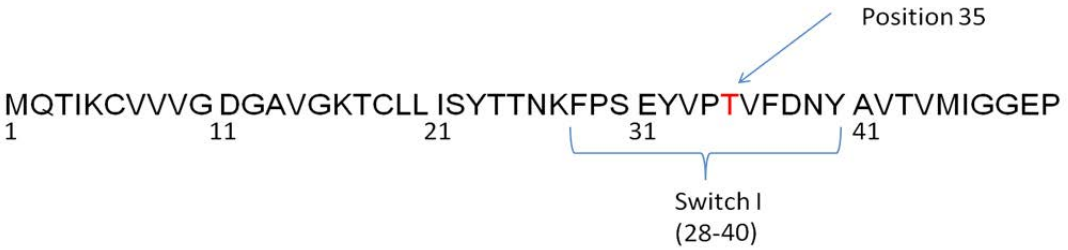

Figure 2. The first 50 amino acids of Cdc42. The Switch I region is where PBD46 binds to the Ras protein. Threonine has been mutated to alanine, making T35A.

Materials and Methods

Protein Expression Cdc42 is expressed in E. Coli strain BL21(DE3) from pET-15b vectors as a hexa-histidine tagged protein. For large scale expressions, Cdc42 was grown in 500 mL of LB with 0.1 mg/mL ampicillin (same concentration for all LB samples) overnight at 37 °C. Six flasks of 1.5 liters of LB each were inoculated with 75 mL of the seed culture. The fresh cultures were allowed to grow to an optical density at 600 nm (OD_{600}) in the range of 0.4 – 0.6. Ideally, this takes approximately 1 to 1.5 hours. The cultures were induced with1.0 mM isopropyl β-D-thiogalactopyranoside (IPTG) and allowed to incubate for 3.5 hours at 37 °C. Then, the cells are centrifuged at 6500 rpm for 15 minutes at 4 °C and washed with a 40 mM Tris-base solution. The cells are centrifuged again, and the pellet is stored at -80 °C until needed.

Before and after induction, 1 mL aliquots were taken from each flask. These cells were spun down by centrifugation at 14000 rpm for 15 minutes at 4 °C. The pellet was resuspended with 120 µL of 8 M urea and stained with 40 µL of 4x loading dye. The aliquots were incubated at 90 °C for 2 – 5 minutes and stored at 4 °C afterwards. These aliquots were designated for gel electrophoresis on 15% sodium dodecyl sulfate (SDS) gels.

Cdc42(T35A) was expressed in the same manner, but PBD46 had alterations. PBD46 was allowed to grow to an OD_{600} range from 0.8 – 1.0. Induction was allowed to transpire for 4 to 5

hours. Finally, the PAK was washed with PBS buffer (0.14 M NaCl, 0.0030 M KCl, 0.01 M Na_2HPO_4 x 7 H_20, 0.0018M KH_2PO_4 at pH 7.3) instead of a Tris-base solution.

Prior to large scale expression, test expressions were performed to guarantee that the protein of interest was produced effectively. This entails a 10-mL overnight culture of protein with ampicillin and an inoculation of 500 µL into fresher LB. After uninduced and induced samples are taken, the cultures can be properly discarded.

Protein Purification Procedures are performed on ice unless otherwise indicated. The stored pellet of Cdc42 was resuspended in a lysis buffer (30 mL Tris binding buffer, 30 mg lysozyme, 300 µL Halt Protease Cocktail, 3.5 mg PMSF, with 1 mM GDP per liter of culture being resuspended). Sonicate on ice 5 times for 20 seconds with 1-minute rest periods. The cells were incubated on ice for 30 minutes with occasional stirring. A small amount of DNase is added to the cells, and they incubate at room temperature for 15 minutes. The cells are centrifuged at 19500 rpm for 15 minutes at 4 °C, separating the lysate and pellet. The lysate is filtered, and aliquots of both the supernatant and pellet are taken. The lysate of Cdc42, being kept on ice, is ran over a nickel affinity column on the fast protein liquid chromatography (FPLC) machine with Tris binding buffer for nickel column purification (0.040 M imidazole, 0.100 M NaCl, 0.050 M Tris-HCl, 0.010 M $MgCl_2$ x $6H_2O$ at a pH of 8.0). The column is coated with nickel ions, so the hexa-histidine tag of Cdc42 can bind to it. After running the lysate, the higher concentration of imidazole in the elution buffer (0.250 M imidazole, 0.100 M NaCl, 0.050 M Tris-HCl, 0.010 M $MgCl_2$ x $6H_2O$ at a pH of 8.0) allows for Cdc42 to be purified. Fragments from the suspected Cdc42 absorbance peak are collected for dialysis. A dialysis (molecular weight cut off = 6-8 kDa) of the purified Cdc42 in 5 liters of Tris binding buffer was allowed to spin overnight at 4 °C, removing final traces of impurities. The following day, the absorbance at 280 nm was taken and the protein concentration of the purified protein was determined using Beer's law. The protein is stored at -80 °C until needed.

Cdc42(T35A) is purified in the same manner. The general method of purification is the same for PBD46, but there are numerous differences. For PBD46, 30 mL of PBS buffer is used for the lysis buffer instead of Tris binding buffer. Also, GDP is not added. Since PBD46 is GST-tagged, the column for PBD46 is a glutathione column, allowing the protein to bind via disulfide bonds. The GST-tag must be removed if PBD46 is to form a stable complex with Cdc42. Therefore, after purifying PBD46-GST with GST elution buffer (0.020 M Tris-HCl, 0.010 M reduced glutathione), the protein is put back on a glutathione column. Thrombin is added to cleave the tag and allowed to rock overnight. Once the thrombin and PBD46 are washed out of the column, the sample solution flows over a heparin column, allowing the removal of thrombin. The purified PBD46 is dialyzed overnight in 5 liters of PBS buffer every time it goes across a column. The concentration of the protein is determined by taking the absorbance and using Beer's law. PBD46 is also stored at -80°C until needed.

Data Collection

To verify that the protein of interest was actually expressing, gel electrophoresis of 15% SDS gels were performed. SDS gels consist of stacking and separating segments utilized to separate proteins based on their size. Their ingredients include acrylamide, water, SDS, tetramethylethylenediamine (TEMED), ammonium persulfate, and a Tris buffer of pH 8.8 for the stacking gel and pH 6.8 for the separating gel. All samples are run alongside a molecular weight

marker ranging from 17 to 175 kilodaltons (kDa). This allows experimenters to approximate the molecular weight of expressing proteins.

Results and Discussion

Purification of Cdc42 After the concentration of imidazole was increased on the nickel column, an absorbance peak is observed at fragments A4-A7 for the wild type protein, as shown in Figure 3. This is suspected to be Cdc42(WT), so samples of each fragment were taken for gel electrophoresis. Cdc42 is approximately 21 kDa. As indicated on the SDS gel, the samples corresponding to the suspected absorbance peak contain proteins of about 21 kDa. Furthermore, the significant difference between the lysate and the flow through is also at 21 kDa as expected. This verifies that Cdc42(WT) has, in fact, been purified.

As indicated above, the T35A mutant is expressed and purified in the same fashion as that of the wild type. Two lysates of the mutant were put on the same column, consecutively. When the concentration of imidazole was increased, the T35A absorbance peak is visible on both chromatograms as expected. Both absorbance peaks corresponds to fragments A5-A9, which are sampled on the SDS gel. The bands for the pools before and after dialysis indicate that the protein is about 21 kDa. Once again, the most notable difference between the lysate and the flow through is a band of approximately 21 kDa. This leads to a comfortable declaration that T35A has also been purified.

Purification of PBD46 Altogether, PBD46 goes across 3 columns for purification. In Figure 5, there is a chromatogram of the final step of purification on the heparin column. Considering that PBD46 does not have a notable affinity to heparin, it begins to elute instantly in fragments A2-A5. However, concluding that PBD46 has been purified cannot be confirmed with the molecular weight marker used. The smallest shown band on the ladder is 17 kDa, but PBD46 is only 5 kDa. Although a significant band is shown well below the 17 kDa marker, it is not reliable to assume this is the desired protein. The sample was sent in for MALDI mass spectroscopy, but no traces of PBD46 were found.

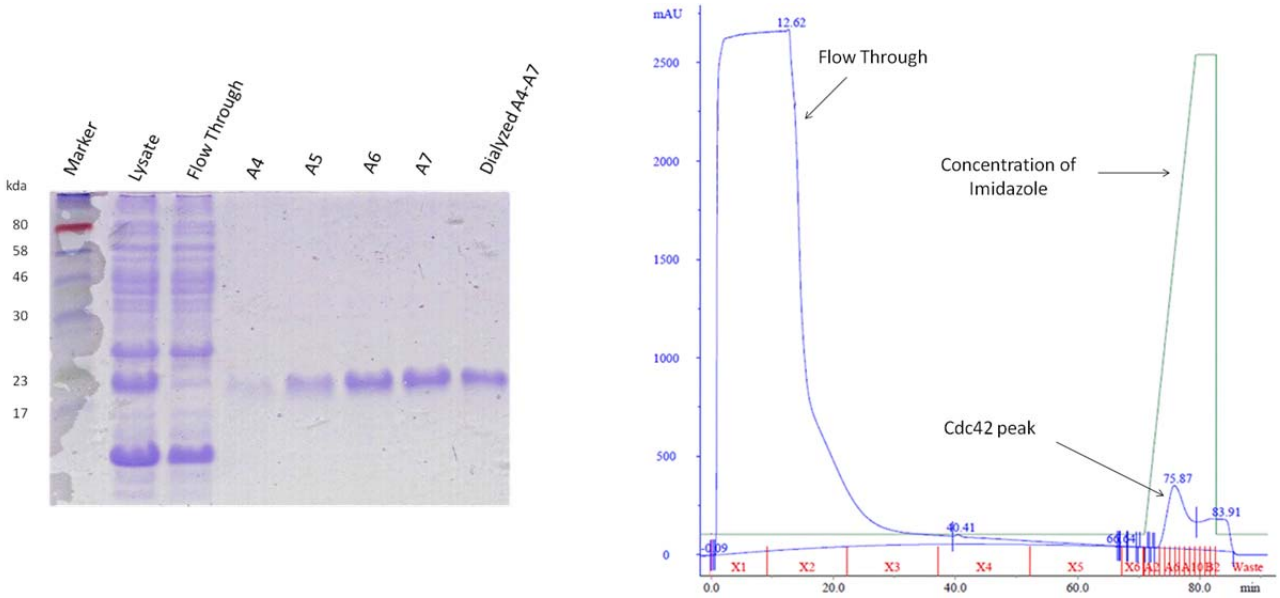

Figure 3. Chromatogram and SDS gel of Cdc42(WT) purification.

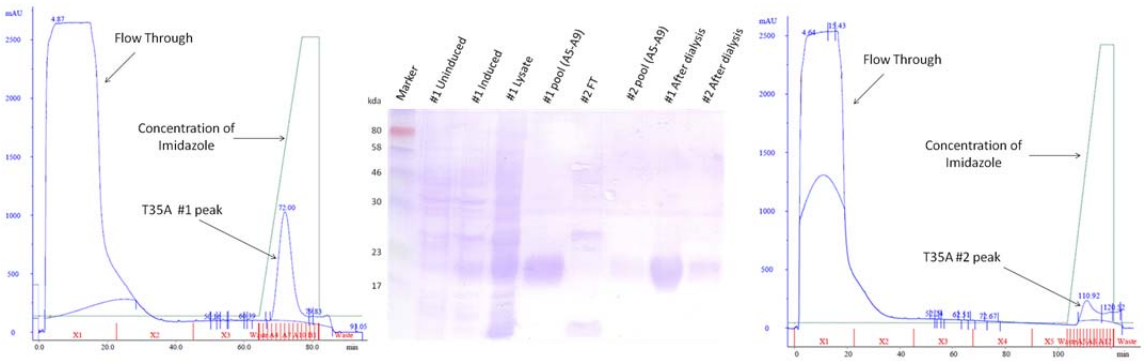

Figure 4. Chromatograms and SDS gel of Cdc42(T35A) purification.

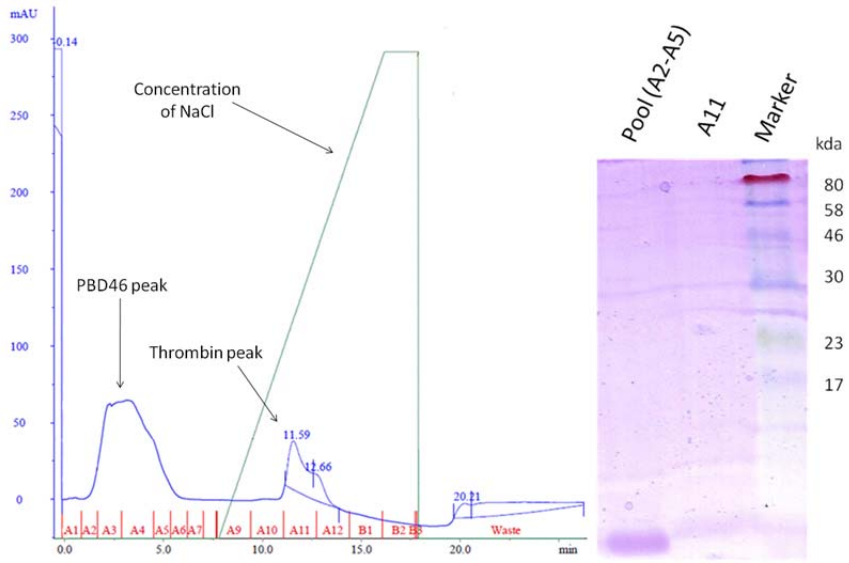

Figure 5. Chromatogram of Heparin column and SDS gel of PBD46 purification.

Protein Concentration After dialysis, the protein concentration of the wild type, the mutant, and PBD46 was determined by taking the absorbance at 280 nm of diluted samples. Using Beer's law, the protein concentration was extrapolated from the absorbance values. The concentrations for Cdc42(WT), T35A #1, T35A #2, and PBD46 were 10.7 mg/mL, 2.2 mg/mL, 0.5 mg/mL, and 0.1 mg/mL, respectively.

Conclusion

With the use of affinity column chromatography, both Cdc42(WT) and T35A have been expressed and purified in sufficient amounts to perform assays in the future. However, there is not enough evidence to conclude that PBD46 has been properly isolated. Even so, 0.1 mg/mL is not sufficient to perform a reasonable number of experiments.

Future Work

It is essential to purify PBD46 in sufficient amounts to perform experimentation on Cdc42 activity. Ideas for optimizing the isolation of this effector have already been conjured. A

different buffer for the lysis of cells and overnight dialysis may present a better yield. PBS buffer has a pH of 7.3. However, this pH may be unsuitable for the protein. Also, it may be favorable to use gel beads rather than pre-packed columns. This will allow for better thrombin cleavage.

After effective purification of the proteins, isothermal titration calorimetry and fluorescence tests may be performed to determine thermodynamic data regarding the binding affinity of Cdc42 to PBD46. This will enable affinity comparisons of the Switch I region with and without threonine in the 35^{th} position.

Acknowledgements

A great level of appreciation goes to Dr. Paul D. Adams, the Adams lab group, Dr. Willyerd Collier, NSF-REU CHE-0851505 for funding, and NIH-ABI for grants to Dr. Adams.

References

1. Guo, W., Sutcliffe, M. J., Cerione, R. A., and Oswald, R. E. (1998) Identification of the Binding Surface on Cdc42 for p21-Activated Kinase, *Biochemistry*, 37, 14030 – 14037.
2. Chandrashekar, R., Salem, O., Krizova, H., McFeeters, R., and Adams, P. D. (2011) A Switch I Mutant Exhibits Less Conformation Freedom, *Biochemistry*, http://pubs.acs.org/doi/pdf/10.1021/bi2004284.
3. Wheatley, E. and Rittinger, K. (2005) Interactions between Cdc42 and the scaffold protein Scd2: requirement of SH3 domains for GTPase binding, Biochem. J., 388, 177-184.
4. Elliot-Smith, A. E., Owen, D., Mott, H. R., and Lowe, P. N. (2007) Double Mutant Cycle Thermodynamic Analysis of the Hydrophobic Cdc42-ACK Protein-Protein Interaction, *Biochemistry*, 46, 14087-14099.

Redox-Magnetohydrodynamic Microfluidics Using Multiple Electrode Pairs and Sweep-Step Potential Waveforms

Elaine Haas, Spring Hill College
Mobile, Alabama

Abstract

Microfluidics is integral for automating lab-on-a-chip (LOAC) devices, especially if it is possible to program fluid flow. Redox-magnetohydrodynamics (MHD) offers unique fluid control for LOAC devices, which is not possible with existing microfluidic pumps. The MHD array setup induces fluid flow while eliminating the need for channels, thus reducing the complexity of the detection system. This project addresses a complication associated with redox-MHD: the need for the presence of redox species. In order to minimize interference with a sample and detection, a strategy to immobilize them to the electrodes was investigated. The redox species, hexamine ruthenium chloride, was tethered to the electrodes using the polymer Nafion. Characterization with cyclic voltammetry showed that the positively-charged redox species indeed loaded into the negatively-charged Nafion polymer (through electrostatic interactions). Because there is a finite number of redox species at the modified electrodes, they will deplete quickly under electrolysis conditions. Thus, a method of redox replenishment was also investigated, but with redox species in solution for preliminary studies (0.1 M potassium ferricyanide, 0.1 M potassium ferrocyanide in 0.1 M potassium chloride). A chip was used with an array of individually-addressable microelectrodes to serve as the anodes and another array to serve as the cathodes. With a multipotentiostat, different pairs of anodes and cathodes were activated with a stepped potential (0 V to 0.3 V at the working electrode). Then at 0.220 s, one set underwent a sweep which reversed its potential (in one experiment, a fast sweep over 0.220 s was used, and in another case a slow sweep over 0.660 s was used). The sweeps replenished the redox species to their original state. This sequence was performed for 6 cycles. The fluid speed was twice as great with both sets during the potential step than when one set was swept back. The results are encouraging that recovery of redox species in this manner should be possible. In the future, the plan is (using another instrument) to program a potential waveform using two or more separate active redox-modified electrode pairs with the waveforms out of phase of each other, in order to produce a continuous fluid flow, without interference of redox species with the sample.

Introduction

There is great interest in microfluidics and LOAC devices that allow for chemical analysis on a miniature scale, thus reducing time, materials and power compared to benchtop analysis. Microfluidics is concerned with the control and behavior of liquids that are entrapped in a very small area. These fluids exhibit entirely different properties and behaviors than do fluids on a large scale. This project investigates fundamental properties of redox-magnetohydrodynamics (redox-MHD) such that it might someday be used to fine-tune microfluidic pumping and stirring for LOAC applications. MHD offers some unique capabilities to control local fluid motion that other micropumps cannot.[1,2] As illustrated in Figure 1a and 1b, MHD utilizes a convective force, $\mathbf{F_B}$, driven by a magnetic field, **B**, in the presence of ion

current, **j**. This convective force in turn directs fluid flow, based on the cross product relationship, $\mathbf{j} \times \mathbf{B} = \mathbf{F_B}$. This project in particular makes use of the MHD theory in conjunction with a silicon microchip with two sets of gold electrode arrays. Preliminary studies are also included using a gold macrochip coated with a polymer film that immobilizes redox species to the surface with minimal loss. It should be noted that programming the potentials at the electrodes can oxidize and reduce the redox species, producing **j** in a controlled manner. Several publications describe this concept.[3-6]

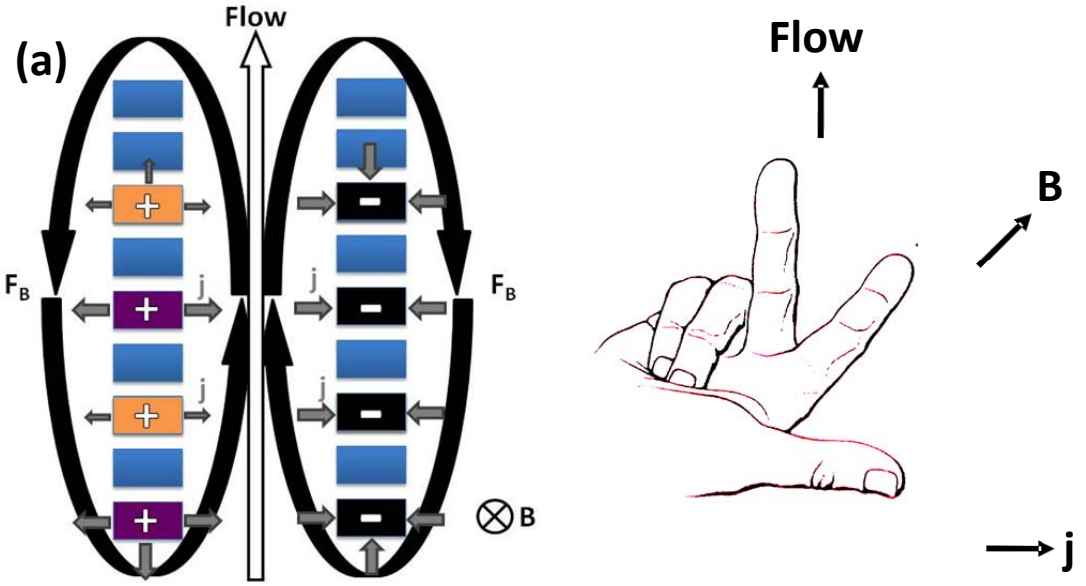

Figure 1. MHD Theory. The right hand rule dictates the direction of fluid flow between the anode and cathode electrode pairs through the array region on the microelectrode chip. The magnetic field (**B**) in this diagram points into the page. The ion flux (**j**) in this diagram points to the right between anode and cathode pairs. The resuting MHD force and consequent fluid flow (Flow) thus points upward. Other **j** vectors are shown in the array diagrams, pointing away from the anodes and toward the cathodes, resulting in the circular flow.

The polymer studies in this project were conducted with the sulfonated fluoropolymer, Nafion, and the redox species, hexamine ruthenium (II/III) chloride. Because of its negative charge, the cations in the Nafion are expected to undergo ion exchange with the $[Ru(NH_3)_6]^{3+/2+}$.[7,8] It is proposed that if the redox species can be tethered to the electrode by exchanging into the polymer film, it will be possible to conduct redox-MHD microfluidics without the redox species mixing and interfering with the surrounding sample fluid, which has been a concern about redox-MHD in the past. The ion current will be sustained with the aid of switching potential waveforms to sequentially activate sets of electrodes in the array, allowing previously activated sets to recover when the redox species deplete.

When a sufficient potential difference is applied between two electrodes in the presence of a redox species the anode will cause oxidation ($Ru(NH_3)^{2+} = Ru(NH_3)^{3+} + e^-$) and the cathode will cause reduction ($e^- + Ru(NH_3)^{3+} = Ru(NH_3)^{2+}$), creating a current to flow between the electrodes. This change in charge must be compensated for somehow. The surrounding

electrolyte or buffer solution should effectively provide the necessary ions for the ion current in solution. Other studies from our research laboratory have shown that ion current compensation from the electrolyte can indeed take place well into the bulk solution between the electrodes. These arguments and results suggest that it might only be necessary to place redox species at the electrodes (i.e. tethered) for oxidation and reduction, and therefore the redox species will not interfere with LOAC samples.

There are several anticipated challenges with a tethered redox species**.** First, appropriate redox-species and tethering chemistries must be identified. Second, the thin layer of tethered redox species will deplete in a short time period (estimated 220 ms for a 500 nm Nafion film). And third, a switching or potential waveform that allows recovery of redox species is needed.

For these reasons, this project focuses on the initial investigation of tethering redox species at electrode surfaces (results shown here for the sulfonated fluoropolymer Nafion in conjunction with the redox species ruthenium hexaamine chloride ($Ru(NH_3)_6Cl_3$ and $Ru(NH_3)_6Cl_2$)).[7] Also, it explores potential waveforms that should allow for the recovery of redox species. Initial studies are shown here with unmodified electrodes and redox species in solution for the same time period and approximate concentrations as expected for modified electrodes, varying electrode configuration, timing, potential waveform, and switching.

When studying the efficiency and effectiveness of LOAC devices that use fluid-flow cells, it is necessary to determine the optimal setup for high speed fluid flow. When the potential is stepped past the E_0 value in such a system, a transient fluid flow occurs immediately after the step but quickly deteriorates over time according the faradaic current flow (which decreases at $t^{1/2}$ as time progresses). It is also important to note that during fluid-flow experiments, the ideal situation is one in which the fluid movement remains swift for a desired period of time. Due to the shortness of time that the transient current occurs and complete depletion for a finite number of redox species at an electrode, we require a means of tuning fluid flow in spite of these two natural occurrences. Thus, this project proposes a sweep-step function that will utilize two separate sets of anode-cathode pairs of electrodes. One sweeps from 0.3 V (oxidation) to 0.0 V (re-establishing a 1:1 mole ratio of oxidized and reduced forms) and then steps to 0.3 V at different times (at the working electrode side of the pair) and for a number of cycles while the working electrode of a second set of electrodes is held at the oxidizing potential of 0.3 V.

Experimental Procedures

Chemicals and Materials. All chemicals were reagent grade and used as received. Aqueous solutions were prepared with high purity deionized water from Ricca Chemical Co. (Arlington, TX). Polystyrene latex microspheres (10 μm diameter, 2.5 wt % dispersion in water) and ruthenium (II) hexaamine chloride were purchased from Alfa Aesar (Ward Hill, MA). Potassium chloride was from VWR (West Chester, PA). Ultra high purity compressed argon gas was obtained from AirGas. Inc. (Radnor, PA). Potassium ferricyanide ($K_3Fe(CN)_6$) was purchased from EM Science (Gibbstown, NJ) and potassium ferrocyanide trihydrate ($K_4Fe(CN)_6 \cdot 3H_2O$) was purchased from Aldrich Chemical Co. (St. Louis, MO). Nafion perfluorinated ion-exchange-resin (5 wt% in a mixture of aliphatic alcohol and 45% H_2O) was purchased from Sigma Aldrich (St. Louis, MO).

Experimental Setup.

Configuration 1: For gold macroelectrodes. To characterize the gold macroelectrodes, a 3-electrode set up was established using a Ag/AgCl (saturated KCl) reference electrode and Pt wire counter electrode. The working electrode was a 1.3 cm × 1.3 cm gold macroelectrode chip secured in solution by an alligator clip. The area of the electrode immersed in the electrolyte was 1.3 cm x 0.6 cm. A solution of 0.1 M $Ru(NH_3)_6Cl_3$ (redox species) in a supporting electrolyte of 0.1 M KCl was freshly prepared prior to all experiments. A supporting electrolyte was used to minimize the influence of ion migration on the measured faradaic current, it is not electroactive in the potential range of interest, and it reduces the resistance to the point where electric fields in bulk solution are small. The CHI 760B potentiostat was used throughout these studies (CH Instruments, Austin, TX) to perform cyclic voltammetry (CV) and chronoamperometry (CA). All macroelectrodes were stored, covered, at room temperature prior to experimentation.

Using a Nafion perfluorinated ion-exchange resin, 5 wt% in a mixture of aliphatic alcohols and 45% H_2O (Sigma Aldrich, St. Louis, MO), gold macrochips (1.3 cm × 1.3 cm) were spin coated until completely covered by polymer. In order to ensure a uniform coating, the chip was covered with Nafion solution completely before the spin coating cycle was initiated. Macrochips were spin coated at 5 different RPM: 1000, 2500, 3500, 4000, and 6000. Thus, the macrochips with the thinnest coating of Nafion were those spun at the fastest RPM, 6000. Approximate thicknesses were measured with a Dektak 3030 and are reported in Table 1. The Nafion-coated macroelectrodes were cured for one hour at 80°C and allowed to sit in air, covered, at room temperature for two days before experiments.

Nafion Thickness on Macroelectrodes	
Speed of Spin Coating / RPM	Approximate Thickness / nm
1000	557
3500	371
4000	288
6000	183

Table 1. The measured thicknesses of the Nafion polymer on the gold macroelectrodes obtained with a Dektak 3030.

Configuration 2: For microelectrode array device. See Figure 2 for a schematic of the setup with the microelectrode array device. Figure 2a is a photograph of the 20-electrode microchip array device. Prior to MHD experiments, each of the 20 individually addressable electrodes were checked by characterization in a solution of 0.1 M KCl, 0.1 M $K_4Fe(CN)_6$, and 0.1 M $K_3Fe(CN)_6$. The characterization experiments utilized a 3-electrode setup was used with a gold pseudoreference separate from the array, and a counter electrode which was also separate from the array. Figure 3 shows an overlay of CV responses from one such characterization (Chip number CN13). For MHD experiments, a two-electrode configuration was used with the working electrode on one side of the array and the reference and counter leads shorted together on the opposite array. A CHI 1030A multipotentiostat was used to apply the potential waveforms throughout MHD experiments. A 760 μm polydimethylsiloxane (PDMS) gasket was placed on the microchip to hold the solution and define the size of the cell (14.0 mm x 6.0 mm). The experimental setup is depicted in Figure 2b.

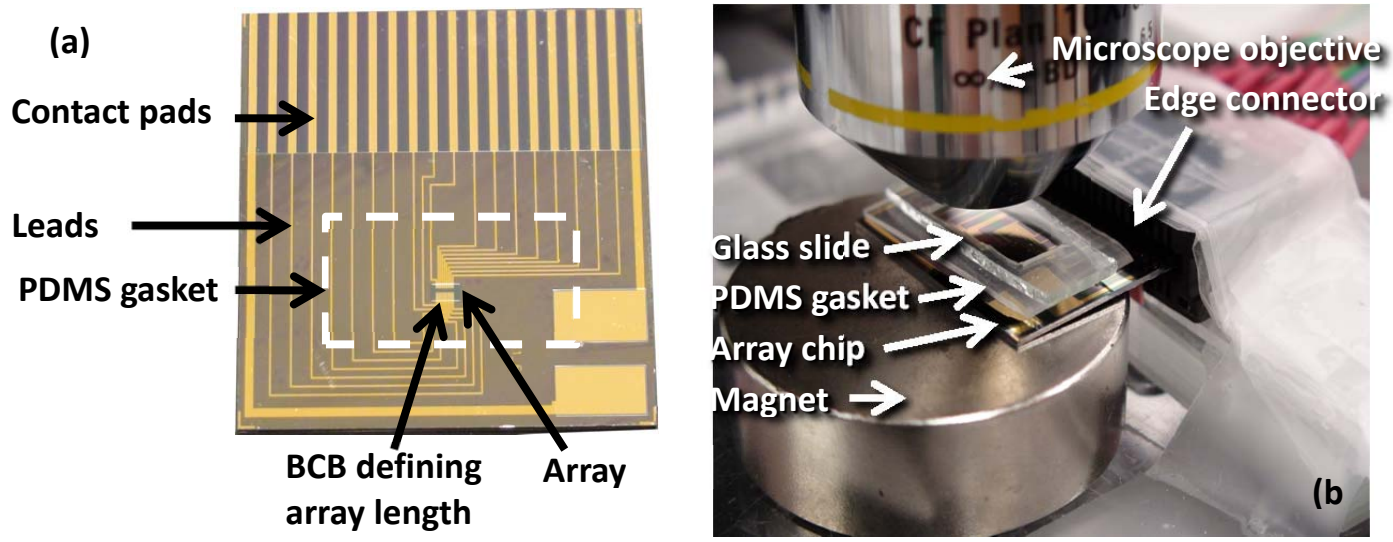

Figure 2. Schematic of experimental setup for microchip array redox-MHD experiments. (a) Photograph of microchip array device CN4. The dashed line traces the boundaries of the cutout in the PDMS gasket that contains solution (defining cell sidewalls). The magnet is not shown. **(b)** Photograph of experimental setup. The PDMS gasket used to define the experimental cell was 760 μm in height, with an inner region cut out (14.0 mm x 6.0 mm). The NdFeB permanent magnet exhibited an average magnetic field of 0.34 T, and was 1.5 inches in diameter and 0.5 inches in height.

Sweep-Step Redox-MHD studies. A CH Instruments 1030A multipotentiostat was used in the redox-MHD sweep-step studies. Working electrode 1 was swept from 0.3 V to 0 V at 1.36 V/s or 0.45 V/s and then held 0.3 V for 0.220 s. This sequence was repeated for 6 cycles. Working electrode 2 was held at a potential of 0.3 V for the entirety of the two-working electrode experiments. The counter and reference electrodes were shorted together opposite the working electrode, on the array region. The NdFeB permanent magnet used in these studies was 1.5" in diameter, 0.5" in height, was purchased from Amazing Magnets (Irvine, CA), and generates field of 0.34 T, which was measured with a DC Magnetometer. A Nikon Eclipse ME600P microscope was interfaced to a Sony Handycam digital camera (model no. HDR-XR500V; 30 frames per second with 1920 x 1080 pixels per frame) to record solution movement. Polystyrene latex microspheres (10-μm diameter) were used to visualize solution movement. A fresh redox species-bead mixture (0.04 vol of 2.5% bead solution : 1 vol redox solution) was used for each experiment. Bead speeds were tracked using particle imaging velocimetry (PIV) software (DynamicStudio v.3.00 software, Dantec Dynamics). The PIV software is able to take several sequential frames of video and create an average image (eliminating background noise) on which the speeds of moving beads are averaged and plotted. Video MPG files were converted to single images with 1 step (30 Hz) between each image. The images generated were then imported into the Dantec software and processed via the average correlation method. The speeds in Table 2 were obtained as an average of three separate experimental trials. Data was taken from the region on the array only between the active set(s) of working electrodes (see designated electrodes in Figures 6 and 8). Speeds occurred at 300 μm above the floor of the cell. The speeds reported for the sweep segments were taken as an average over the entire sweep.

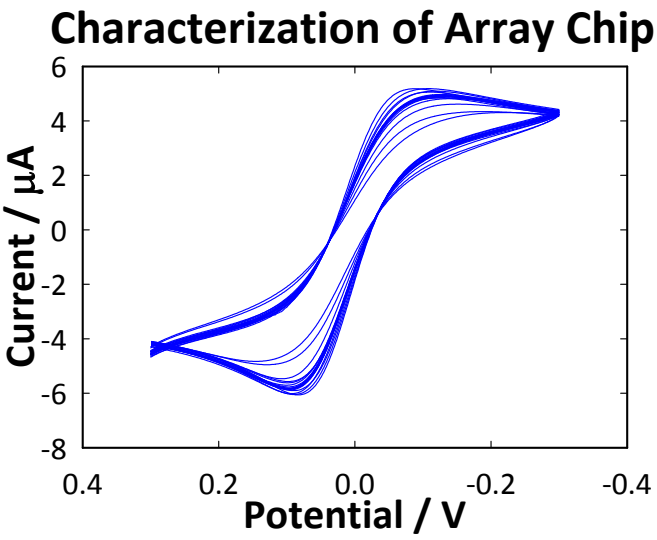

Figure 3. Cyclic Voltammograms of the Characterization of Microchip Array Device CN13 in redox solution of 0.1 M $K_4Fe(CN)_6$ and $K_3Fe(CN)_6$ in 0.1 M KCl showing that the device is functional. This figure depicts the peak cathodic and anodic currents that occur at each of 18 individually addressable electrodes in the potential window 0.3 V to -0.3 V at 0.05 V/s, sweeping toward the negative potential. On the forward sweep (i_{pf}) the $Ru(NH_3)_6Cl^{3+}$ is reduced. On the reverse peak (i_{pr}) $Ru(NH_3)_6Cl^{2+}$ is oxidized. Cathodic and anodic peaks behave similarly for electrodes 2 through 19 on the microelectrode array chip (CN13). E° ≈ 0.0 V vs. on-chip gold pseudo-reference electrode. The counter electrode was on-chip but also separate from the array.

Results and Discussion

With experimental configuration 1 (for gold macroelectrodes) and subsequent experiments, the electrochemistry for each of five different Nafion polymer thicknesses was compared using redox species "loading" experiments. Results showed that the thicker films produced more reproducible interactions with $[Ru(NH_3)_6]^{3+/2+}$ solution. Table 1 shows the five speeds at which Nafion polymer was spin coated in addition to corresponding measured thicknesses. Figure 4 illustrates one such "loading" experiment using a gold macrochip that was coated with Nafion at 2500 RPM (Nafion thickness at this speed was not measured). The overlay of CV responses in Figure 4 shows the behavior of a Nafion film in three sequential experiments: (1) the expected background current in 0.1 M KCl electrolyte alone before loading, (2) diffusion-limited current from redox species in solution during loading, and (3) expected shift in $E_{1/2}$ due to stabilization of oxidized form loaded in negatively-charged Nafion. Because of this shift, we see that there are electrostatic interactions between the Nafion polymer and the postively charged redox species, $Ru(NH_3)_6^{3+}$.

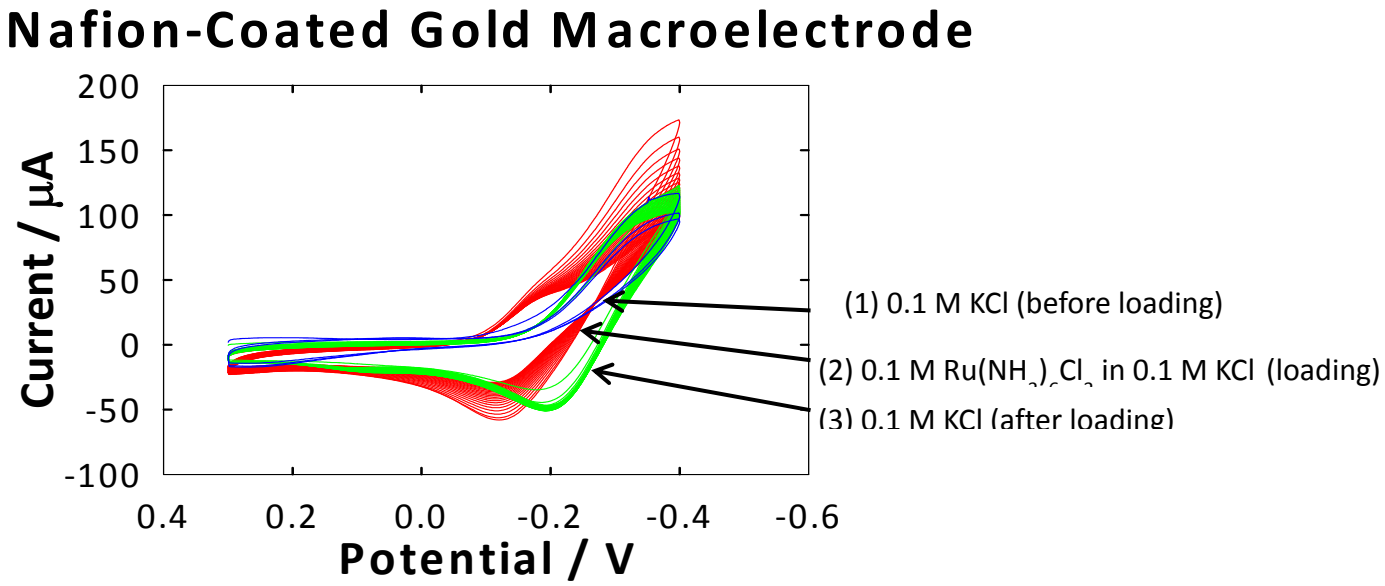

Figure 4. Nafion-Coated Gold Macroelectrode studies. This overlay of CV responses shows the expected behavior of a Nafion film in three sequential experiments.

As can be seen in Figure 4, the 0.1 M KCl (the supporting electrolyte in the $Ru(NH_3)_6Cl_3$ solution) is negligible. There is a peak that occurs from approximately -0.3 V to -0.4 V, but this is due to the reduction of oxygen in solution. Preliminary studies with the redox-polymer combination shown here indicate that the combination does exhibit tethering to the electrode surface, thus it is promising for decreasing interference in redox-MHD future studies. More work needs to be done in determining the best redox-modfied electrodes suitable for redox-MHD microfluidics.

These polymer studies, however, segued to the investigation of tuning fluid flow and redox species replenishment at the electrode array region, again using the array chip depicted in Figure 2a in the experimental setup depicted in Figure 2b. To this end, a series of studies were performed in solution containing redox species using different potential waveforms. Two waveform combinations were utilized, one for short sweep-step studies (Figure 5) and another for long sweep-step studies (Figure 7). Images obtained using PIV analysis of videos (Figures 6 and 8) allowed for the comparison of bead speeds for control experiments and for experiments utilizing one and two pairs of active electrodes, separately.

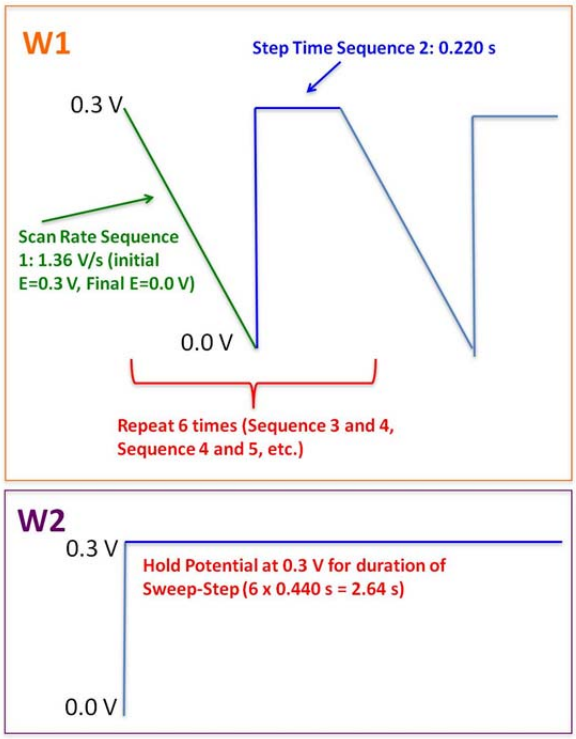

Figure 5. Waveform Diagram for Short Sweep-Step Studies.

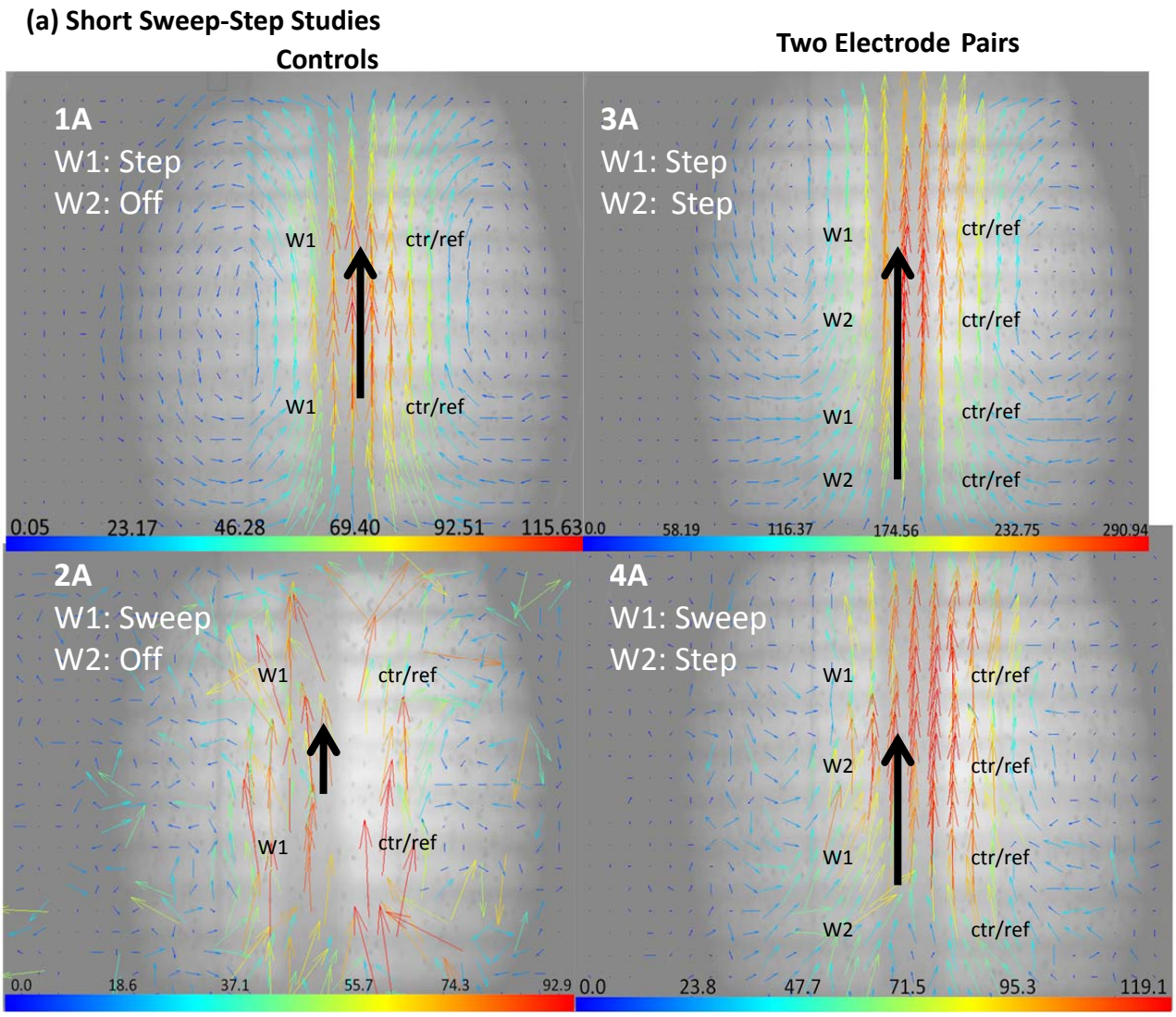

Figure 6. PIV Analyses for Short Sweep-Step Studies. During these experiments, the sweep across potential window 0.3 V to 0.0 V (towards more negative potentials) was programmed to last 0.220 s at 1.36 V/s for 6 sequential cycles. The large dark arrows were overlayed to represent the net fluid flow in the region between active electrodes. Speeds (Table 2) from greatest to least were measured: 3A>1A, 4A>2A.

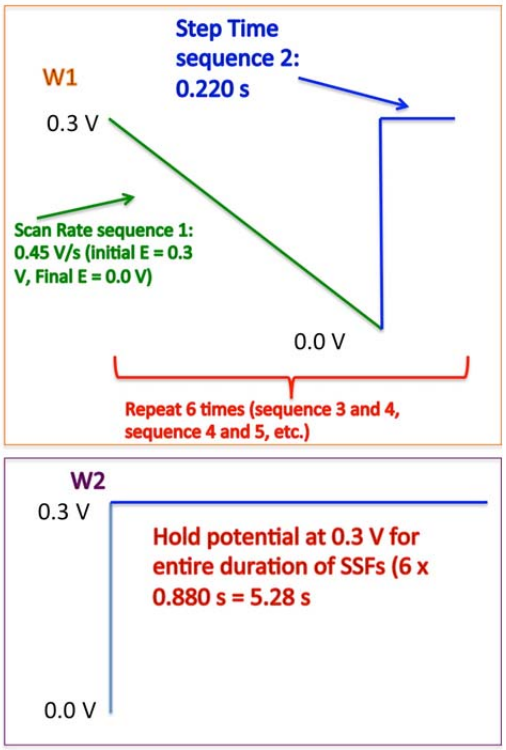

Figure 7. Waveform Diagram for Long Sweep-Step Studies.

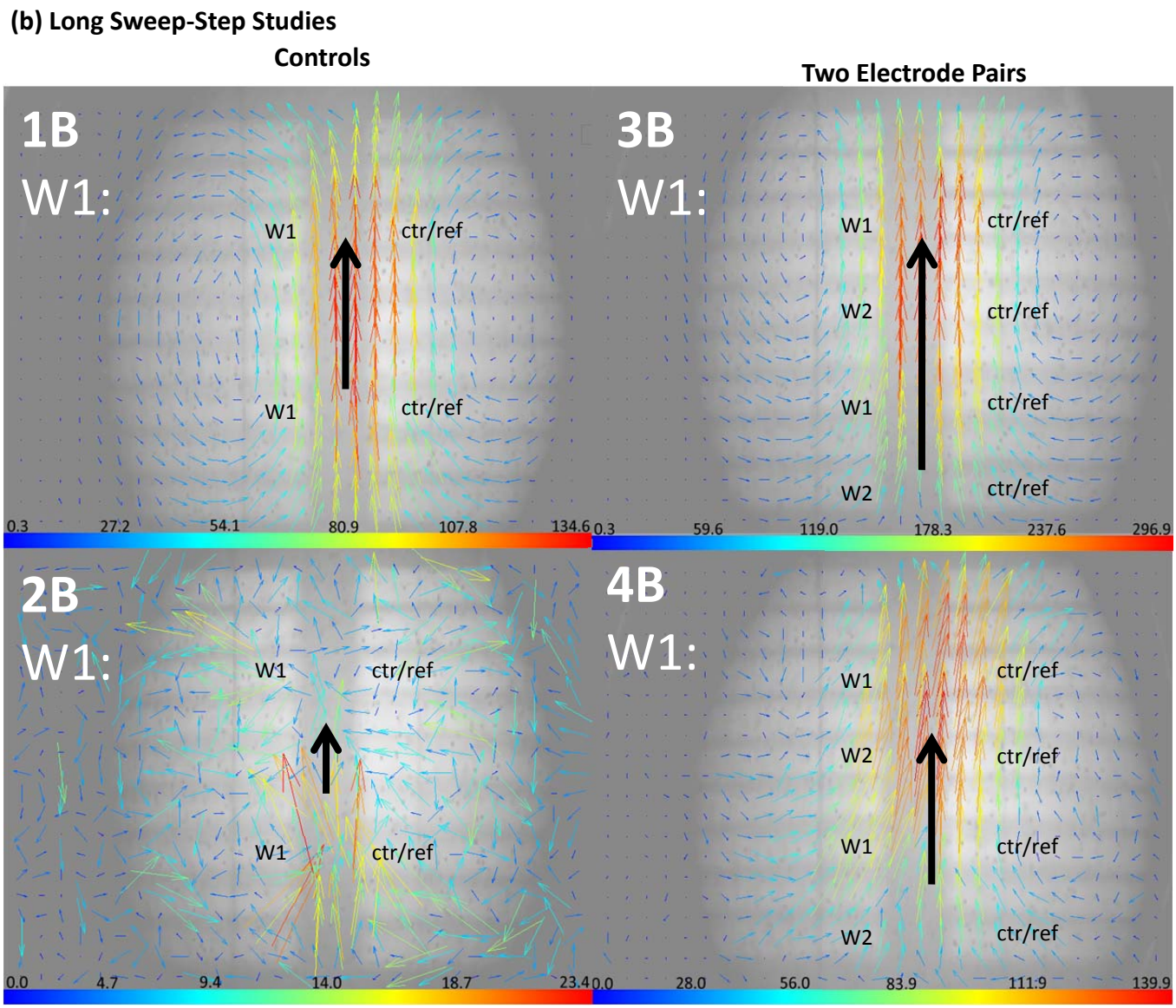

Figure 8. Long Sweep-Step Studies. The working electrode is opposite a counter electrode shorted to the reference electrode, all on the array region. During these experiments, the sweep across potential window 0.3 V to 0.0 V (towards more negative potentials) was programmed to last 0.660 s at 0.45 V/s for 6 sequential cycles. The large dark arrows were overlayed to represent the region between active electrodes. Speeds (Table 2) from greatest to least were measured: 3B>1B, 4B>2B.

PIV analysis of the control experiments, which employed only one working electrode pair (with the counter electrode and reference electrode shorted together on the opposite array as indicated) are shown in Figures 6 and 8 (1A, 2A, 1B, and 2B). Speeds are reported in Table 2. The average bead speed was measured from the region of the array only between active electrodes and at a height of 300 µm from the floor of the cell. During the step part of the cycle (1A and 1B), fluid flow occurs between active electrodes in a fairly flat flow profile. For the sweep part of the cycle (2A and 2B), the beads slow to a stop when going from +0.3 V to 0.0 V. This was expected because the current is lower during the slower sweep. Then, at 0.0 V, a 1:1

mole ratio of oxidized-to-reduced forms is produced (E = E°) and that is the starting composition of the solution, thus no net current is generated. Without any current, $|\mathbf{j}| = 0$ and therefore $|\mathbf{F_B}| = 0$ and velocity of the fluid is zero.

In experiments utilizing two sets of electrode pairs (3A and 3B), the combined step produces twice the fluid speed of that for a single set of paired electrodes in the control experiments. This was expected to occur with twice the active electrodes and twice the current and with reinforcing flow enhancement. When the W1 electrode set begins its sweep (4A and 4B), the fluid slows to half the speed but continues to flow, because the W2 set of electrodes continues to produce a current at the 0.3 V potential step, as expected.

Bead Speed During Sweep-Step Studies	
Experiment	*Speed* / μm·s^{-1}*
1A	113.1 ± 19.8
2A	41.3 ± 20.0
3A	232.3 ± 19.9
4A	105.3 ± 21.5
1B	120.6 ± 1.6
2B	14.3 ± 7.1
3B	234.0 ± 18.7
4B	108.8 ± 20.8

Table 2. Bead Speeds for Sweep-Step Studies (corresponding to experiments labeled in Figure 6 and 8). The bead speeds occurred as predicted. Fluid flow was greater during sweep-step experiments with the second working electrode held at a potential than during sweep-step experiments with a second electrode at open circuit. *Speeds are averages calculated from three experimental trials, each from Cycle 1.

Thus, it is observed that fluid continues to flow while alternating electrodes are swept to recover redox species. In addition to increasing the time that the species has to replenish, a longer sweep time allows more electrode sets to be included with sweep-step functions that are out of phase with each other to ensure continuous fluid flow over long times. When future studies include more functions out of phase with one another, different instrumentation must be used. A diagram of the ideal waveform sequence has been drawn in Figure 9. Again, this setup will allow electrodes the be stepped while others are sweeping to allow for continuous replenishment of species.

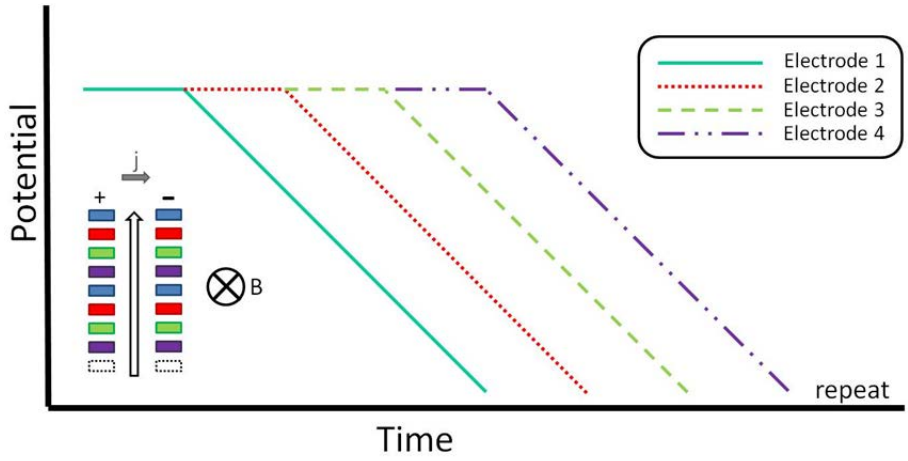

Figure 9. Waveform diagram intended for future studies with a different instrument.

Conclusions

The sweep-step studies investigated here show that fluid flow is increased by twofold as the number of electrode pairs is doubled. This suggests that the maximum velocity can be tuned to a specific application by increasing or decreasing the number of electrode pairs that are activated simultaneously. The current during a sweep decreases with time, and likewise beads slow to a stop as the sweep progresses in both the short and long sweep studies. Thus, the working electrodes that are sweeping decrease their contribution to the overall fluid flow. As long as other electrode pairs are activated with a step, fluid continues to flow, but at a lower velocity.

If new electrode pairs are stepped to oxidizing potentials only when old electrode pairs begin their sweep-recovery cycle, then the fluid should achieve a fairly constant velocity with small pulses at the switching times. However, this kind of switching will require modification and reprogramming of existing instrumentation. In the future, we hope to be able to create waveforms such as the one pictured in Figure 9, where cycles are performed on multiple pairs of electrodes, out of phase with one another, allowing for continued pumping of fluid at some electrodes while replenishment of redox species occurs at others. The cycles will be repeated such that fluid flow is sustained over long periods of time. Also in the future, work needs to be done to tether redox species to electrodes. There was not enough time to investigate the Nafion/$Ru(NH_3)_6^{3+/2+}$ system thoroughly. Many other possible systems are reported in the literature. However, the most optimized conditions will be those where redox species are covalently attached to avoid loss into surrounding fluid, films are as thin as possible to maximize electron transfer and diffusion rates (e.g. monolayer), and redox concentrations are high to minimize frequency of recovery cycles.

Acknowledgements

The National Science Foundation is acknowledged for financial support through grant CHE-0719097 and a REU through grant NSF CHE-0851505/REU. Support has also been provided in part by the Arkansas Biosciences Institute, the major research component of the Arkansas Tobacco Settlement Proceeds Act of 2000. Special thanks go to Ingrid Fritsch, Christena Nash, and the Fritsch Research Group.

References

(1) M. C. Weston; M. D. Gerner; I. Fritsch, “Magnetic Fields for Fluid Motion.” Anal. Chem. **2010**, *82*, 3411-3418

(2) S. Qian; H. H. Bau, “Magneto-hydrodynamics based microfluidics.” Mech. Res. Commun. **2009**, *36*, 10-21.

(3) E. C. Anderson; I. Fritsch (2006). "Factors Influencing Redox Magnetohydrodynamic-Induced Convection for Enhancement of Stripping Analysis." Analytical Chemistry **78**: 3745-3751.

(4) E. C. Anderson; M. C. Weston; et al. (2010). "Investigations of Redox Magnetohydrodynamic Fluid Flow at Microelectrode Arrays Using Microbeads." Analytical Chemistry **82**(7): 2643-2651.

(5) M. C. Weston, E. C. Anderson, et al. (2006). "Redox magnetohydrodynamic enhancement of stripping voltammetry: toward portable analysis using disposable electrodes, permanent magnets, and small volumes." The Analyst **131**: 1322-1331.
(6) Weston, M. C., C. K. Nash, et al. (2010). "Redox-Magnetohydrodynamic Microfluidics Without Channels and Compatible with Electrochemical Detection Under Immunoassay Conditions." Analytical Chemistry.
(7) Buttry, D. A. and F. C. Anson (1983). "Effects of Electron Exchange and Single-File Diffusion on Charge Propagation in Nafion Films Containing Redox Couples." Journal of the American Chemical Society **105**(4): 685-689.
(8) Szentirmay, M. N. and C. R. Martin (1984). "Ion-Exchange Selectivity of Nafion Films on Electrode Surfaces." Analytical Chemistry **56**(11): 1898-1902.

Chemical Synthesis of Pd_xFe_y-Pt Nanoparticles as Electrocatalysts

Jonathan Janzen, Northeastern State University
Tahlequah, Oklahoma

Abstract

Platinum (Pt) catalysts used in fuel cells are in need of much improvement, especially regarding the oxidation reduction reaction (ORR) on the cathode side of the fuel cell. An approach designed to reduce the amount of Pt used and enhance the catalytic ability of the catalysts is described, using a core-shell structure with a palladium-iron alloy as a core and Pt as the shell. Nanoparticles made of mainly Pd with trace amount of Fe were synthesized using combination of thermal decomposition and reduction in the presence of different capping ligands. The initial attempt to make core-shell structures is unsuccessful due to the self-nucleation of Pt.

Introduction

The fuel cell has become the object of much interest due to its ability to convert chemical energy directly into electricity. In the fuel cell, fuel is separated from oxygen by an electrolyte membrane. At the anode of the fuel cell, fuel is oxidized as it comes in contact with a catalyst ($H_2 \rightarrow 2H^+ + 2e^-$). The proton travels across the electrolyte membrane while the electrons travel through an external circuit. At the cathode side, the oxygen reduction reaction (ORR) takes place. Oxygen reacts with the electrons and protons, forming water ($½O_2 + 2e^- + 2H^+ \rightarrow H_2O$). The catalysts for these reactions are generally Platinum (Pt), Pt-based alloys, or carbon-supported catalysts (Pt/C). The catalyst at the anode can have low Pt amounts without performance loss[1]; however, slower kinetics at the cathode requires the use of much more platinum[2]. This is an issue because of the rarity and the cost of Pt. The problem is that OH tends to adsorb strongly to the catalyst, blocking the oxygen from reaching it[3].

There are several ways to overcome this problem. The surface of a catalyst is what catalyzes a reaction, and the different facets of a crystal catalyst have different catalytic abilities. The ORR of a Pt octahedron enclosed by {111} is higher than cube enclosed by {100}[3,4,5]. The reason is the OH adsorption on the crystal surface on the {111} plane is less than on the {100} plane, allowing more oxygen to access the surface of the catalyst[3]. Also, alloying Pt with 3d-transition metals (e.g. Fe, Ni, or Co) amplifies catalytic ability due to electron coupling[2,5]. Noble metals, such as gold, silver and palladium, can enhance the ORR activity by balancing the strength of adsorption of O and OH. A Pt/Pd alloy is expected to have a very high ORR activity[6]. To reduce the amount of Pt used, a core-shell structure can be a potential solution, where only the surface of the nanocrystal consists of Pt. In this work, attempts were made to synthesize core materials made of Pd_xFe_y, following by addition of Pt to the core.

Experimental Sections

Chemicals. Palladium (II) acetylacetonate ($Pd(acac)_2$, Pd 34.7%), platinum (II) acetylacetonate ($Pt(acac)_2$ Pt 48.0%), potassium tetrachloroplatinate (II) (K_2PtCl_4, 99.9%, Pt 46.0%), iron (II) chloride tetrahydrate ($FeCl_2 \cdot 4H_2O$, 99%), iron (II) stearate ($Fe(St)_2$, Fe 9%), stearic acid (HSt, 90%), tetramethylammonium hydroxide (TMAOH, 25% w/w in methanol), iron (III) chloride

hexahydrate ($FeCl_3 \cdot 6H_2O$, 97-102%), oleic acid (OA, 90%), 1-octadecene (ODE, 90%), and iron pentacarbonyl ($Fe(CO)_5$,99.99%) were purchased from Alfa Aesar. Iron (III) acetylacetonate ($Fe(acac)_3$, 99+%) and tungsten hexacarbonyl ($W(CO)_6$, 99%) were purchased from Acros Organics. Oleylamine (OLA, 70%) was purchased from Aldrich. Tri-*n*-octylphosphine (TOP, 90%) was purchased from TCI America. All chemicals were used as received without further purification.

Synthesis Methods.

1. Synthesis of Iron (III) stearate. In a beaker, 5.0 mmol $FeCl_3 \cdot 6H_2O$ was added to 6.3 mL of methanol and stirred until dissolved. Then 15.0 mmol of HSt was added to the solution and methanol was added for a total of about 30 mL of methanol. The solution was then heated to boiling and all of the HSt was dissolved. Afterward, 15.0 mmol of TMAOH was added by slow squirting, and dark, red-brown clumps formed. The solution was kept at 30°C for 30 minutes to allow the reaction to complete. The gummy product was washed with boiling methanol in a Buchner funnel. The product was analyzed using an FT-IR and was washed until the peak at ~1740 cm^{-1} from the carbonyl in HSt was no longer visible.

2. Synthesis of sample 1. Into a three-neck flask, 0.05 mmol of $FeCl_2 \cdot 4H_2O$ and 0.05 mmol of $Pd(acac)_2$ were loaded with 6.0 mL of OLA. The flask was degassed to remove oxygen using a flow of argon for 10 minutes at room temperature (RT), and it was stirred vigorously for the remainder of the experiment. The temperature was then set to 130 °C. In a separate vial, 0.05 g of $W(CO)_6$ (~1.4 mmol) was added to 2.0 mL of OA and 2.0 mL of OLA and degassed under argon. Using heating, shaking and ultrasonication, the $W(CO)_6$ was dissolved in the vial forming a bright lime colored solution. When the three-neck flask reached 130 °C, the solution in the vial was injected into the flask via a glass syringe. The solution in the three-neck flask was then set to 240 °C and allowed to react for 20 minutes. The flask was removed from heat and allowed to cool to RT. The product was then washed twice using methanol, centrifuging at 4,000 RPM, and removing the supernatant. It was then washed four more times in a similar way using a small amount of toluene with the methanol.

3. Synthesis of sample 2. For this reaction, 0.05 mmol of $Fe(St)_2$ was used as the iron precursor instead of $FeCl_2 \cdot 4H_2O$, and the reaction at 240 °C went for 45 minutes. All other experimental conditions remained the same as the synthesis for Sample **1**.

4. Synthesis of sample 3. For this reaction, 0.05 mmol of $Fe(acac)_3$ was used as the iron precursor. All other experimental conditions remained the same as the synthesis for Sample **2**.

5. Synthesis of sample 4. For this reaction, 0.05 mmol of synthesized $Fe(St)_3$ was used as the iron precursor. All other experimental conditions remained the same as the synthesis for Sample **2**.

6. Synthesis of sample 5. In a three-neck flask, 0.05 mmol $Pd(acac)_2$ was added along with 2.0 mL of OA, 2.0 mL of OLA, and 4.0 mL of ODE. It was degassed under a flow of argon for 10 minutes. Then 1.0 mL of TOP was injected and the flask was degassed for 30 minutes. Following this, 0.4 mmol of $Fe(CO)_5$ in 1.0 mL of ODE was injected into the flask, and it was degassed for 30 minutes. The flask was set to 300 °C and reacted at that temperature for 30 minutes. It was then removed from heat and cooled to RT. The product was washed in a similar manner as described in the synthesis of Sample **1**.

7. Addition of Pt to sample 5. As-synthesized sample **5** was put in a three-neck flask with 4.0 mL of OLA and 4.0 mL of ODE. Then 0.05 mmol of K_2PtCl_4 was added. The flask was degassed under argon at RT for 30 minutes, then reacted at 100 °C for two hours. The reddish Pt precursor was still visible, so the flask temperature was increased to 200 °C and reacted for 90

minutes. As an alternative method, K_2PtCl_4 was added to 4.0 mL of OLA in a three-neck flask and stirred under argon at RT. Then it was slowly heated to 75 °C to attempt to dissolve it under vigorous stirring, and cooled to RT. Sample **5** was added to 4.0 mL of ODE and injected into the flask. It was subsequently raised to 160 °C for 1 hour. It was then washed in a similar manner as described in the synthesis for Sample **1**, except acetone was used instead of methanol.

Characterization Method. X-ray diffraction (XRD) patterns were collected using a Rigaku Miniflex II X-ray diffractometer equipped with a Cu Kα radiation source (λ = 1.5406 Å) operating at 30 kV/15 mA. Transmission electron microscope (TEM) images were taken on a Fei Titan 80-300 microscope with an accelerating voltage of 300 kV. Infrared spectra were obtained using a Bruker Tensor 27 FT-IR spectrometer.

Results and Discussion

The nanoparticles made of Pd and Fe were synthesized using various iron precursors in an organic solution of OLA and OA. Both can serve as capping ligands for nanocrystals, and OLA also serves as a reducing agent[5]. Figure 1 shows the TEM images of the nanocrystals prepared in samples **1**-**4**. The nanoparticles noticeably aggregated in a toluene solution and they were not very dispersed in the TEM images.

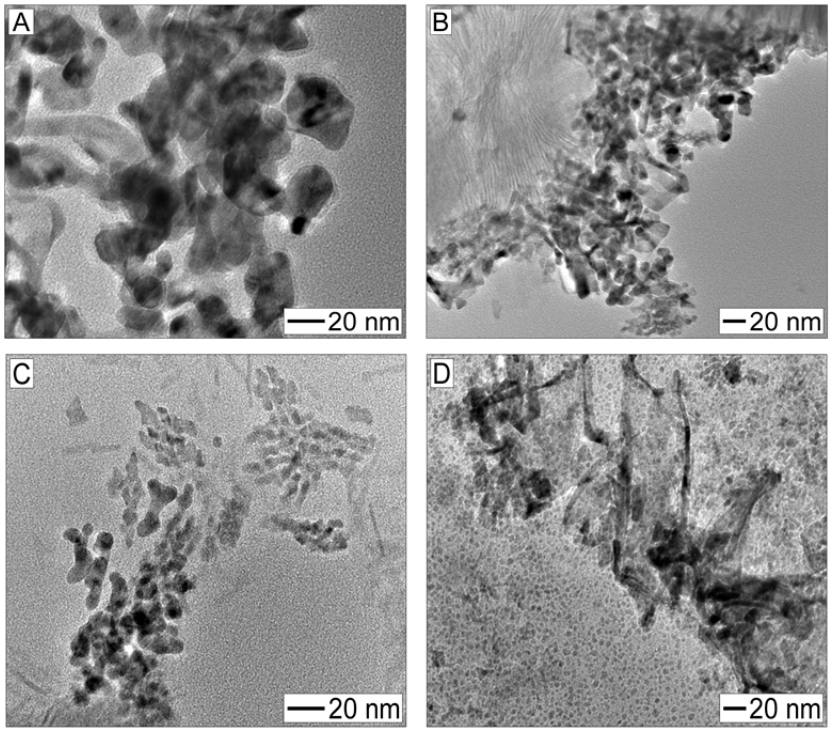

Figure 1. TEM images of nanocrystals made of Pd and Fe as synthsized from different iron precursors: (A) iron (II) chloride tetrahydrate, (B) iron (II) stearate, (C) iron (III) acetylacetonate, and (D) iron (III) stearate.

Figure 2 shows the XRD pattern of samples **1**-**4**. The first two samples look virtually the same, exhibiting peaks that are quite consistent with face-centered cubic (*fcc*) crystal structure, similar to Pd. The slight shift of the peak position is attributed to the composition of Fe (4%) in

the nanoparticles. The black vertical bars represent the relative position and peaks of that alloy. Samples **3** and **4** show a few other peaks that are not consistent with a Pd/Fe alloy. The peak at 23 degrees is indicative of an iron oxide, hematite (Fe_2O_3). The peaks around 30, 54, and 63 degrees are from other type of iron oxide, magnetite (Fe_3O_4). This result suggested that there are iron oxides present in the samples **3** and **4** in addition to the Pd/Fe alloy.

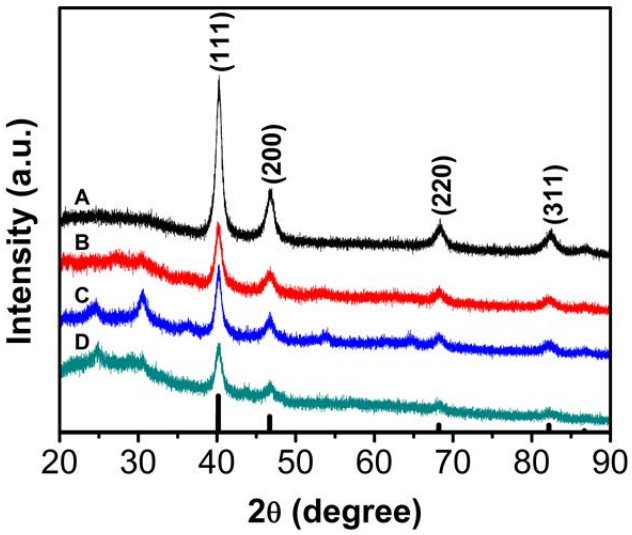

Figure 2. XRD patterns of palladium-iron nanoparticles prepared from different precursors: A) iron (II) chloride, B) iron (II) stearate, C) iron (III) acetylacetonate, and D) iron (III) stearate. The black vertical lines at the bottom show the relative standard peaks of $Pd_{0.96}Fe_{0.04}$.

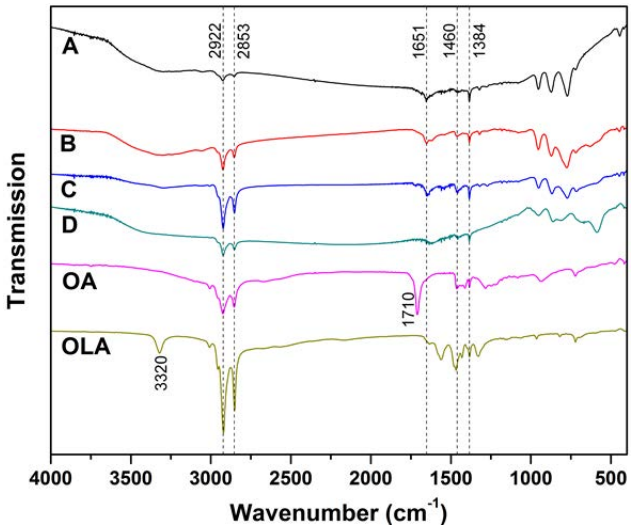

Figure 3. IR spectra of the ligands on the four samples compared with oleic acid (OA) and oleylamine (OLA). Samples were prepared using various iron precursors, A) iron (II) chloride, B) iron (II) stearate, C) iron (III) acetylacetonate, and D) iron (III) stearate. The chart on the right shows what functional groups are responsible for the different peaks.

Two possible capping agents were used in the synthesis of these nanoparticles. To determine whether OLA and/or OA were the actual capping ligand, the samples were analyzed using FT-IR. Figure 3 shows the IR spectra of samples **1** through **4**, along with OLA and OA as control. The peak assignments were listed in Table 1. The peaks at ~2853 and ~2922 cm^{-1} are due to the symmetric and asymmetric CH_2 stretching modes[7,8]. The peak at 1710 cm^{-1} for the OA is from the C=O stretching[8]. The peak at 1710 cm^{-1} is missing in the samples, while the peaks at ~1651 and ~1384 cm^{-1} are present in the samples. Both of these two peaks arise from the asymmetric and symmetric vibration of the metal carboxylate[7] which is typically in the range of 1650-1510 cm^{-1} and 1400-1280 cm^{-1}, respectively[9]. The peak at ~1460 cm^{-1} may also be due to the symmetric stretching of the carboxylate group[8]. This result implies that the nanoparticles in all samples were capped by OA. The peak at 3320 cm^{-1} for OLA is from –NH stretching which is also disappeared in all the samples possibly due to the amine group on the OLA bound to the surface of nanoparticles.

Table 1. IR peak assignment

Peak (cm^{-1})	Assignment
3320	NH stretch
2922	CH_2 asymmetric stretch
1710	CH_2 symmetric stretch
1651	C=O metal asymmetric stretch
1460	COO^- symmetric stretch
1384	COO^- metal symmetric stretch

The Pd/Fe nanoparticles were also synthesized using TOP as capping ligand. These nanoparticles were very uniform spheres which were used for Pt coating. The reactions were performed at high temperature and low temperature. Figure 4 shows the typical TEM images of the products. At high temperature, the reduction was very fast. As a result, the reduced Pt atoms were self-nucleated and formed large agglomerates. At low temperature, the reduction slowed down and fewer agglomerates were found in the production. However, in both cases, no Pt shell was deposited on the core particles. This is possibly due to two main reasons: 1) the hinderance of the capping ligand on the nanoparticles blocking the Pt atom diffusion onto their surfaces, and 2) the fast reduction kinetics promoting the self-nucleation of the Pt nanoparticles.

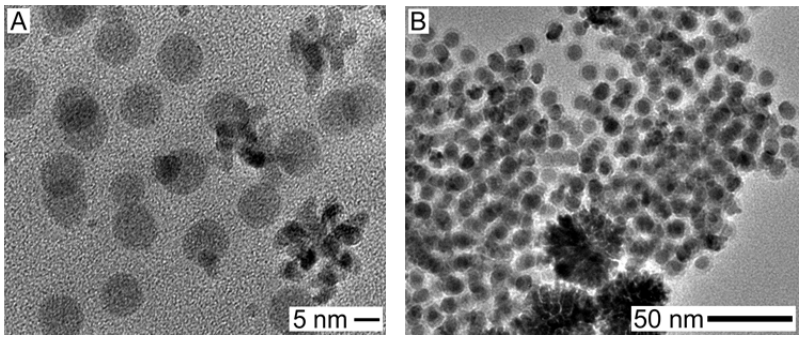

Figure 4. TEM images of Pd/Fe nanoparticles with the addition of Pt at two different conditions: (A) high temperature and (B) low temperature.

Conclusion

Nanoparticles made of Pd and Fe were synthesized in solution phase reaction with different capping ligands. The crystal structures were characterized by XRD. The products were dominated by Pd component. Depending on the types of Fe precursors, the final products may contain iron oxide impurities. The initial attempt to make core-shell structures is unsuccessful due to the self-nucleation of Pt. Future work includes optimization of the core morphology and composition, as well as control of the reaction kinetics for the Pt shell formation.

Acknowledgements

I would like to acknowledge the NSF CHE/REU 0851505. Also, I would like to thank Dr. Jingyi Chen for her mentorship and Shutang Chen for his help in this project.

References

(1) Gasteiger, H. A.; Panels, J.E.; Yan, S.G., Dependence of PEM Fuel Cell Performance on Catalyst Loading. *Journal of Power Sources* **2004,** *127,* 162-171.
(2) Gasteiger, H. A.; Kocha, S.S.; Sompalli, B.; Wagner. F.T., Activity Benchmarks and Requirements for Pt, Pt-alloy, and Non-Pt Oxygen Reduction Catalysts for PEMFCs. *Applied Catalysis B: Environmental* **2005,** *56,* 9-35.
(3) Markovic, N. M.; Ross, P. N., Surface Science Studies of Model Fuel Cell Electrocatalysts. *Surface Science Reports* **2002,** *45,* 117-229.
(4) Wu, J.; Zhang, J.; Peng, Z.; Yang, S.; Wagner, F. T.; Yang, H., Truncated Octahedral Pt_3Ni Oxygen Reduction Reaction Electrocatalysts. *Journal of the American Chemical Society* **2010,** *132,* 4984-4985.
(5) Zhang, J.; Yang, H.; Fang, J.; Zou, S., Synthesis and Oxygen Reduction Activity of Shape Controlled Pt_3Ni Nanopolyhedra. *NanoLetters* **2010,** *10,* 638-644.
(6) Ramírez-Caballero, G. E.; Ma, Y.; Callejas-Tovar, R.; Balbuena, P. B., Surface Segregation and Stability of Core-Shell Alloy Catalysts for Oxygen Reduction in Acid Medium. *Physical Chemistry Chemical Physics* **2010,** *12,* 2209-2218.
(7) Kishore, P. N. R.; Jeevanandam, P., Sythesis of Silver-Iron oxide Nanocomposites by Thermal Decomposition. *Journal of Nanoscience and Nanotechnology* **2011,** *11,* 3445-3453.
(8) Lewis, W. K.; Rosenberger, A. T.; Gord, J. R.; Crouse, C. A.; Harruff, B. A.; Fernando, K. A. S.; Smith, M. J.; Phelps, D. K.; Spowart, J. E.; Guliants, E. A.; Bunker, C. E., Multispectroscopic (FTIR, XPS, and TOFMS-TPD) Investigation of the Core–Shell Bonding in Sonochemically Prepared Aluminum Nanoparticles Capped with Oleic Acid. *Journal of Physical Chemistry C* **2010,** *114,* 6377-6380.
(9) Bronstein, L. M.; Huang, X.; Retrum, J.; Schmucker, A.; Pink, M.; Stein, B. D.; Dragnea, B., Influence of Iron Oleate Complex Structure on Iron Oxide Nanoparticle Formation. *Chemistry of Materials* **2007,** *19,* 3624-3632.

Digestive Enzyme Analysis of Rheb (Ras homolog enriched brain)

Ja'Qualane Scales, Philander Smith College
Little Rock, Arkansas

Abstract

Ras homolog enriched brain [Homo sapiens] is a gene consisting of 183 amino acids and a molecular weight of 20.7 kDa. It is a member of the GTPase superfamily and it encodes proteins that are bound to lipids in the cell membrane. Some of the major functions of this protein are cell proliferation, cell differentiation and regulation of growth due to its interaction with mTOR/S6K1/4E-BP1 signaling transduction pathway. The protein has GTPase capabilities and switches between a GDP-form and a GTP-form, which is made possible through phosphorylation, dephosphorylation, and farnesylation ("Rheb ras homolog," 2011). Protein farnesylation plays an essential role in the membrane and the interaction between most eukaryotic proteins. In addition, it is catalyzed by the enzyme farnesyltransferase (FTIs). Current research has brought attention to the biological affects farnesylation may have on cancer cells, actin cytoskeleton, and cell morphology (F., & CL, 2001). Proteolytic digestions with chymotrypsin and trypsin were used on Rheb-His6 and the number of fragmentations produced was compared.

Introduction

Rheb

Rheb binds and activates mTORC1, a metabolic regulator that is vital to cancer cells. Studies have shown that Rheb assists in different stages of cancer development through various tumor-induced mechanisms. These mechanisms may be contributed to late prognosis of patients with cancer overexpressing Rheb. However, there has not been enough sufficient research done to link Rheb with cancer pathogenesis (Lu, 2010).

mTOR/S6K1/4E-BP1

The signaling protein TOR (target of rapamycin; other common names in mammals are FRAP, RAFT, or RAPT) is classified in the superfamily of phosphatidylinositol kinase-related kinase and it controls cell growth and the cell cycle from yeast to flies to mammals. The mammalian target of rapamycin (mTOR) uses nutrients and mitogen signals to control the growth and division of cells. Rapamycin reduces the cells and mTOR keeps the cell from being reduced. Therefore, TOR signaling controls cell growth and cell size. Two signaling pathways that work in conjunction to control mRNA translation also have a dual role as downstream effectors of mTOR. These effectors are ribosomal protein S6 kinase 1 (S6K1) pathway and the eukaryotic translation initiation factor 4E (Eif4E)-binding protein 1 (4E-BP1 or PHAS-I)/eIF4E pathway (Fingar, 2003). Many researchers suggest that S6K1 plays a vital role in the S-phase of the cell cycle. On the other hand, 4EBP1/eIF4E does not have a critical role in the cell cycle progression but it is overexpressed in human tumors. S6K1 and eIF4E pathways function separately to increase cell size along mTOR and it promotes mTOR-dependent cell cycle progression coupled with cell growth during cell proliferation (Yu, Li, Xu, Li, & Guan, 2005).

Protein Purification

Protein purification isolates and breaks down large individual proteins into fragments that can be used to examine protein activity. Proteins can function as enzymes, signals, or receptors. In addition, they play a role in gene expression. Purification is a process that includes three stages: fractionation, purification, and polishing. Fractionation is a preparation step and the beginning of reduction steps. During fractionation, proteins are being separated using a centrifuge, microfilter system, or lysis buffer. The purification step continues to break down the protein and eliminates contaminants by using chromatography. The purpose of chromatography is to separate different cell constituents using chemicals. Polishing removes parts of the protein that is degrading and allows the protein to be preserved and stored over a period of time (Lohrey, 2010).

Digestive Enzymes

Enzymes are highly energized proteins that catalyze biological systems and determine chemical changes (Berg, Tymoczko, & Stryer, 2007). They are specific and bind to particular active sites. These protein molecules are required for the digestion of food, brain stimulation, and producing cellular energy. Digestive enzymes are found in the gastrointestinal tract and their purpose is to break down food so nutrients can be extracted and absorbed easily. Also, enzymes are present in raw foods and they aid in starting the digestion process, which lowers the amount of digestive enzymes secreted. When cooking at moderate to high temperatures, food enzymes get destroyed. However, if the body has to constantly rely on its own enzymes; more stress will be put on the biological system ("Digestive Enzymes").

There are numerous proteolytic enzymes that help break down proteins in the digestive system. Chymotrypsin is an example of a digestive enzyme that slices peptide bonds specifically on the carboxyl-terminal (C-terminal) side of the hydrophobic and aromatic amino acids, such as phenylalanine and methionine. In addition, chymotrypsin is an example of using covalent catalysis because the nucelophile becomes covalently attached to the substrates' unreactive carbonyl carbon. Trypsin is another amino acid that slices peptides on the C-terminal side of lysine and arginine amino acid deposits (Worthington, 2009).

Digestive enzymes are important because they work together as catalysts to aid in absorption and digestion. Enzymes are essential to the body because without them food would not be broken down and nutrients could not get absorbed and transported into the blood stream.

Experimental Procedures

Test Expression and Protein Purification

First, two 1L and one 250ml flasks of LB media were made and autoclaved for an hour [1L water: 25.0g LB media; 250ml water: 6.3g LB media]. Then, the flasks cooled down for 30 minutes. Next, 250µl of ampicillin was pipetted into the 250ml flask and 1ml of the Rheb-His6 protein was pipetted into the same flask. After, the flask was placed on a shaker (37^0C) overnight. The next day the O.D. was measured and the formula $[\frac{X}{1000ml} * O.D. = 0.05]$ was used to calculate how much protein should be used to inoculate the fresh LB media. Then, 1ml of ampicillin was pipetted into both 1L flasks. Next, both flasks were inoculated with the calculated amount of proteins and then placed on a shaker until the cells reached an O.D. between 0.6-0.8. After, a 120µl aliquot (add 20µl 8M urea and 40µl 4xSDS Loading Dye) was taken and labeled (R_{ui}). Then, 400ml of the protein was taken from one of the 1L flasks and

placed in an eppendorf tube. The tube was balanced and spun on maximum in an eppendorf microfuge for 15 minutes. Next, the supernatant was poured into the biohazard trash bin with only the pellet left in the eppendorf tube. The pellet was resuspended in urea (120µl) and 40µl of loading dye was added. Then, the eppendorf tube was placed in the VWR incubator for 2 minutes at 90^0C. Next, the eppendorf tube was labeled (R_i) and stored at -80^0C. Later, 200µl of IPTG was placed in both 1L flasks and incubated at room temperature for 4-5 hours. Next, the cells from the two 1L flasks were poured into 6 centrifuge bottles and balanced. Then, the cells were centrifuged (6500rpm, 15mins, 4^0C). After, the supernatant was discarded and the pellets were left in the bottles. Next, the cells were resuspended in Binding Buffer for PBS-Ni^{2+} - Affinity Purification. 40ml of the buffer was poured into a beaker and 5ml of the buffer was pipetted into each of the 6 bottles. Then, the cells were poured into a 50ml tube, balanced, and centrifuged (Jouan centrifuge) for 15 minutes. After, the supernatant was discarded and the pellets were placed in a -80^0C freezer (not necessary if continuing the procedure). Later, fresh lysis buffer was made and placed on ice, while the cells unthawed on top of the ice for an hour. Next, the cells were resuspended in fresh lysis buffer. Then, the cells were sonicated 5 times for 20 seconds with 1 minute intervals while still in ice. After, the lysate was incubated on ice for 30 minutes. During the incubation period, the FPLC was cleaned. Next, a small scoop of DNAse was added to the lysate and incubated for 15 minutes at room temperature. Then, the lysate was poured into a tube, balanced, and centrifuged (19500rpm, 15 minutes, 4^0C). After, the supernatant and pellet were filtered. Next, an aliquot of the supernatant and the pellet was taken [small scoop of supernatant (R_L=Rheb lysate); pellet+60µl of 8M urea (R_p=Rheb pellet); added 40µl of 4 x Loading Dye to each]. After, the lysate ran over Ni^{2+}-Affinity Column on the FPLC. Next, an aliquot of the flow through (R_{FT}) and Pool Fractions (R_{pool}) were taken. The aliquots were placed in a freezer at -80^0C and the sample was placed in a tube and refrigerated. Later, a 15% SDS gel was loaded and ran (200V, 65mA, 60mins). Then, a dialysis of pure Rheb was done in 1xPBS-Buffer+0.010M $MgCl_2$ x 6 H_20 overnight at 4^0C (MWCO Dialysis Bag=6000-8000 kDa). Later, the protein content was determined. Then, the protein was concentrated and an aliquot was taken.

Digestive Enzyme Assay

First, 2mg/ml of chymotrypsin was made. Then, 7 eppendorf tubes were labeled (0 minutes, 1 minute, 5 minutes, 10 minutes, 20 minutes, 30 minutes., 60 minutes). Next, chymotrypsin to Rheb-His6 concentrations (1:10 ratio) was calculated for incubation. Then, an aliquot of Rheb and chymotrypsin (30µl of Rheb and 30µl of chymotrypsin; 10µl of 4 x loading dye in each) was taken and frozen immediately. After, 500µl of Rheb and 970µl of chymotrypsin were incubated at room temperature in a water bath for 5 minutes. Next, the calculated amount of chymotrypsin to Rheb sample was made and then the extra chymotrypsin was frozen immediately. Then, the Rheb/Chymotrypsin sample was incubated in time intervals of 0 minutes, 1 minute, 5 minutes, 10 minutes, 20 minutes, 30 minutes, and 60 minutes. After each time interval was reached, 30 µl of the sample was placed into the desired eppendorf tube. Then, 10 µl of the 4 x loading dye was added and the eppendorf tube was placed in liquid nitrogen. Lastly, a 15% SDS gel was made and ran. The process was repeated using trypsin.

Results and Discussion

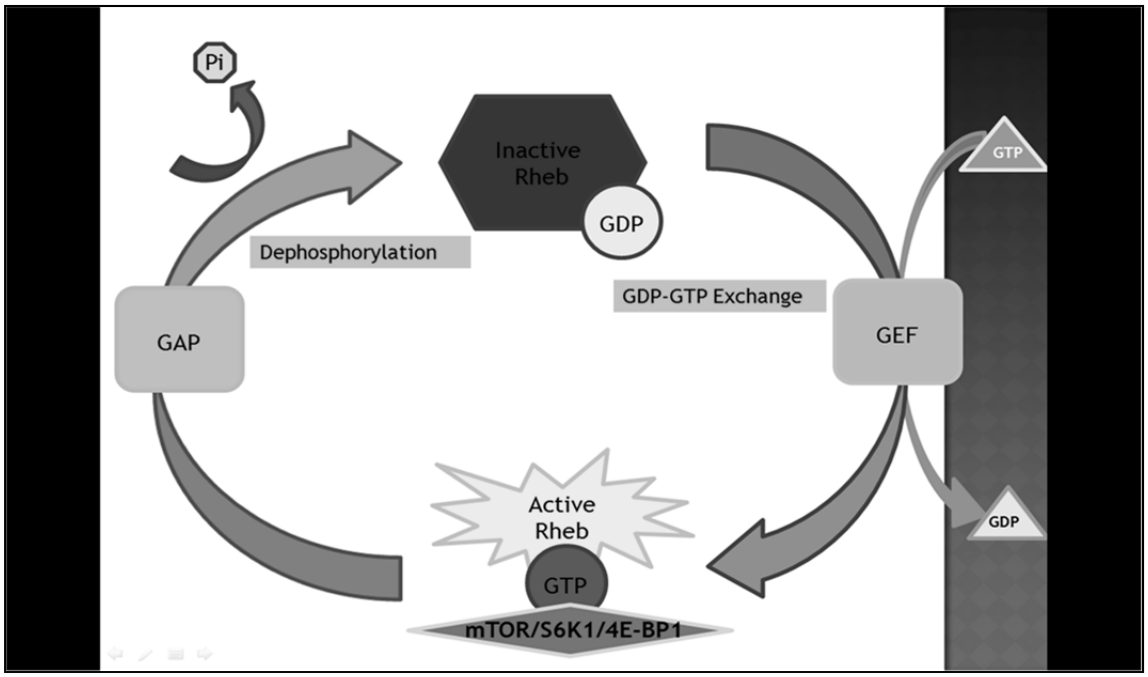

Figure 1: Rheb GTPase Cycle in cell-cycle regulation

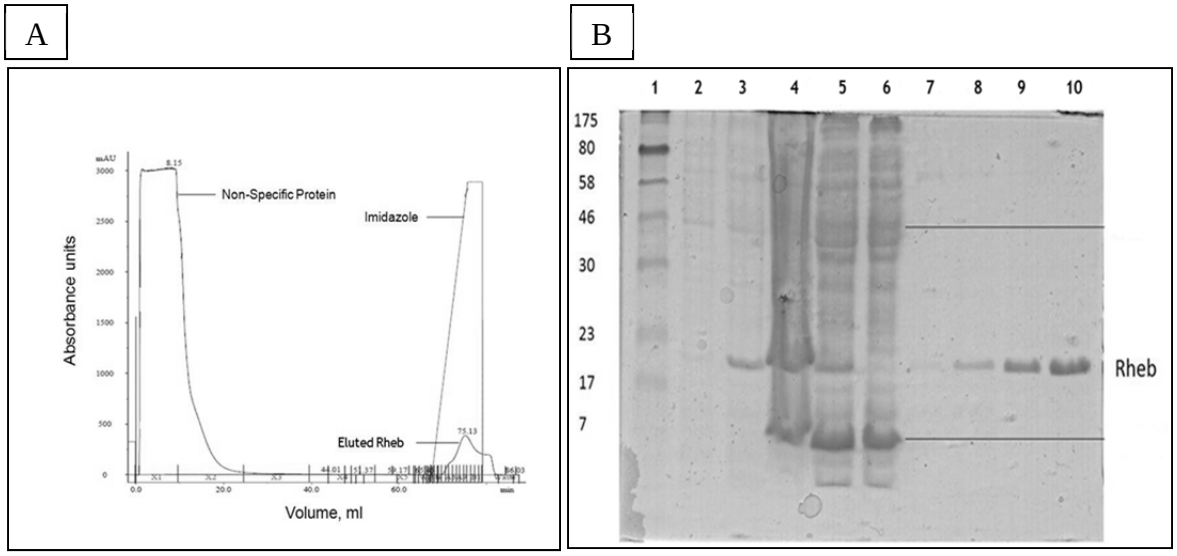

Figure 2. **Purification of Rheb-His6 protein**. **A**, chromatogram from the purification of Rheb-His6; **B**, 15% SDS-GEL analysis of fractions from the purification of Rheb-His6. Lane 1, molecular weight marker (kDa); lane 2, uninduced Rheb; lane 3, induced Rheb; lane 4, protein pellet; lane 5, supernatant; lane 6, flow-through fraction; lane 7-10 eluted protein.

Figure 3. **Chymotrypsin.** Gel electrophoresis of chymotrypsin assay. Lane 1, molecular weight maker (kDa). Lane 2, Rheb. Lane 3, Chymotrypsin. Lane 4, 0 minutes. Lane 5, 1 minute. Lane 6, 5 minutes. Lane 7, 10 minutes. Lane 8, 20 minutes. Lane 9, 30 minutes. Lane 10, 60 minutes.

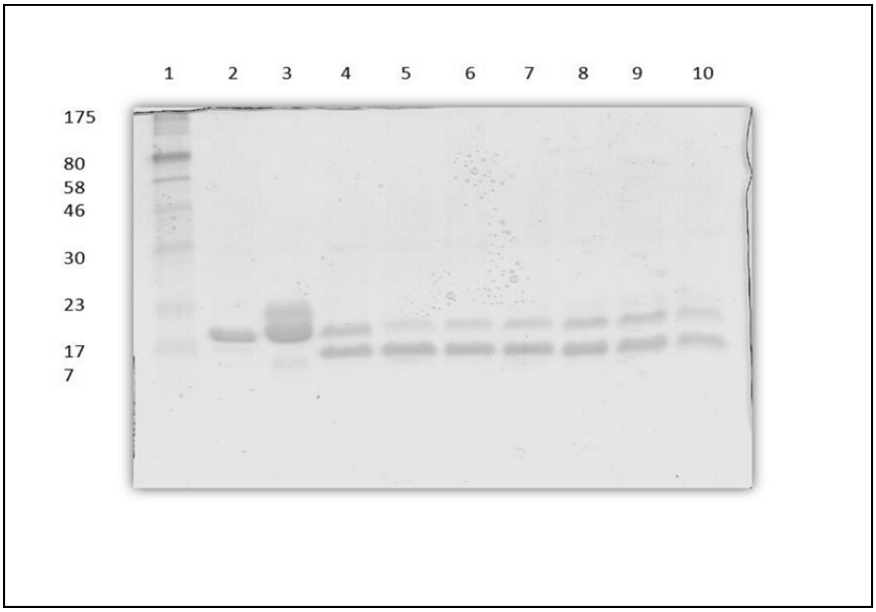

Figure 4. **Trypsin.** Gel electrophoresis of trypsin assay. Lane 1, molecular weight maker (kDa). Lane 2, Rheb. Lane 3, Trypsin. Lane 4, 0 minutes. Lane 5, 1 minute. Lane 6, 5 minutes. Lane 7, 10 minutes. Lane 8, 20 minutes. Lane 9, 30 minutes. Lane 10, 60 minutes.

The digestive enzyme assay was repeated three times to gain better results. Of the four assays, one produced quality results. According to the chymotrypsin SDS-Gel, Rheb was completely digested at zero minutes. However, the trypsin SDS-GEL showed evidence of some fragmentation, even though the intensities of the Rheb bands were not significantly different. Overall, these results show that the ratio of chymotrypsin to Rheb was too low and the incubation period for the trypsin to Rheb sample should be extended to produce more fragments.

Conclusion

The objective of this project was completed but more research is needed to understand the affects chymotrypsin and trypsin has on Rheb. Also, a minor change in the methodology is suggested to produce better results. However, future research studies will be targeted towards analyzing protein patterns and protein interactions; labeling small fragments of the protein that have been cleaved by digestive enzymes; and using fluorescent dye as a control to compare the number of fragmentations produced by each enzyme.

Acknowledgements

This publication was made possible by the National Science Foundation CHE-0851505/REU and NIH & ABI Grant to P.D.A.

I would like to thank my mentor, Dr. Paul Adams, program directors, Dr. David Paul and Dr. Julie Stenken, staff REU coordinator, Mrs. Leslie Johnson, research assistants, Christian Hundshammer and Dr. Reena Chandrashekar, Kyla Morris, Seth Haynes, and Edward Evans.

References

1. Berg, Jj., Tymoczko, J., & Stryer, L. (2007). *Biochemistry*. New York City: W.H. Freeman and Company.
2. Digestive enzymes. (n.d.). *Yourbodycanheal.com*, Retrieved from http://www.yourbodycanheal.com/enzymes.html
3. F., T., & CL, G. (2001). Protein farnesylation in mammalian cells: effects of farnesyltransferase inhibitors on cancer cells. *PubMed.gov*, Retrieved from http://www.ncbi.nlm.nih.gov/pubmed/11706990
4. Fingar, D. (2003). mtor controls cell cycle progression through its cell growth effectors s6k1 and 4e-bp1/eukaryotic translation initiation factor 4e.*Molecular and Cellular Biology*, *24*(1),
5. Lohrey, J. (2010, November 10). *What is protein purification?* Retrieved from http://www.livestrong.com/article/303147-what-is-protein-purification/
6. Lu, Zhi. (2010). Mammalian target of rapamycin activator rheb is frequently overexpressed in human carcinomas and is critical and sufficient for skin epithelial carcinogenesis. *Cancer Research*, Retrieved from http://m.cancerres.aacrjournals.org/content/70/8/3287.abstract
7. Nomanbhoy, T. K., Leonard, D. A., & Manor, D. (1996). Biochemistry. *Investigation of the GTP-Binding/GTPase Cycle of Cdc42Hs Using Extrinsic* , 4602-4608.
8. Rheb ras homolog enriched in brain [homo sapiens]. (2011). *NCBI*, Retrieved from http://www.ncbi.nlm.nih.gov/gene/6009
9. Worthington, K. (2009, July 07). *Trypsin*. Retrieved from http://www.worthington-biochem.com/try/default.html
10. Yu, Y., Li, S., Xu, X., Li, Y., & Guan, K. (2005). Structural basis for the unique biological function of small gtpase rheb. *The Journal of Biological Chemistry*, *280*(17), Retrieved from http://m.jbc.org/content/280/17/17093.full.pdf doi: 10.1074

Tailoring Polymer-Coated Gold Nanocages for Chemical Sampling in a Microdialysis Device

Sweta Shrestha, Cameron University
Lawton, Oklahoma

Abstract

Gold (Au) nanocages have extensive biomedical applications. The polymer poly-*N*-isopropylacrylamide (p-(NIPAAm)) is a thermally responsive polymer that can change its structural conformations with change in temperature with respect to its low critical solution temperature (LCST). Gold nanocages with localized surface plasmon resonance (LSPR) tuned near IR region are coated with p-(NIPAAm) and this polymer controls the release of samples from nanocages with the temperature change. Besides other biomedical applications of p-(NIPAAm) coated nanocages such as drug delivery, photoacoustic imaging, photothermal therapy, and contrast agent, this preliminary study was done to demonstrate as proof of principle if these nanocages can be used for chemical sampling through microdialysis device. Microdialysis sampling is a minimally invasive device that collects samples via diffusion from different tissues and organs with aid of semipermeable hollow fiber membrane. The analyte diffuse into the semipermeable membrane and carried out by perfusion fluid for further chemical analysis. The main objective of our study is to demonstrate if p-(NIPAAm) coated gold nanocages passed in the perfusion fluid could collect analytes through microdialysis sampling. Our study results showed that p-(NIPAAm) coated nanocages can be used for chemical sampling without any damage to microdialysis probe.

Introduction

Gold (Au) nanoparticles have been the part of intensive biomedical applications such as chemotherapy, photothermal therapy, and optical imaging. Gold nanocages are the nanostructures prepared by galvanic replacement reaction where a gold salt precursor (chloroauric acid) is titrated into a solution of sacrificial silver (Ag) nanocube suspension.[1] The interior part of Ag nanostructure is oxidized and reduced Au atoms grow on the surface of nanocubes producing Au nanocages.[5] Au nanocages have porous walls and a hollow interior with unique tunable localized surface plasmon resonance (LSPR) varying the size of nanocages and their pores. For biomedical applications, LSPR peak of Au nanocages should be tuned to near infrared region.[1] Thermally sensitive polymers poly (*N*-isopropylacrylamide) (p-(NIPAAm)) with low critical solution temperature (LCST) of 32^{o}C are used to coat the Au nanocages. When temperature is below LCST, the polymer is hydrophilic in nature and when temperature is above LCST, the polymer becomes hydrophobic.[2]This polymer is heat-sensitive and its conformation changes with temperature with respect to its LCST.[3] Polymer coated nanocages at temperature above LCST results in shrinking of hydrodynamic diameter of polymer leading to exposure of pores of nancoages, and thus releasing samples from the core or entrapping samples inside the core. Temperature below LCST causes polymer to stretch out and covers the pores of nanocages and thus restricting the movement of samples through the pores. This conformational change of polymer controls the release of samples from Au nanocages. So

we attempt to use polymer coated nanocages as carrier for chemical sampling using microdialysis device.

Microdialysis sampling is a minimally invasive device that helps to collect samples via diffusion from different tissues and organs of the body for biochemical studies. It is a simple *in-vivo* technique of collecting samples with the aid of probe consisting of semipermeable hollow fiber membrane with 200-500 μm diameter and 1-30mm length inserted into the different tissues and organs.[4] The analytes diffuse through the semipermeable membrane and they are carried out through outlet impermeable membrane as dialysate. Detection of dialysate can be quantified in mathematical expression called extraction effienciency (EE) which is the ratio of the concentration of analyte extracted from microdialysis sampling (C_{outlet}) to that of analyte stock (C_{inlet}) as expressed in equation 1.[6]

$$EE(\%) = \frac{C_{outlet}}{C_{inlet}} \qquad 1$$

Extraction efficiency of chemical sampling depends on the perfusion flow rate, concentration of perfusion fluid and analyte, diffusion coefficient of analyte, and molecular weight cut off (MWCO), material, and pore size of membrane. Microdialysis sampling has been applied in many areas of neuroscience and biotechnology. A microdialysis probe has shown promising adaptation to diversified applications, and samples analysis that are easily done by available technologies. So our vision is to use polymer coated nanocages for chemical sampling using the microdialysis probe as shown in Figure 1. At temperature above LCST of polymer, polymer coated Au nanocages inside microdialysis membrane can entrap diffused analyte into its core and entrapped analyte can be further analyzed. The main objective of this study is to demonstrate if polymer coated nanocages could act as carrier and entrap samples using microdialysis device.

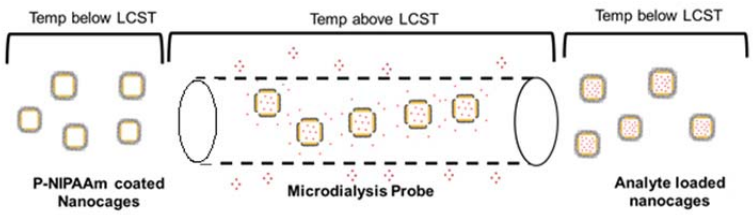

Figure 1: Schematic illustration of polymer-coated-nanocages for chemical sampling in microdialysis device.

Experimental Sections

Synthesisof Ag nanocubes: Ethylene glycol (EG), 50 mL was heated to 150^{o}C and stirred. At 150^{o}C, EG solutions of 0.6 mL of 3mM NaHS, 5 mL of 3 mM HCl, and 12.5 mL of Polyvinylpyrrolidone (PVP) (0.35 g PVP dissolved in 17.5 mL) were added to the solution. After 2 mins, 4 mL of silver trifluoroacetate in EG solution (282) mM was added to the reaction mixture and heated for 35-45 mins at 150^{o}C.

Synthesis of Au nanocages: Deionized water in 100 mL round bottom flask was heated and stirred for 10 mins. 500 μL of Ag nanocube suspension was added to water. Chloroauric acid ($HAuCl_4$) solution (1 mM) was titrated to the Ag nanocube solution. The UV-Vis spectrum

of the sample was taken. NaCl crystals were added to sample until the solution saturated and stored for an hour. The sample was centrifuged at 14000 rpm for 15 mins and clear solution was discarded. The sample was redispersed with 1.5 mL water and washed twice. The sample was resuspended by 0.1 mL water.

Surface coating of Au nanocages by p- (NIPAAm): Thermally responsive polymer p-(NIPAAm) (MW~12,000) (10 mL of 0.33 mM) with LCST 32^{o}C was titrated by 5 mL of 1.6 nM Au nanocages at the rate of 0.2 mL/min. The reaction solution was stirred for 5 days at room temperature. The polymer coated nanocages was centrifuged at 14000 rpm for 15 mins at 20^{o}C and supernatant was discarded. The nanocages were washed 4 times and it was resuspended with 0.6 mL deionized water. For the controlled release of dye, copolymer p-(NIPAAm-*co*-AAm) (poly-*N*-isopropylacrylamide-*co*-acrylamide) with LCST 41^{o}C was used for surface coating of Au nanocages.

Loading of Rhodamine B (RB) dye in copolymer coated Au nanocages: The suspended copolymer coated Au nanocages (0.6 mL)was mixed with 10 mL of RB dye (~18 mM) and it was vortexed and sonicated for 10 mins. It was placed in oil bath at 50^{o}C overnight. The solution was placed in ice bath for an hour. It was centrifuged at 14000 rpm for 15 mins at 20^{o}C and supernatant was discarded. The solution was washed until the absorbance of supernatant at 554 nm was less than 0.05.

RB dye release from copolymer coated Au nanocages: RB dye loaded copolymer coated nanocages were suspended with 0.6 mL warm water (50^{o}C) and vortexed. It was placed in water bath at 50^{o}C for 2 mins and immediately placed in ice bath for 5 mins. It was centrifuged at 14000 rpm for 15 mins at 20^{o}C and UV-Vis spectrum reading of supernatant was taken. After absorbance reading, supernatant was returned back to the nanocages and again it was placed in water bath for next time intervals of conventional heating.

Microdialysis Sampling: The microdialysis setup is shown in Figure 1 and 2. Polymer p-(NIPAAm) coated Au nanocages ranging the concentration from μM to nM were used as perfusion fluid in the microdialysis sampling. The semipermeable membrane was immersed in the analyte solution (dyes) and the flow rate of perfusion fluid was adjusted depending on the experimental setup. The concentration of analyte used was in the range of μM. The microdialysis probe used was PES (Polyethersulfone) of 100 kDa. Chemical sampling was carried out in two different conditions: placing microdialysis probe along with analyte in sand bath (37-40^{o}C) and placing microdialysis setup in warm room (37^{o}C).

Instrumentation: Transmission electron microscope (TEM) images were taken on a FEI Titan 80-300 microscope with an accelerating voltage of 300 kV. The UV-vis spectra were obtained using a UV-vis spectrometer (HP 8453A). The hydrodynamic diameter was measured using a dynamic light scattering (DSL) instrument (Brookhaven ZetaPALS).

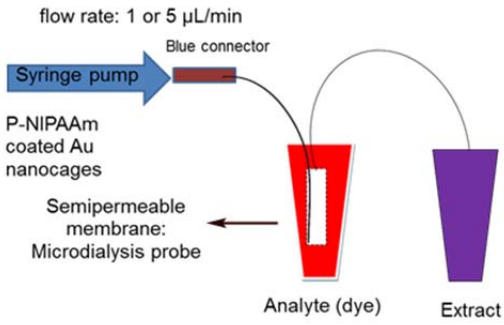

Figure 2: Diagrammatic microdialysis sampling set up

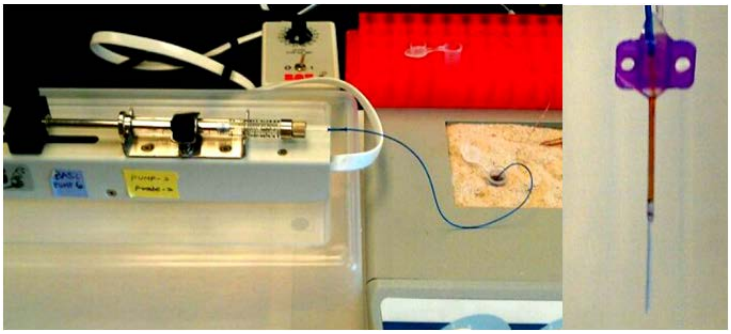

Figure 3: (Left) Microdialysis sampling set up and (Right)Microdialysis probe.

Results and Discussion

Gold nanocages were synthesized by galvanic replacement reaction such that reduced Au replaces the oxidized Ag atoms. When Ag nanocube suspension is titrated with gold salt solution precursor ($HAuCl_4$), Ag atoms get oxidized which dealloys the Ag/Au nanostructures and changes the structural composition of Ag nanocubes into Ag nanocages. With the increase in titrated volume of $HAuCl_4$ solution into the Ag nanocube suspension, there was a red shifting of LSPR peak to near IR region and the observation of series of color change from yellow, orange, maroon, purple, navy blue to fading blue (Figure 4). The LSPR peak of Au nanocages can be tuned to desired wavelength and for this experimental purpose there was requirement of LSPR peak to be tuned near IR region (780-800 nm). Most of Au nanocages synthesized had their LSPR peak wavelength ranging from 775 nm to 805 nm.

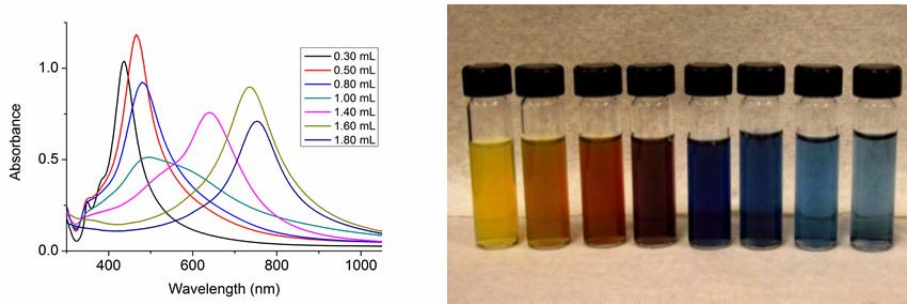

Figure 4: Tuning of LSPR peaks of Au nanocages at different wavelengths: (Left) UV-Vis spectra of samples prepared by different titrated volumes of $HAuCl_4$ solution were taken. With the increase of titrated volume of $HAuCl_4$ solution on Ag nanocube suspension, the LSPR peak wavelength red shifted. (Right) Photograph of the sample solution (going from left to right) with the increase in titrated volume of $HAuCl_4$ solution on Ag nanocube suspended solution.

Figure 5 shows the TEM image of p-(NIPAAm) coated Au nanocages and the UV-Vis spectra for both PVP-coated and p-(NIPAAm) coated Au nanocages. The size of the nanocages is 40±5 nm. There was observation of red-shifting of LSPR peak after replacing PVP polymer by p-(NIPAAm) on surface of Au nanocages. In order to further confirm the exchange of PVP polymer by p-(NIPAAm) polymer on the surface of Au nanocages as well as to observe the change of hydrodynamic diameter of p-(NIPAAm) coated Au nanocages above and below its LCST (32^{o}C), the DLS experiment was carried out (Figure 6). At two different temperatures, 25 ^{o}C and 37^{o}C, the change of diameter of p-(NIPAAm) coated nanocages was observed unlike PVP coated nanocages. The PVP coated nanocages exhibited negligible change in diameter with temperature change whereas, p-(NIPAAm) coating showed significant changes such that above LCST (37^{o}C) diameter decreased (shrinked) and it reversibly expanded below LCST (25^{o}C) as shown in Figure 6. At 37 ^{o}C, the hydrodynamic diameter of the nanocages was measured to be 105±1 nm and 121±4 nm for PVP-coated nanocages and p-(NIPAAm) coated nanocages, respectively.

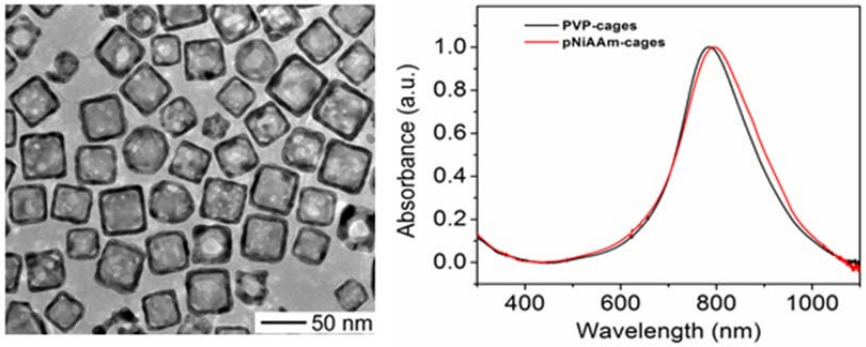

Figure 5: (Left) TEM imageof p-(NIPAAm) coated Au nanocages and (Right) Red-shifting of LSPR peak with the change of polymer coated on Au nanocages. LSPR peak of PVP nanocages is at 789 nm and that of p-(NIPAAm) nanocages is at 795 nm.

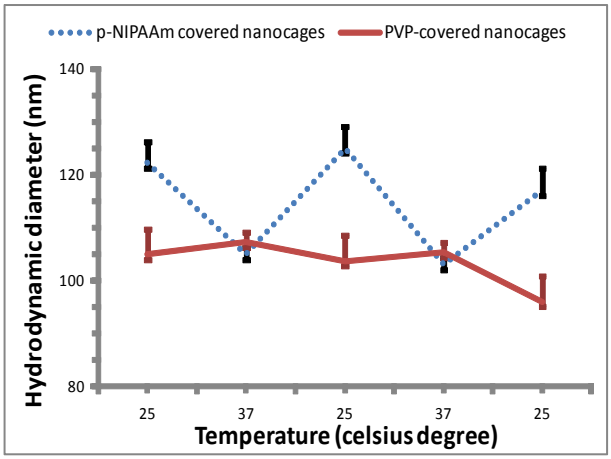

Figure 6: Observation of diameter change with change in temperature with respect to LCST of polymer p-(NIPAAm).

Gold nanocages with LPSR peak at near IR region were coated with thermally responsive copolymer p-(NIPAAm-*co*-AAm) having LCST 41^{o}C. The RB dye (~18mM) was loaded on copolymer coated Au nanocages in order to figure out how the temperature affects the release of dye from the nanocages and also to check the functionality of nanocages as shown in Figure 7. It was observed through UV-Vis spectra of supernatant at 554 nm that with the increase in time intervals of conventional heating beyond LCST of copolymer, there was increase in the amount of RB dye released from the nanocages. The copolymer has the LCST 41^{o}C so when copolymer coated nanocages was placed in water bath of 50^{o}C at certain time intervals, copolymer shrinks as a result of which porous walls of nanocages get exposed and releases dye in supernatant.

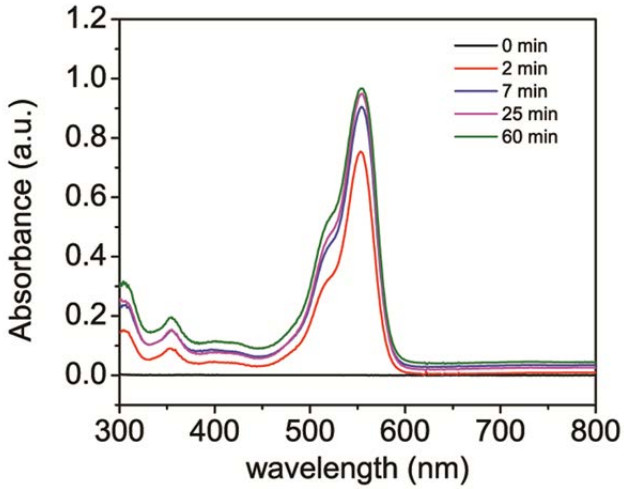

Figure 7: Controlled release of RB dye from copolymer coated Au nanocages with LCST 41^{o}C: Absorption spectra of RB dye released at 554 nm were measured for different time intervals of conventional heating. It demonstrated that the higher time interval of heating of RB dye loaded nanocages, the more release of dye from nanocages.

Microdialysis sampling was carried out using methyl orange dye (MO) and p-(NIPAAm) nanocages of concentration 16.7 μM. The absorbance peak of MO dye is at 465 nm. The

microdialysis probe was immersed in the analyte MO stock solution. The analyte was placed in sand bath at temperature 40^{o}C. Flow rate of perfusion fluid is one of the important factor to affect the extraction efficiency (EE%) of chemical sampling. As shown in Table 1, EE% of analyte sampling increased with the decrease in the flow rate of perfusion fluid. Maximum EE% could be achieved using slow perfusion flow rate because it allows more time for diffused analyte to get entrapped or adsorbed by polymer coated nanocages.

Table 1: Flow rate of perfusion fluid affects the extraction efficiency of microdialysis sampling.

Flow rate (μL/min)	Perfusion Fluid	Analyte	Inlet concentration μM	Outlet concentration μM	(EE) %	Std. dev. %	Recovery of Nanocages %
1	pNIPAAm nanocages	MO	20.5	4.3	21.1	-	Not measured
5	pNIPAAm nanocages	MO	20.3	1.4	6.8	-	~100

For the next experimental set-up, 1 μL/min perfusion flow rate was used. Microdialysis sampling was carried out in warm room at 37^{o}C temperature using p-(NIPAAm) coated nanocages (0.1 nM) and water (control) as perfusion fluid, as shown in Table 2.The EE% of microdialysis sampling using p-(NIPAAm) nanocages as perfusion fluid was less than using water (Control). The possible reason might be due to not being able to detect the dye entrapped inside the nanocages. But the results demonstrated that p-(NIPAAm) nanocages can be used in microdialysis sampling in order to collect analyte comparing the EE% of chemical sampling using p-(NIPAAm) coated nanocages versus water. These nanocages can be applied in microdialysis sampling without probe damage as they are recovered completely through outlet.

Table 2: Comparison of EE% of chemical sampling

Perfusion Fluid	Analyte	Inlet concentrationμM	Outlet concentration μM	Extraction Efficiency (EE) %	Standard Deviation %	Recovery of Nanocages %
pNIPAAmnanocages	MO	16.8	5.6	33.2	0.7	~100
Water	MO	21.9	9.1	41.4	1.3	Not measured

To determine the non-specific adsorption of dye on the p-(NIPAAm) coated nanocages, the control experiments were performed at room temperature. The result in Table 3 shows that a small amount of MO dye was lost when the MO solution was incubated with the p-(NIPAAm) coated nanocages. This loss of the MO could be attributed to the adsorption of dye by the p-(NIPAAm).

Table 3. Non-specific adsorption of dye on p-(NIPAAm) coated nanocages.

Temperature(^{o}C)	MO stock (μM)	MO in supernatant (μM)	MO loss (μM)
25 (R.T.)	21.6	20.2	1.4

Conclusion

The p-(NIPAAm) coated nanocages can be used for the collection of samples through microdialysis sampling. There is no damage of microdialysis probe because of these nanocages are fully recovered through microdialysis probe. The results of this study showed that the extraction efficiency of analyte using p-(NIPAAm) nanocages as perfusion fluid increased with the decrease in perfusion flow rate. On the other hand, the extraction efficiency of analyte using perfusion p-(NIPAAm)nanocages is less compared to water (control). The possible reason might be due to the dye entrapped inside the nanocages. Further experiments need to be carried out to quantify the entrapped dye by releasing them from the nanocages. As per our objective, p-(NIPAAm) coated nanocages can be used as perfusion fluid to carry out chemical sampling. The sampling efficiency of microdialysis can be optimized by concentration, porosity, and coating layer of perfusion nanocages.

Acknowledgement

I would like to thank Drs. Jingyi Chen and Julie Stenken for their mentorship. I would also like to thank graduate students Leanne Mathurin and Randy Cabrera for their help in the project.

References

1. Skrabalak, S. E., Au, L., X. & Xia, Y. Facile synthesis of Ag nanocubes and Au nanocages. *Nature Protocols* **2,** 2181-2190 (2007).
2. Yavuz, M. S. *et al*. Gold nanocages covered by smart polymers for controlled release with near – infrared light. *Nature Materials* **8**, 935 (2009).
3. Li, Weiyang*et al.* Gold nanocages covered by thermally- responsive polymers for controlled release by high-intensity focused ultrasound. *Nanoscale* **3**, 1726 (2011).
4. Stenken, J.A.Microdialysis sampling in *Encyclopedia of Medical devices and Instrumentation*, Second edition. New York. John Wiley & Sons. 2006
5. Skrabalak, S. E., Chen, J., Sun, Y., Lu, X., Au, L., Cobley, C. M., and Xia, Y. Gold Nanocages: Synthesis, Properties, and Applications. *Accounts of Chemical Research;***41,** 1587-1595 (2008).
6. Bungay, P.M., Morrison, P.F., and Dedrick, R.L. Steady-State theory for quantitative microdialysis of solutes and water in vivo and in vitro. *Life Sci.,* **46**, 105-119 (1990).

Expanding the Scope of the Catalytic Dynamic Resolution of *N*-Boc-2-Lithiopiperidine

Jin Sun Woo, Mount Holyoke College
South Hadley, Massachusetts

Abstract

The scope of the catalytic dynamic resolution (CDR) of *N*-Boc-2-lithiopiperidine 1 has been expanded toward the scaled-up synthesis of (*R*)-pipecolic acid methyl ester 3.

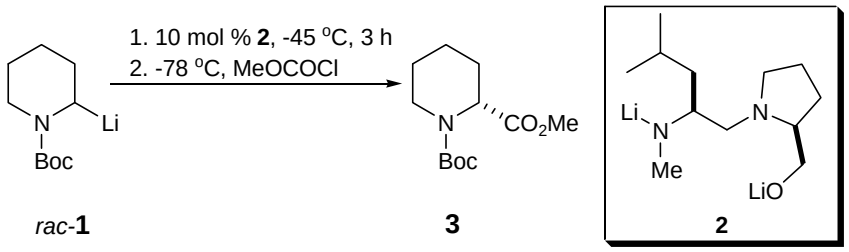

Introduction

Optically active piperidine derivatives are prevalent in natural products and are used in thousands of clinical and preclinical trials.[1] For example, (-)-swainsonine is a potentially useful antimetastasis drug for cancer treatment,[2] and conhydrine is a poisonous alkaloid in hemlock[3] (Figure 1). The pipecolic moiety is a key structure in antamiscomicin B[4]. The enantioselective synthesis of piperidine derivatives has been the subject of investigation by many researchers.[5] Recently, Beng and Gawley discovered a catalytic dynamic resolution (CDR) of *N*-Boc-2-lithiopiperidine using dilithiated diamino alkoxide ligands (*S*,*S*)-**2** and (*S*,*R*)-**2**, which afford either enantiomer of the 2-substituted piperidine in good yields and excellent enantioselectivity[6] (Scheme 1). In small scale reactions (<5 mmol), the authors synthesized both enantiomers of the proline homologue, pipecolic acid as well as the ester and amide derivatives in >97:3 er. In the wake of the important finding, there is a growing interest in implementing the CDR methodology as an alternative to a classical resolution, which is still the most practical way to obtain enantiopure compounds on an industrial scale.

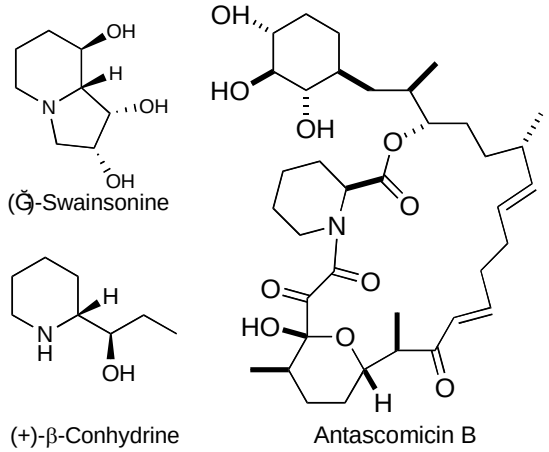

Figure 1. Piperidine alkaloids.

Scheme 1. CDR of *N*-Boc-2-lithiopiperidine **1**[6]

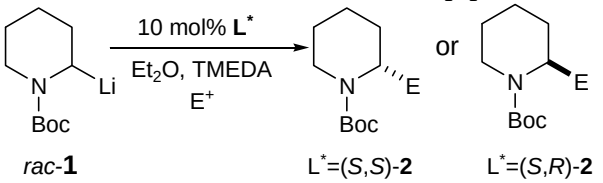

E^+:	Yield (%)	er (*R*:*S*)
CO_2	78	98:2
MeOCOCl	88	>99:1
MeOCOCl	85	>99:1
PhNCO	68	>99:1

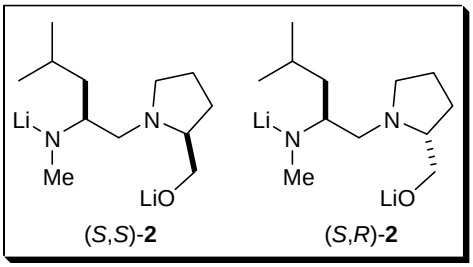

Objective

The goal of this project was to synthesize multigram quantities of enantioenriched pipecolic acid or its derivatives, for use in the total synthesis of antascomicin B.

Results and Discussion

As the starting material, *N*-Boc-piperidine was prepared by the reaction of di-*tert*-butyl dicarbonate and piperidine in dichloromethane (Scheme 2). 24.30 g of the desired product was obtained as an oil in 100% yield, data as reported.[6]

Scheme 2. Synthesis of *N*-Boc-Piperidine.

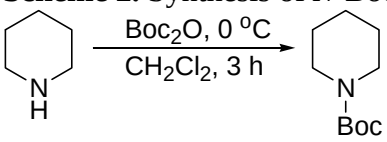

Toward the synthesis of (*S*,*R*)-**2**, the (*S*,*R*)-dipeptide ester **4** was synthesized by peptide coupling reaction of (*S*)-*N*-Boc-leucine and *D*-proline methyl ester hydrochloride in the presence of EDCI and HOBt in chloroform (Scheme 3). 1.26 g (76%) of the dipeptide ester was obtained. The reduction of the dipeptide ester was followed. 1.15 g of the conjugate acid of crude (*S*,*R*)-**2** was obtained as viscous oil.

Scheme 3. Synthesis of the conjugate acid of (*S*,*R*)-**2**.

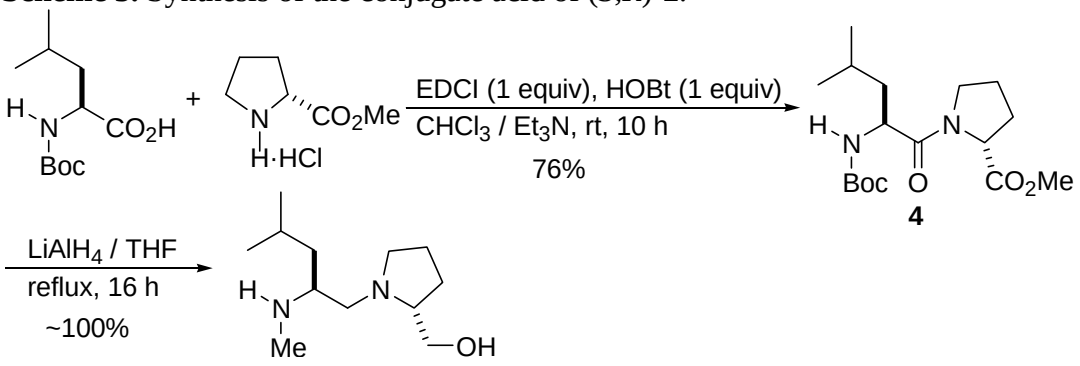

The conjugate acid of diastereomeric ligand (*S*,*S*)-**2** was also synthesized in the same way, to give 0.56 g (71%) of the product.

R-**3** was synthesized by CDR using ligand (*S*,*S*)-**2** (Scheme 4). After deprotonation of *N*-Boc-piperidine using *s*-BuLi and TMEDA at –80 °C for 3 h, the addition of 10 mol% of (*S*,*S*)-**2** and 3 h of equilibration were followed. After cooling to –80 °C, methyl chloroformate was added. CSP-GC traces showed one peak thus indicating that enantiopure *R*-**3** was obtained.

Scheme 4. Synthesis of *R*-**3** by CDR

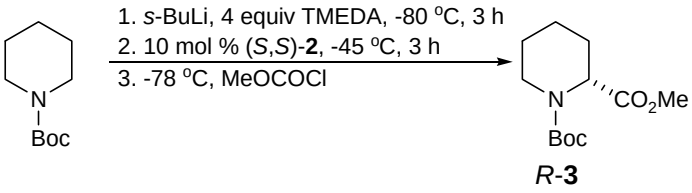

Experimental

N-Boc-Piperidine.
To a 250 mL round bottom flask containing piperidine (9.89 g, 131.5 mmol, 1.0 equiv), di-*tert*-butyl dicarbonate (28.7 g, 131.5 mmol, 1.0 equiv) in CH_2Cl_2 (100 mL) was added slowly by dropping funnel at 0 °C. The mixture was stirred for 3h and washed with saturated NaCl (3 x 50mL) and with H_2O (2 x 50 mL). The combined organic layers were dried over $MgSO_4$ and filtered and evaporated.

Conjugate acid of (S,R)-2.
Step 1. Boc-(*L*)-leucine (2.12 g, 4.83 mmol, 1.0 equiv) was dissolved in $CHCl_3$ (20 mL) in 100 mL round bottom flask. EDCI (0.95 g, 4.83 mmol, 1.0 equiv) and HOBt (0.73 g, 4.83 mmol, 1.0 equiv) were added. The mixture was stirred for 10 min. *D*-Pro-OMe·HCl (0.80 g, 4.83 mmol, 1.0 equiv) in $CHCl_3$ (10 mL) and Et_3N (2 mL) was added to the mixture slowly. The mixture was stirred at room temperature for 10 h. The solvents were evaporated. Ethylacetate (10 mL) was added, and the mixture was stirred for 30 min. The suspension was filtered. The filtrate was washed with10% citric acid (3 x 10 mL) and with 10% $NaHCO_3$ (2 x 10 mL). The organic layer was dried over $MgSO_4$ and evaporated.
Step 2. A stirred suspension of $LiAlH_4$ (1.4 g, 36.80 mmol, 10.0 equiv) in THF (100 mL) was

cooled to 0 °C. A solution of the (*S*,*R*)-**4** (1.26 g, 3.68 mmol, 1.0 equiv) in THF (30 mL) was added dropwise to the suspension. The mixture was stirred for 10 min at room temperature and refluxed for 16 h. The mixture was cooled to 0 °C and Et_2O (50 mL) was added. The mixture was carefully quenched by slow addition of 50% $NaOH_{(aq)}$ (100 mL) while stirring until all salts appeared white. The solvent was decanted, and the white solid was washed with Et_2O. The combined organic layers were dried over $MgSO_4$ and evaporated. The crude was purified by Kugelrohr distillation.

NMR spectra of (*S*,*R*)-2

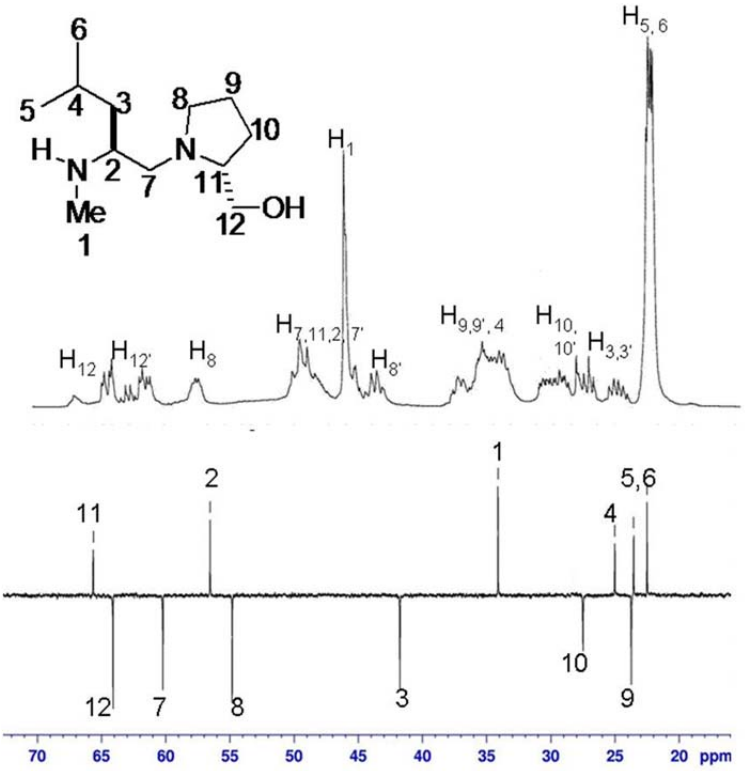

NMR spectra of (*S*,*S*)-2

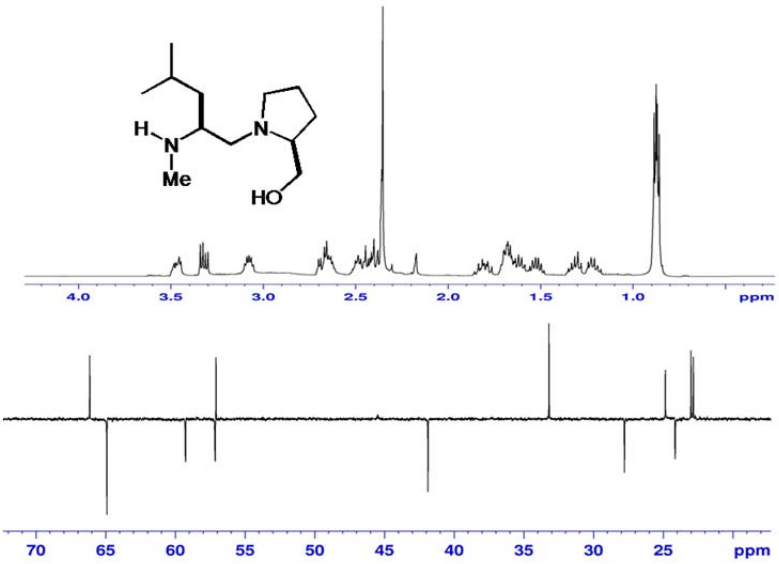

***Synthesis of R*-3.**

In an oven-dried, septum-capped 25 mL round bottom flask equipped with a stir bar, *N*-Boc-piperidine (0.185 g, 1 mmol, 1 equiv) and freshly distilled TMEDA (.15 ml, 4 mmol, 4.0 equiv) were dissolved in freshly distilled Et_2O (10 mL) under argon. The solution was cooled to –80 °C and *s*-BuLi (1.2 equiv) was added slowly by means of a syringe over a ten minute period. The mixture was stirred for 3 h. The conjugate acid of (*S*,*S*)-**2** (0.022 g, 0.1 mmol, 10 mol%) in Et_2O (10 mL) was treated with freshly titrated *s*-BuLi (20 mol%). The preformed alkoxide *S*,*S*-**2** was added and the flask was quickly transferred to a second thermostatted bath at –45 °C, and allowed to stir for 3 h. The mixture was cooled to –80 °C and rapidly quenched with methyl chloroformate (0.23 mL, 3 mmol, 3.0 equiv). After 2 h, MeOH was added and the mixture was stirred for 5 min. After warming to room temperature, 2 M HCl was added. The layers were separated and the aqueous layer was extracted with Et_2O. The combined organic layers were dried over $MgSO_4$ and evaporated to obtain the crude product . The er was determined by CSP-GC.

CSP-GC trace of the *rac*-3 and *R*-3 of >99:1 er

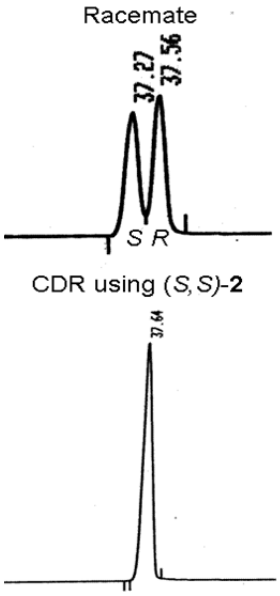

Acknowledgements

I thank National Science Foundation (CHE 1011788) for the support of this work. I appreciate Dr. Gawley for help and nurturing an inexperienced student. I appreciate Dr. Beng for tremendous guidance. I also thank Abigail, Barry, Scott, and Elizabeth for being helpful companies in the group.

Reference

1. Watson, P. S.; Jiang, B.; Scott, B., A diastereoselective synthesis of 2,4-disubstituted piperidines: scaffolds for drug discovery. *Org. Lett.* **2000,** *2*, 3679-3681.
2. Pyne, S. Recent Developments on the Synthesis of (-)-Swainsonine and Analogues.*Current Organic Synthesis* **2005**, *2*, 39-57.
3. Voituriez,A; Ferreira,F;Chemla, F. Short and Efficient Asymmetric Synthesis of (-)-r-Conhydrine.*J. Org. Chem.* **2007**, *72*, 5358-5361
4. Qi, W.; McIntoch, M. C. Toward the synthesis of antascomicin B. Synthesis of a model of the C22–C34 fragment via Ireland–Claisen and allylic diazene rearrangements. *Tetrahedron*, **2008**, *64*, 7021-7025.
5. (a) Bailey, W. F.; Beak, P.; Kerrick, S. T.; Ma, S.; Wiberg, K. B. *J. Am. Chem.Soc.* **2002**, *124*, 1889. (b) Stead, D.; Carbone, G.; O'Brien, P.; Campos, K. R.; Coldham, I.; Sanderson,A. *J. Am. Chem. Soc.* **2010**, *132*, 7260. (c) Coldham, I.; Raimbault, S.; Chovatia, P. T.; Patel, J. J.; Leonori, D.; Sheikh,N. S.; Whittaker, D. T. E. *Chem. Commun.* **2008**, 4174. (d) Beng, T. K.; Yousaf, T. I.; Coldham, I.; Gawley, R. E. *J. Am. Chem. Soc.* **2009**, *131*, 6908.
6. Beng, T. K.; Gawley, R. E. *J. Am. Chem. Soc.***2010**, 132, 12216-12217.
7. Beak, P.; Lee, W. K., α-Lithioamine synthetic equivalents: syntheses of diastereoisomers from Boc derivatives of cyclic amines. *J. Org. Chem.* **1993,** *58*, 1109-17.

Synthesis of JWH-018 Metabolite

Patience Wright, Spring Hill College
Mobile, Alabama

Abstract

Beginning in 2004, herbal mixtures with the name "Spice" or "K2" were sold in "headshops" and on the internet. These mixtures contain 1-pentyl-3-(1-napthoyl)indole, also known as JWH-018. Although JWH-018 and delta-9-tetrahydrocannabinol (Δ^9-THC) have different structures, both give cannabis-like effects after consumption. Hallucination, distorted perception, and tachycardia are common effects of usage. Due to this, the Drug Enforcement Agency (DEA) is conducting further studies to determine if these mixtures should be permanently placed on the controlled substances list prohibiting their sale and consumption. For this project, the authors synthesized a JWH-018 metabolite and analyzed the products using gas chromatography-mass spectroscopy (GC/MS). The metabolite was synthesized to mimic the metabolized product found in K2 users' urine after its consumption. Hydroxylation on the alkyl chain is the most common metabolite found in urine; therefore, the authors choose to synthesize it to act as an analytical standard to compare to urine samples of K2 users. Since the carboxylic acid form is the second most common metabolite found, future studies will work toward continuing the synthesis.

Introduction

In 2004, interest in herbal mixtures with the names "K2" and "Spice" became apparent as these blends began appearing in "headshops" and online. Although some of these mixtures come in packages with warnings suggesting that they are not for human consumption (Figure 1), the mixtures have been used as "herbal highs."

The most common ingredient reported in these mixtures is 1-pentyl-3-(1-napthoyl)indole, also known as JWH-018. While JWH-018 has cannabis-like effects similar to delta-9-tetrahydrocannabinol (Δ^9-THC) found in marijuana, they do not have similar structures (Figure 2). Both of these substances interact with the cannabinoid receptors, CB_1 and CB_2, with a higher binding affinity reported for JWH-018 compared to Δ^9-THC [1,2]. Less JWH-018 is, therefore, needed in the body to have the same effects as a higher dose of Δ^9-THC. Hallucination, distorted perception, and tachycardia are common effects of usage for JWH-018 and Δ^9-THC.

Previous studies of JWH-018 have included detection in incense packets using GC/MS [3]. These studies have allowed these mixtures to be monitored before they become available on the market. Determining appropriate methods for detecting metabolic products is beneficial for law enforcement agencies. This is especially applicable since the Drug Enforcement Agency (DEA) is conducting studies to determine if mixtures containing JWH-018 should be placed on the controlled substances list prohibiting their sales [4].

The purpose of this study is to synthesize a JWH-018 metabolite where hydroxylation occurs on the alkyl chain. This is the most common metabolite predicted in K2 users' urine by studies with rat liver microsomes reported by Wintermeyer et al [5]. The synthesized metabolite will then be used as an analytical standard to quantitate the metabolite found in K2 users' urine.

The presence of this metabolite has only recently been confirmed with liquid chromatography-mass spectrometry (LC-MS/MS) [6]. Developing a GC/MS method and improving the method validation is needed for conclusive determination of a history of abuse.

Since previous studies in the group have shown that better detection limits are achieved when the metabolite is derivatized with the same protecting groups used in the synthesis, the synthetic target of this study was the silane derivative shown in Figure 3. The overall synthetic scheme can be found in Figure 3 with the different reagents and conditions regarding each step. In further studies, the removal of the protecting group and addition of the hydroxyl group will take place. This will allow the hydroxyl group to be oxidized into a carboxylic acid which is the second most common metabolite found in K2 users' urine [6].

Figure 1. Different brands of 'Spice' herbal products illustrating differences in packaging and herbal blend appearance. Some packages indicate not intended for human consumption.

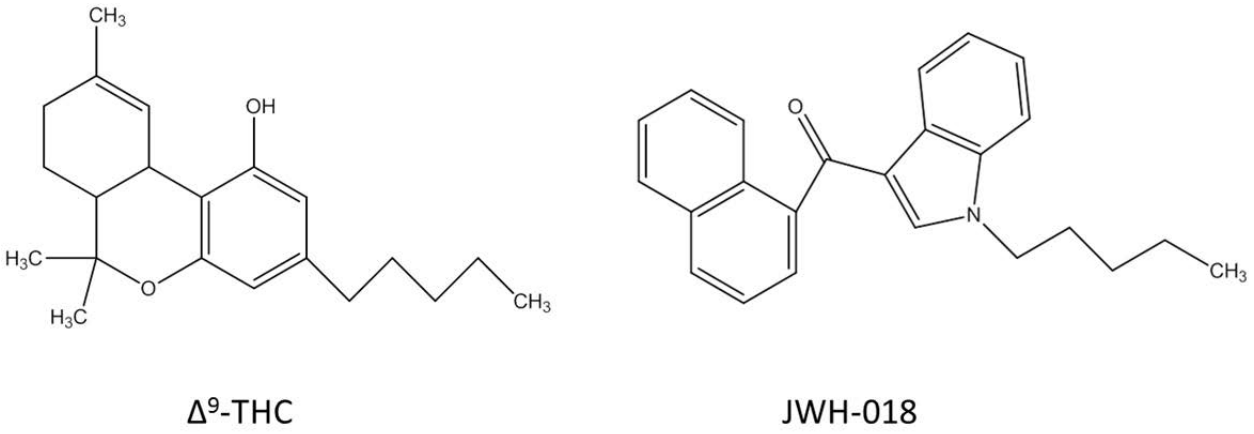

Figure 2. Structural formulas for Δ^9-THC and JWH-018.

Experimental Procedures

Materials and Instrumentation. The solvents and reagents were purchased from EMD Chemicals (Gibbstown, NJ), Sigma Aldrich (St. Louis, MO), and TCI America (Portland, OR). The samples were analyzed using a Varian 450 gas chromatography system combined with a Varian 320 MS. The GC had an injector temperature fixed at 300 °C, a split 10:1 ratio, and a Zebron ZB-5HT Inferno 30M x 0.25 ID column. The temperature programming of the GC varied for the steps. Steps 1 and 2 were held at 65 °C (2 min) then increased with a rate of 25 °C/min until 280 °C (2 min). For step 3, the temperature was held at 80°C then increased at a rate of 25 °C/min to reach 310 °C (15 min). The MS conditions were as follows: scanning 50-500 amu and 1 sec/scan.

Compound 1 (1-*t*-butyldimethylsilyl-5-bromopentane). 5-bromo-pentan-1-ol (3.6 mL, 29.7 mmole), imidazole (5.1 g, 74.9 mmole), and tert-butyldimethylsilyl chloride (TBDMSCL) (5.9 g, 39.1 mmole) were dissolved in 10 mL DMF under N_2 at 0 °C. The reaction stirred overnight at room temperature. After the overnight reaction, the solution was diluted with 20 mL ethanol and quenched with 10 mL 1 M HCl. The clear, colorless solution was extracted three times with petroleum ether (50 mL), dried with Na_2SO_4, and filtered. The petroleum ether was removed by rotary evaporation and a clear oil (compound 1) was recovered and purified using a silica column (petroleum ether/ethanol, 50:1 v/v) [7].

Compound 2 (1-(5-t-butyldimethylsilylpentyl)indole). Compound 1 (8.0 g, 28.5 mmol), KOH (0.5 g, 8.9 mmol), and 1.1 g indole (1.1 g, 9.4 mmol) were dissolved in 20 mL DMF and the reaction was stirred overnight. The mixture was quenched after this time with 50 mL H_2O. After the addition of H_2O, the solution formed a white precipitate with an orange oil on top of the solution. The solution was extracted three times with petroleum ether (50 mL), washed three times with H_2O (50 mL), dried with $MgSO_4$, and filtered. Rotary evaporation was used to remove the petroleum ether which was followed by purification by a silica column (petroleum ether/diethyl ether, 9:1 v/v) [8].

Compound 3 (1-(5-t-butyldimethylsilylpentyl)-3-(napthoyl)indole).. Compound 2 (0.7 g, 2.2 mmol) was dissolved in CH_2Cl_2 (10 mL, 156.6 mmol) and cooled to 0 °C under N_2. To this solution, Me_2AlCl (3.4 mL, 36.6 mmol) was added drop-wise and allowed to stir for 30 min. After this time, 1-naphthoyl chloride (0.4 mL, 2.6 mmol) was added in dry CH_2Cl_2 (10 mL, 156.6 mmol) to the pink solution and stirred for 2 hrs. After the solution changed to a bright

orange color, DMF was removed by rotary evaporation to recover a brown oil. The oil was purified with a silica column (petroleum ether/ethyl acetate, 9:1 v/v) to give a faint yellow oil [9].

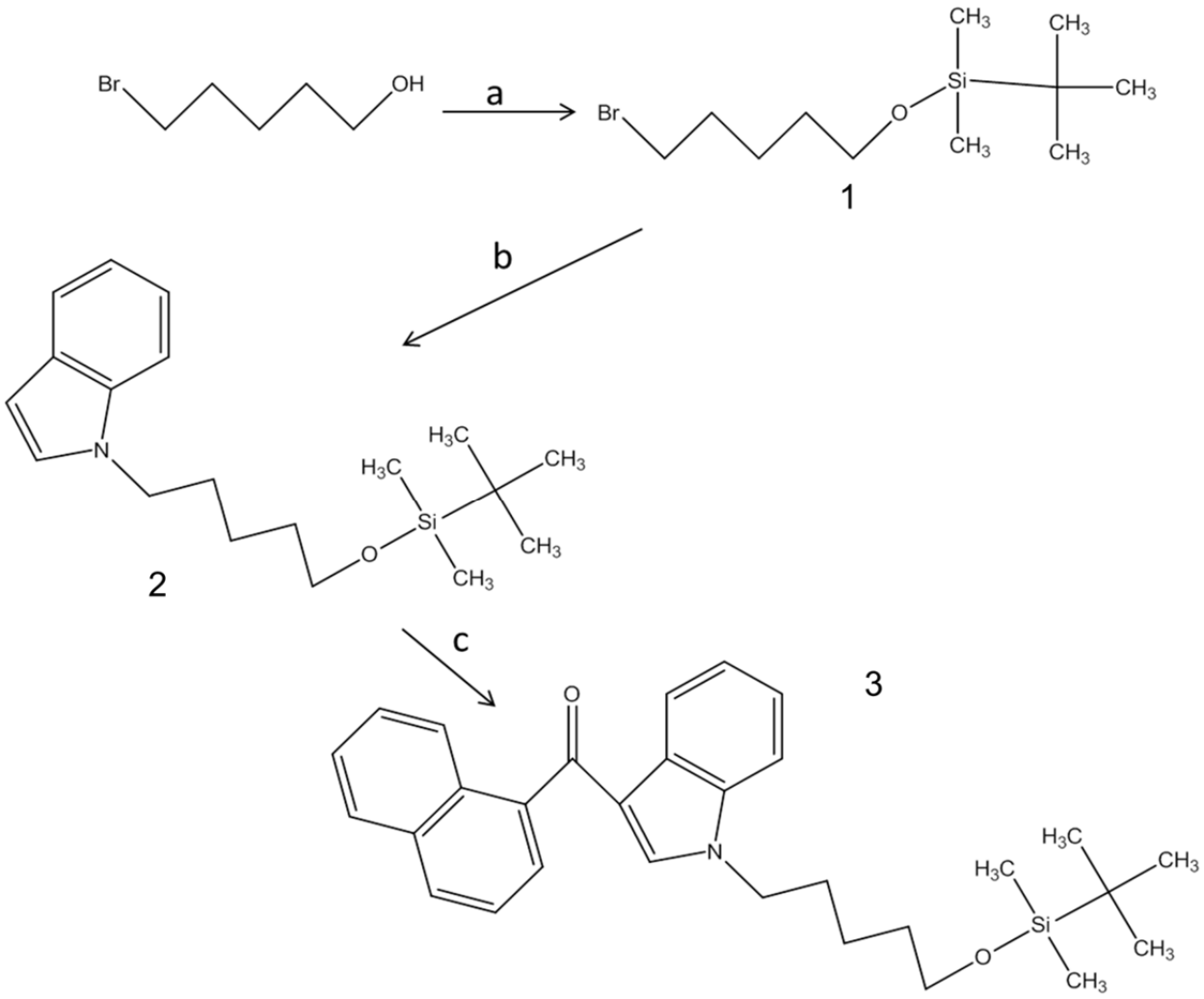

Figure 3. Reagents and conditions for the synthesis of JWH-018 hydroxylated metabolite; (a) TBDMSCl, imidazole, DMF, 0°C to room temperature; (b) DMF, indole, KOH; and (c) 1-naphthoyl chloride, CH_2Cl_2, Me_2AlCl, 0°C.

Results and Discussion

During the synthesis of the JWH-018 metabolite, each compound was analyzed using GC/MS to confirm product formation. The gas chromatogram, corresponding mass spectrum, and fragmentation pattern were determined for each product.

The GC/MS data and fragmentation patterns for compound 1 are shown in Figures 4. Compound 1 should have a molecular ion at *m/z* 281; however, this ion is not visible in the mass spectrum (Figure 4B). In previous studies by this group, chemical ionization (CI) was used for confirmation. In this instance, a molecular ion at *m/z* 281 was observed. The current GC/MS

method uses electron ionization (EI) which did not fragment the compound in the same manner. EI uses a hard ionization technique, whereas, CI is often referred to as a soft ionization technique. EI may cause rearrangement of the chain to form a cyclic structure. A cyclic structure will not produce a molecular ion at *m/z* 281.

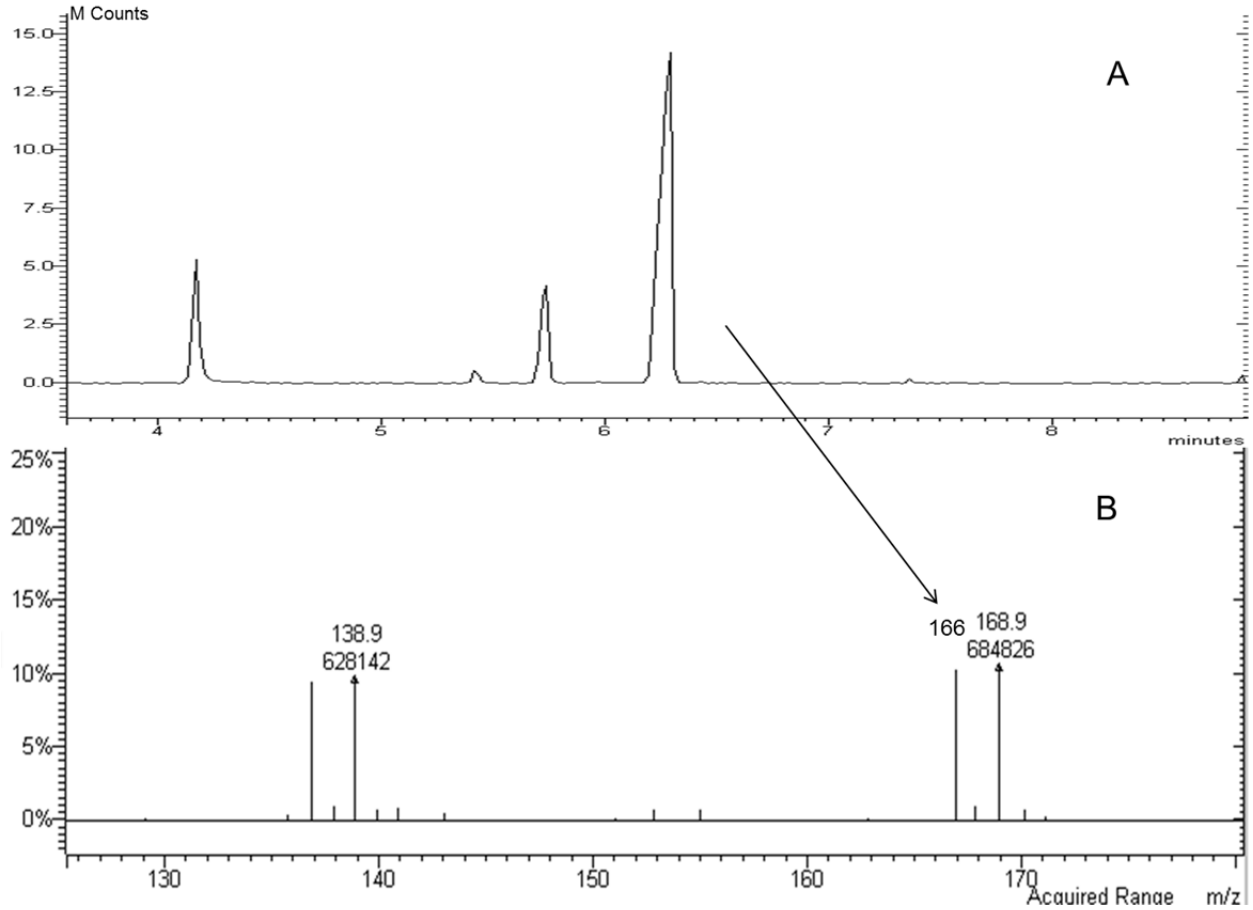

Figure 4. (A) GC chromatogram of compound 1; and (B) corresponding MS spectrum.

It appears that compound 1 fragments in the MS to form an ion at *m/z* 166 as illustrated in Figure 5. This ion occurs due to the breaking of the Si and O bond.

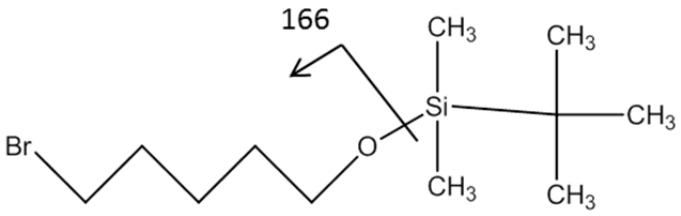

Figure 5. Fragmentation patterns of compound 1.

The product was also analyzed by ^{1}H NMR. Peak assignments for compound 1 are shown in Figure 6 and are labeled in the NMR spectrum (Figure 7) as follows: peaks 1 and 5 are

triplets, peak 2 is a pentet, peaks 6 and 7 are singlets and peaks 3 and 4 is an unresolved multiplet. These assignments correspond to those predicted thus confirming product formation.

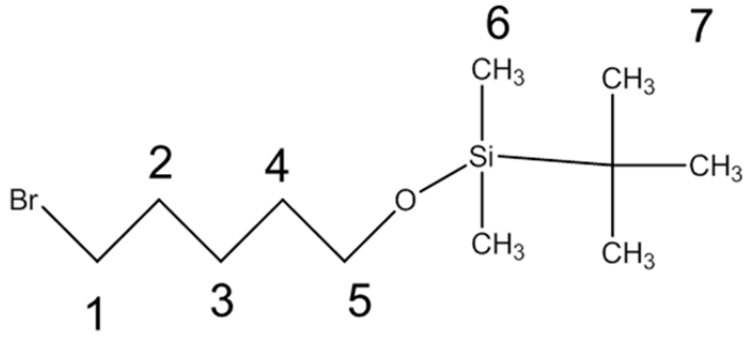

Figure 6. Structure of compound 1 with NMR peak assignments

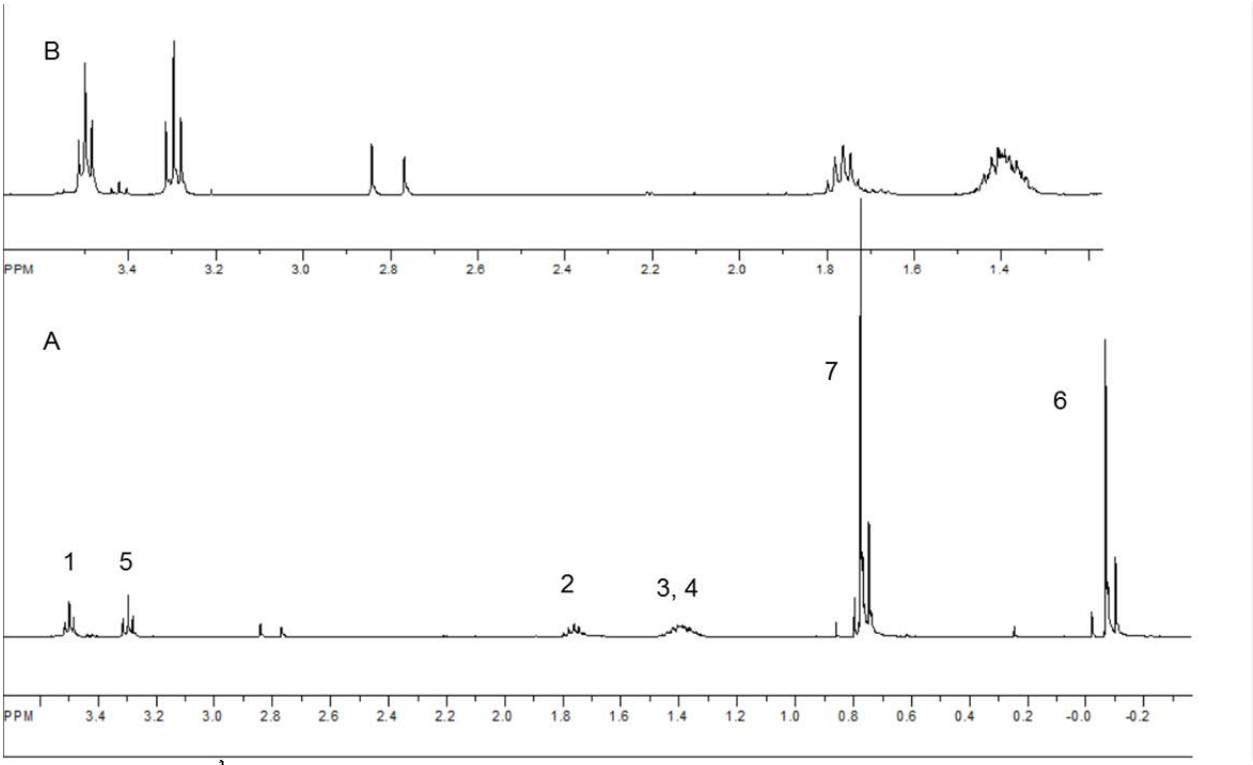

Figure 7. (A) H^1 NMR of compound 1; (B) enlarged view of spectrum A centered around 1.2-3.4 ppm.

The GC/MS and fragmentation patterns of compound 2 are shown in Figure 8. The molecular ion of compound 2 is found at *m/z* 317 and is visible in the mass spectrum (Figure 8B). Other abundant ions are found at *m/z* 130 and *m/z* 260. These ion formations indicate that compound 2 was formed.

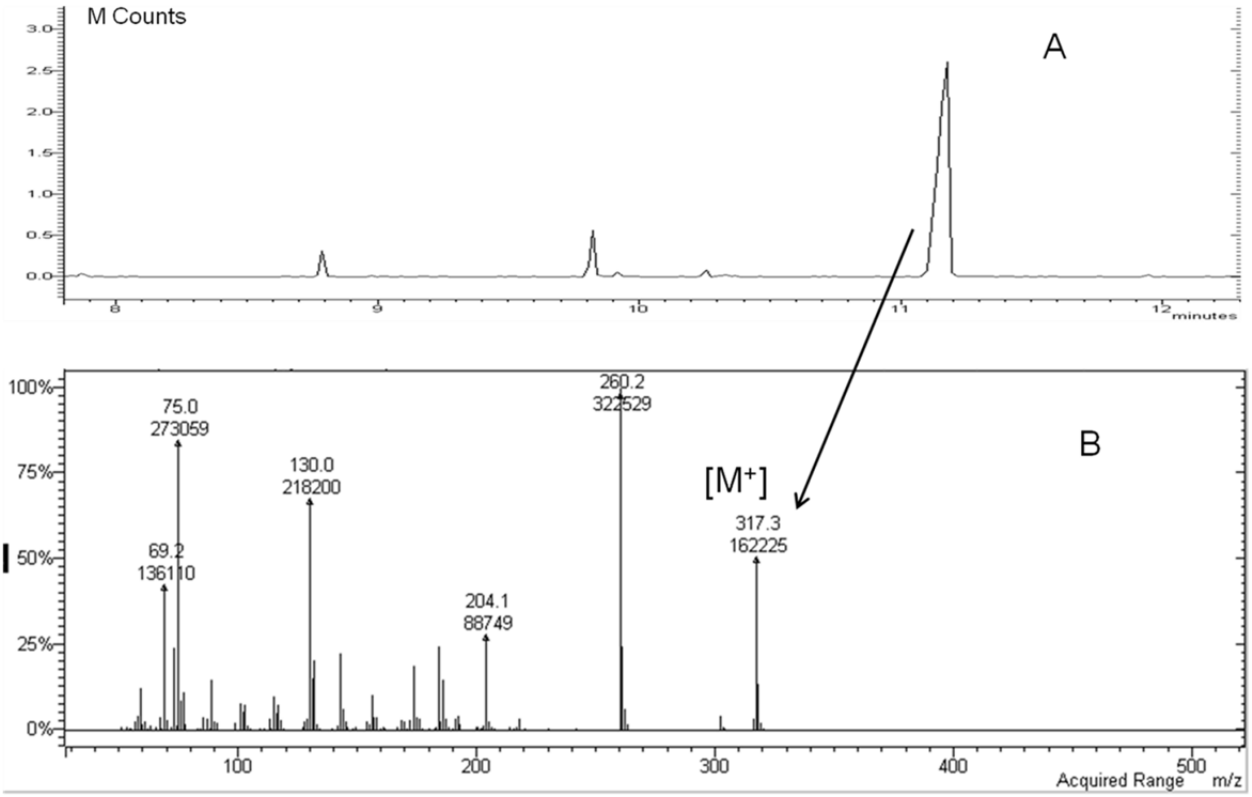

Figure 8. (A) GC chromatogram of compound 2; and (B) corresponding MS spectrum.

The fragmentation patterns of compound 2 are shown in Figure 9. The ion at *m/z* 130 is formed through loss of the butyl side chain and protecting group ($-\dot{(}CH_2)_4OSi(CH_3)_2C(CH_3)_3$). The ion at *m/z* 260 is formed from loss of the tert butyl on the protecting group ($-\dot{C}(CH_3)_3$).

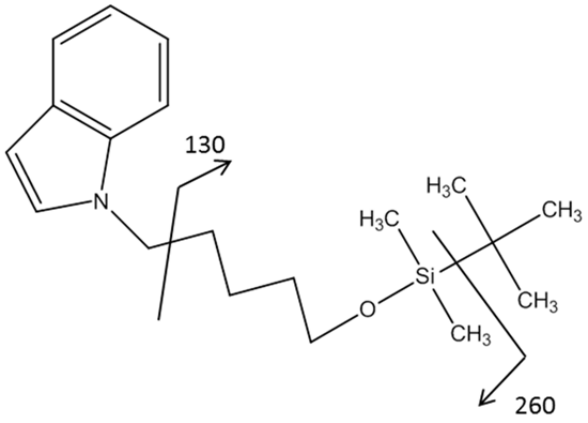

Figure 9. Fragmentation patterns of compound 2.

The GC/MS data and fragmentation patterns for compound 3 are visible in Figure 10. Compound 3 has a molecular ion at *m/z* 471 visible in the mass spectrum (Figure 10B). The other ions noted in the fragmentation patterns are at *m/z* 127 and 155.

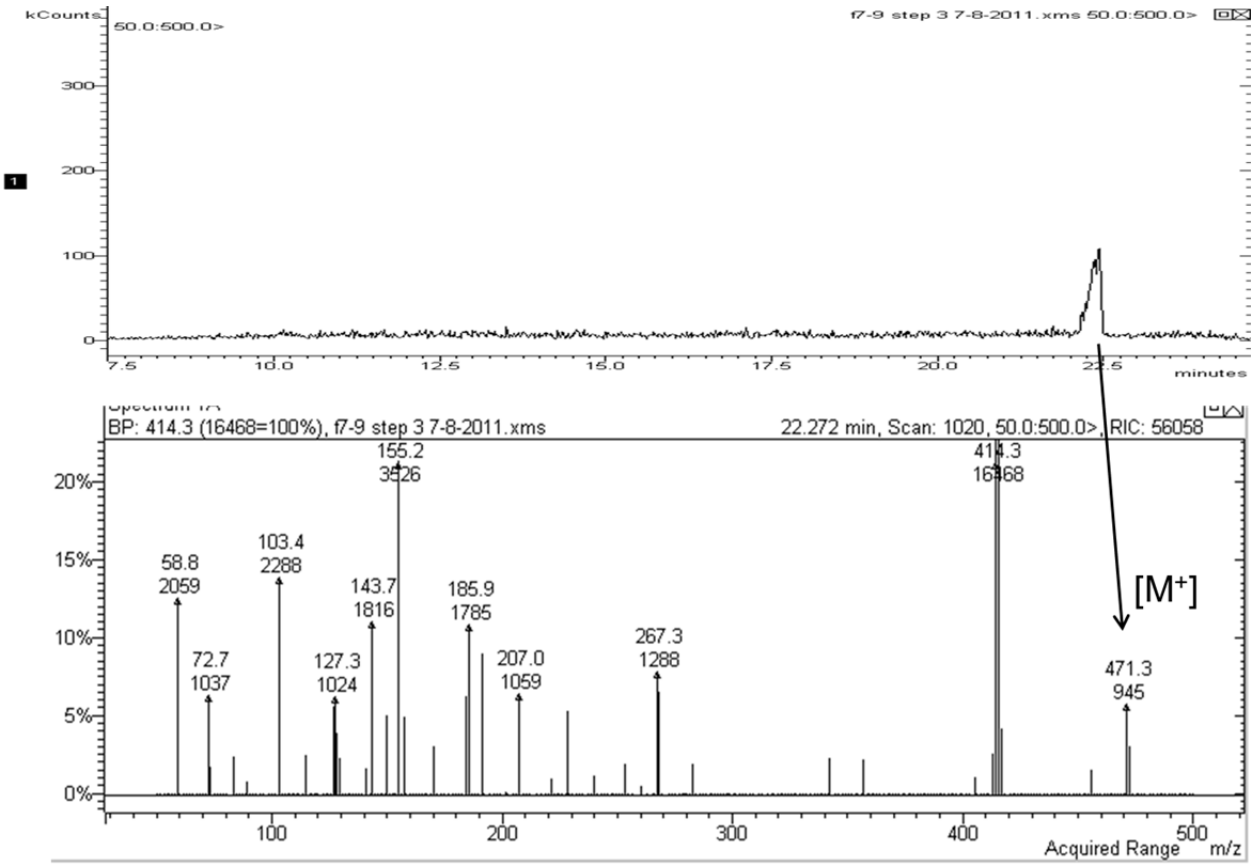

Figure 10. (A) GC chromatogram of compound 3; and (B) corresponding MS spectrum.

The ions at *m/z* 127 and 155 are from naphthalenyl and carbonylnaphthalenyl, respectively. Another abundant ion is at *m/z* 414, which corresponds to loss of tert butyl from the protecting group (-·C(CH_3)$_3$). This loss is identical to the loss found in compound 2 at *m/z* 260. The molecular ion and other ion formations indicate that the proper compound was formed during synthesis.

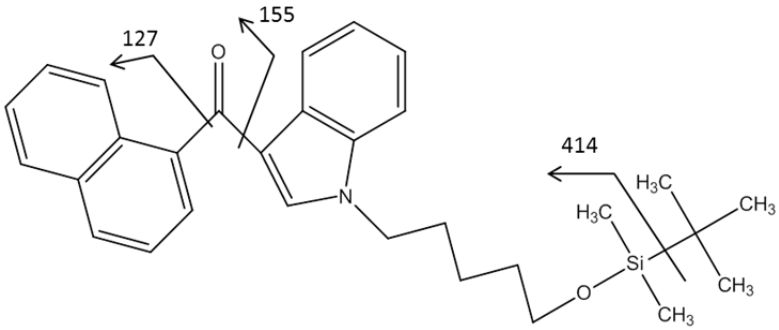

Figure 11. Fragmentation patterns of compound 3.

Conclusion

In conclusion, the JWH-018 metabolite was formed with the protecting group attached in place of the hydroxyl group (Figure 3 compound 3). This proved to have better detection limits

with GC/MS than the hydroxylated form of the metabolite. The appropriate GC/MS methodology was determined during this project which will help in future studies regarding this metabolite. Proper analytical standards are crucial to compare the standard retention time and mass spectrum fragmentation patterns to metabolites found in the urine of K2 users.

Future Work

In future studies, the synthesis will be continued to form the hydroxylated metabolite which can then be oxidized to form the carboxylic acid. Both metabolites will then be compared to those found in K2 users' urine. After the hydroxylated metabolite is formed, the detection limits of the metabolite will be determined. In addition, future work will compare the methods of GC/MS to the established one for LC-MS/MS. As a result of the gas chromatogram and mass spectrum of compound 1 using EI, future studies will also analyze different brominated alkyl chains to determine which chain lengths react to form cyclic structures.

Acknowledgements

I would like to thank Dr. Durham and Beth Emerson for guiding me through the synthesis and helping me understand the significance of this project. Also, I want to thank Carrie Synder and the rest of the Durham group for helping me in the laboratory this summer. Dr Lay and Jennifer Gidden deserve thanks for allowing me to use the Arkansas Statewide Mass Spectrometry Facilities. Lastly, I would like to thank the National Science Foundation CHE-0851505/REU for financial aid.

References

(1) Sobolevsky, T.; Prasolov, I.; Rodchenkov, G., Detection of JWH-018 metabolites in smoking mixture post-administration urine. *Forensic Science International* 2010, 200 (1-3), 141-147.

(2) Grigoryev, A.; Savchuk, S.; Melnik, A.; Moskaleva, N. j.; Dzhurko, J.; Ershov, M.; Nosyrev, A.; Vedenin, A.; Izotov, B.; Zabirova, I.; Rozhanets, V., Chromatography-mass spectrometry studies on the metabolism of synthetic cannabinoids JWH-018 and JWH-073, psychoactive components of smoking mixtures. *Journal of Chromatography B* 2011, 879 (15-16), 1126-1136.

(3) Dresen, S.; Ferreiros, N.; Putz, M.; Westphal, F.; Zimmermann, R.; Auwarter, V., Monitoring of herbal mixtures potentially containing synthetic cannabinoids as pshychoactive compounds. *Journal of Mass Spectrometry* 2010, *45*, 1186-1194.

(4) Drug Enforcement Administration, Schedules of Controlled Substances: Temporary Placement of Five Synthetic Cannabinoids Into Schedule I. *Microgram Bulletin* 2011, 44 (3), 21-27.

(5) Wintermeyer, A.; Moller, I.; Thevis, M.; Jubner, M.; Beike, J.; Rothschild, M. A.; Bender, K., In vitro phase I metabolism of the synthetic cannabimimetic JWH-018. *Analytical and Bioanalytical Chemistry* 2010, 398, 2141-2153.

(6) Moran, C. L.; Le, V.-H.; Chimalakonda, K. C.; Smedley, A. L.; Lackey, F. D.; Owen, S. N.; Kennedy, P. D.; Endres, G. W.; Ciske, F. L.; Kramer, J. B.; Kornilov, A. M.; Bratton, L. D.; Dobrowolski, P. J.; Wessinger, W. D.; Fantegrossi, W. E.; Prather, P. L.; James, L. P.; Radominska-Pandya, A.; Moran, J. H., Quantitative Measurement of JWH-018 and JWH-073 Metabolites Excreted in Human Urine. *Analytical Chemistry* 2011, 83 (11), 4228-4236.

(7) Li, C.; Xu, W.; Vadivel, S. K.; Fan, P.; Makriyannis, A., High Affinity Electrophilic and Photoactivatable Covalent Endocannabinoid Probes for the CB1 Receptor. *Journal of Medicinal Chemistry* 2005, *48* (20), 6423-6429.

(8) Dehaen, W.; Hassner, A., Annulation of Heterocycles via Intramolecular Nitrile Oxide-Heterocycle Cycloaddition Reaction. *Journal of Organic Chemistry* 1991, *56* (2), 896-900.

(9) Huffman, J. W.; Zengin, G.; Wu, M.-J.; Lu, J.; Hynd, G.; Bushell, K.; Thompson, A. L. S.; Bushell, S.; Tartal, C.; Hurst, D. P.; Reggio, P. H.; Selley, D. E.; Cassidy, M. P.; Wiley, J. L.; Martin, B. R., Structure-activity relationships for 1-alkyl-3-(1-naphthoyl)indoles at the cannabinoid CB(1) and CB(2) receptors: steric and electronic effects of naphthoyl substituents. New highly selective CB(2) receptor agonists. *Bioorganic & Medicinal Chemistry* 2005, *13* (1), 89-112.

APPENDIX

Student Posters
Candid Pictures

Phospholipid Analyses by Utilizing GC-MS

Terry Anderson II[1]
[1] Department of Chemistry, Philander Smith College, 900 Daisy L. Gaston Bates Dr., Little Rock, Ar, 72202

UNIVERSITY OF ARKANSAS
2011 Summer REU Experience

PHILANDER SMITH COLLEGE EST 1877

Introduction:

A GC-MS is two part Instrument, A) a Gas Chromatograph (GC) for separating volatile compounds; and B) a Mass Spectrometer (MS) for analyzing the mass-to-charge ratio of the substances exiting the GC.

The purpose of this research was the development of a proper analytical methods and their applications to tissue samples to properly profile the phospholipids. The only way to profile lipids in a GC-MS is an esterfication process which is necessary to make the lipid more volatile, or as a Fatty Acid Methyl Ester(FAMES) to move through the GC-MS column. A tissue extraction process has to be performed to obtain the lipids. Then esterfication process must be done on the extract.

The lipids that were used in this project: Phosphatidylcholine(PC), Phosphatidylinostiol(PI), are of the glycreophospholipids lipid classification, and Sphingomyelin(SM) of the sphingolipids lipid classification, are some of the most abundant lipids that are found in nature.

Phosphatidylcholine (PC):

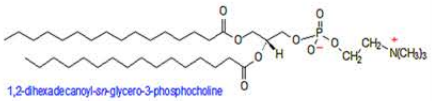

1,2-dihexadecanoyl-*sn*-glycero-3-phosphocholine

Phosphotidylinositol (PI):

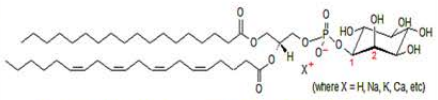

1-octadecanoyl, 2-(5Z,8Z,11Z,14Z-eicosatetraenoyl)-*sn*-glycero-3-phospho-(1'-*myo*-inositol)

Sphingomyelin (SM):

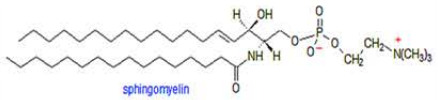

sphingomyelin

All Pictures Courtesy of: The ACOS Lipid Bank (lipidback.acos.org)

Experimental Methods/Procedures:

GC-MS Lipid Standard Fatty Acid Methyl Ester's (FAMES) Preparation:

- 2mg of the lipid is placed into a 16 X 125 mm Pyrex screw cap culture tube
- 2ml of BF_3-CH_3OH 12%(w/w), or $NaOCH_3$(0.5 M) is added to the lipid
- The mixture is heated for 5-10 min. at 60°C
- Cool mixture at room temp. for 10 min., before adding 1ml of H_2O (distilled) and 1ml of C_6H_{14}
- Agitate the mixture, and allow to separate
- Take the top layer and dry in anhydrous Na_2SO_4
- Remove top layer and place into a GC-MS Vial

GC-MS Tissue Lipid Extraction & FAMES Preparation:

- A small amount of freeze-dried tissue was ground up and placed in to a 16 X 125 mm Pyrex screw cap culture tube
- A Chloroform-Methanol (2:1 vol/vol) solution is placed in the test tube, before 2ml of BF_3-CH_3OH 12%(w/w), or $NaOCH_3$(.5 M) is added
- The mixture is heated for 1.5 hrs. at 60°C
- Cool Mixture at room temp. for 10 min., before adding 2ml of $NaHCO_3$ and 3ml of C_6H_{14}
- Agitate and centrifuge the mixture,to allow for separation
- Take the top layer and dry in anhydrous Sodium Sulfate-Potassium Carbonate (10:1 wt/wt)
- Remove top layer and place into a GC-MS Vial

GC-MS Temperature Gradient Method:

-The initial GC oven temperature was set at 140°C(hold 5 min)

-Temperature was increased at a rate of 4°C/min, until reaching 240°C(hold 15 min)

-Total Time: 45 min.

Data/Results:

➢**GC-MS Lipid Catalyst Comparison: BF_3 Vs. $NaOCH_3$**

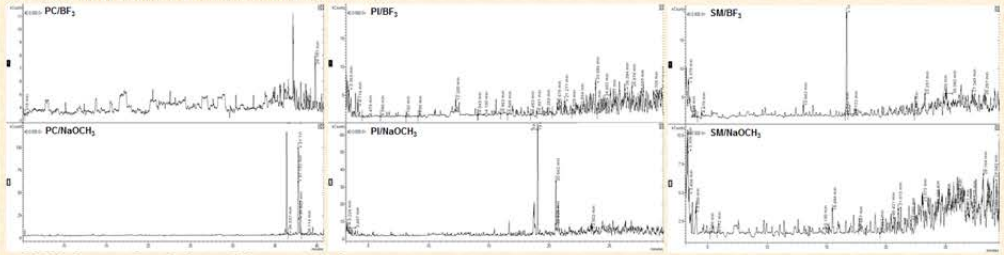

➢**GC-MS Spectra: Standards vs. Mixture vs. Beef Tissue Sample**

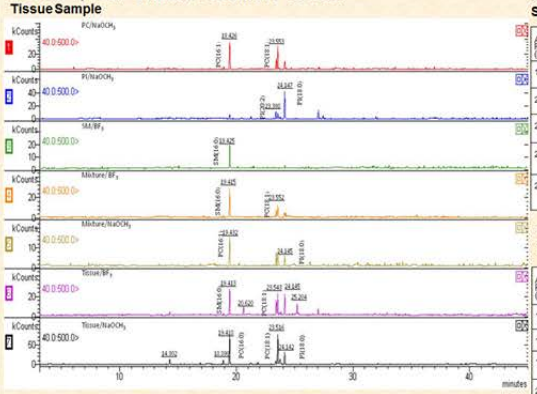

➢**6) GC-MS Retention Time Identification for Beef Tissue/BF_3 Sample**

Average Retention Time (min)	Systematic Name	Formula	m/z	Shorthand Designation	RSD	Phospholipid Source
19.413 ± 0.0072	Hexadecanoic Acid, methyl ester	$C_{17}H_{34}O_2$	270.2559	16:0	0.04%	SM
20.620 ± 0.0092	Dodecane, 1,1-dimethyl-	$C_{14}H_{30}O_2$	230.2246		0.04%	Other lipid
23.543 ± 0.0010	16- Octadecanoic acid, methyl ester	$C_{19}H_{38}O_2$	296.2715	18:1	0.004%	PC
24.145 ± 0.0050	Undecanoic acid, methyl ester	$C_{12}H_{24}O_2$	200.1776	11:0	0.02%	Other lipid
25.204 ± 0.0052	4,5 Bis-dimethoxymethyl-octanedioic acid, dimethyl ester	$C_{15}H_{30}O_8$	350.1941		0.02%	Other lipid

➢**7) GC-MS Retention Time Identification for Beef Tissue/$NaOCH_3$ Sample**

Average Retention Time (min)	Systematic Name	Formula	m/z	Shorthand Designation	RSD	Phospholipid Source
14.302 ± 0.0065	Methyl Tetradecanoate	$C_{15}H_{30}O_2$	242.2246	14:0	0.05%	Other lipid
18.890 ± 0.0095	Unknown				0.05%	Other lipid
19.418 ± 0.0065	Hexadecanoic acid, methyl ester	$C_{17}H_{34}O_2$	270.2559	16:0	0.03%	PC
23.516 ±0.0551	9-Octadecanoic acid (Z)-, methyl ester (C19:1)	$C_{19}H_{36}O_2$	296.2715	18:1	0.23%	PC
24.142 ± 0.0044	Octadecanoic acid, methyl ester	$C_{19}H_{38}O_2$	298.2872	18:0	0.02%	PI

Conclusion:

- The GC-MS data shows that the FAMES synthesis procedure created methyl esters, for GC-MS analysis

-The catalyst $NaOCH_3$ allows for the PC&PI lipid FAMES to be analyzed with least amount of noise interference, where as BF_3 allows SM to be analyzed with the least amount of noise

-Lipid extraction from the beef tissue was successful, although lipid FAMES were better identified with $NaOCH_3$ catalyst than BF_3

-GC-MS Method: Higher heat, longer amount of time equates to better separation

-Relative Standard Derivative (RSD) is below 1%; Retention times are reproducible with small error percentage

Future Studies:

- MALDI- MS/MS of the tissue sample for more accurate analysis

-Compare health live tissues to diseased live tissues to identify lipid intensity changes utilizing MALDI-TOF MS

- Identify the interaction of the lipids: PC, PI, SM when in a mixture through MALDI-TOF, i.e. Suppression effects or-, structural rearrangement

References:

- Busboom, J. R., C. T. Gaskins, M. L. Nelson, and J. V. OFallon. "A direct method for fatty acid methyl ester synthesis: Application to wet meat tissues, oils, and feedstuffs". Journal of Animal Science.(2007)

- Arnhold, J., K. Arnold, B. Fuchs, J. Lebig, M. Muller, M. Petkovic, J. Schiller, H. Spaltenholz, R. Sub, O. Zschornig. "Matrix-assisted Laser Desorption and Ionization time-of-flight (MALDI-TOF) mass spectrometry in Lipid and Phospholipid research". Progress in Lipid Research.(2004): 449-488

- Jackson, Shelly N., Amina S. Woods. "Direct profiling of tissue lipids by MALDI-TOF". Journal of Chromatography B. (2008)

- Folch, Jordi, M. Lees, and G. H. Sloane Stanley. "A Simple Method For The Isolation and Purification Of Total Lipides From Animal Tissues". McLean Hospital Research Laboratories, Waverley, and the Department of Biological Chemistry, Harvard Medical School, Boston, Massachusetts. (1965)

Acknowledgments:

Beth Emerson
Dr. Jennifer Gidden
Dr. Frank Hahn
Dr. Jack Lay
Dr. Julie Stenken
Dr. Rohana Liyanage

NSF-REU 0851505

Fluorescence labeling of cpSRP43 to monitor the protein standard dynamics by single molecule FRET

Jasmine Brown, Feng Gao and Colin D. Heyes
Philander Smith College, Little Rock , Arkansas
University of Arkansas at Fayetteville

INTRODUCTION

- cpSRP is a chloroplast protein signal recognition particle (1).
- Transports light-harvesting chlorophyll proteins to the thylakoid membrane (2).
- Composed of a combination of chromodomains (CD) and ankyrins (Ank) (2).
- Proteins of interest are cpSRP43 and cpSRP54.
- Protein 1 contains chromodomain 3 and ankyrin 2.
- Protein 2 contains chromodomain 2 and ankyrin 2.

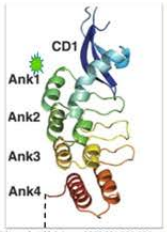

K F Stengel et al. Science 2008;321:253-256 (3DEO in PDB)

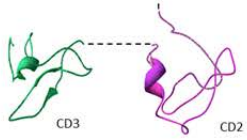

Leena PST, Sivaraja, Kumar TKS, Merry R., Yu C. (Unpublished, IX3P in PDB)

Sivaraja, Kumar TKS, Merry R., Yu C. (Unpublished, IX3O in PDB)

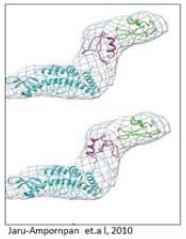

Jaru-Ampornpan et.a l, 2010

Jaru-Ampornpan et.al, 2010

OBJECTIVES

- To examine interaction and structural changes between cpSRP43 and cpSRP54 upon interaction.
- The cpSRP43 and cpSRP54 heterodimer binds to light-harvesting chlorophyll binding protein (LHCP) to transport it to the thylakoid membrane to be used in photosynthesis.
- Understanding this transport mechanism will hopefully impact the development of efficient solar energy devices.

METHODS

- Label proteins with fluorescent dyes.
- Separate dyes and labeled proteins with size elusion chromatography.
- Measure ensemble fluorescence and absorbance spectra.
- Measure single molecule Förster Resonance Energy Transfer (FRET).

Labeling Possibilities

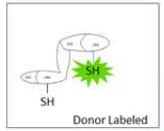

Creates donor only peak in FRET histograms (see below)

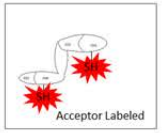

No Significance – not visible in FRET histograms

Reactions

Maleimide dye — Fluorescent labeled protein

Maleimide dye — Fluorescent labeled protein

	Method 1	Method 2	Method 3	Method 4
Alexa546 Concentration	1mM	3mM	3mM	3mM
Alexa488 Concentration	1mM	1mM	3mM	3mM
Add Urea	No	No	No	Yes
Time Elapsed between adding acceptor and donor	0	2 and 6 Hours	1 Hour	1 Hour
Labeling Ratio	1 : 0.9 : 1.8	1 : 0.2 : 2.8	1 : 1.9 : 3.9	1 : 1.7 : 3.7

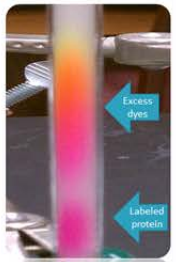

Gel Filtration

RESULTS

- Labeled proteins located in fraction 3.
- Decrease in donor-only labeled proteins with method 4 – best for single-molecule FRET (smFRET).
- Data shows that the ensemble fluorescence and smFRET are consistent.
- At least 3 states present in cpSRP43 determined from smFRET. High FRET efficiency state increases as cpSRP54 is added

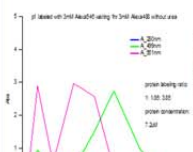

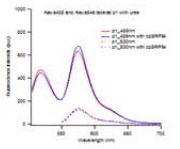

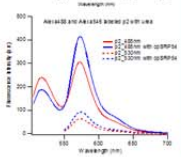

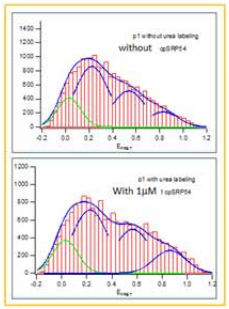

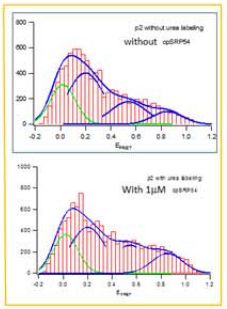

CONCLUSIONS

- Modified protocol increased FRET-labeled protein.
- Data suggests ankyrin2 is difficult to label, possibly the cysteine residue is not exposed to the solvent
- Urea exposes both cystines on protein to fluorescent dyes.
- Found various states of cpSRP43. population of states changes as cpSRP54 is added.
- FRET changes between Ank2-CD2 and Ank2-CD3 labeled proteins upon addition of cpSRP54 are different.

FUTURE GOALS

- To identify reason for difference in FRET signal in Ank2-CD2 and Ank2-CD3 FRET labeled proteins
- Identify molecular structural changes in cpSRP43 from single molecule FRET data during interaction with cpSRP54.
- To label a mutant cpSRP43 in both CD2 and CD3 to identify structural changes in these domains.

REFERENCES

1. Kathir, K., Rajalingam, D., Sivaraja, V., Kight, A., Goforth, R., Yu, C., et al. (2008). Assembly of Chloroplast signal Recognition Particle involves structural rearrangement in cpSRP43. *NIH Public Access* , 49-60.
2. Stengel, K. F., Holdermann, I., Cain, P., Robinson, C., Wild, K., & Sinning, I. (2008). Structural Basis for Specific Substrate Recognition by the Chloroplast Signal Recognition Particle Protein cpSRP43. *Science* , 253-256.
3. Jaru-Ampornpan, P., Shen, K., Lam, V., Ali, M., Doniach, S., Jia, T., et al. (2010). ATP-independent reversal of a membrane protein aggregate by a chloroplast SRP subunit. *Nature Structural and Molecular Biology* , 696-703.

ACKNOWLEDGEMENTS

- National Science Foundation CHE-0851505/REU
- Dr. David Paul
- Dr. Julie Stenken
- Leslie Johnson

CONTACT INFORMATION

Jasmine Brown
Email: jasmine.nbrown08@gmail.com

Synthesis and Characterization of a Ru-Pd Bimetallic Complex

Ryan Christman and Nan Zheng
University of Arkansas, Fayetteville

Introduction

Direct arylation via C-H functionalization, is a specific research area within the field of organic chemistry that has many advantages over current synthetic methods. By performing chemistry directly on carbon-hydrogen bonds, the need for pre-functionalized groups is eliminated. This allows for more efficient synthetic methods, eliminating waste and saving time and money. Activation of carbon-hydrogen bonds requires the use of transition metals as catalysts. Traditionally, the accepted mechanism for palladium, one of the common catalyst choices, was a Pd(II)-Pd(IV) redox cycle. Recently though, bimetallic Pd(III) has been shown to be the active catalyst in direct arylation reactions. Due to few examples of previous reactions involving Pd(III), little is known about its reactivity.

Figure 1. Bimetallic Palladium catalyst structure. Pd(III) is the active catalyst.

Goal

In order to address this lack of knowledge, Dr. Zheng devised a bimetallic ruthenium-palladium model to study palladium in its third oxidation state. The mononuclear Pd(III) complex is supposed to be an unstable and short-lived species. By using complex **1.11** as a model, we hope to be able to study these species. Through flash photolysis, Ru(II) is easily oxidized to Ru(III) in the presence of viologen. The electron transfer between the metal centers should then only produce Pd(III), as the process is strictly a one-electron process. This electron transfer process involving the use of a Ru center to oxidize another metal center intramolecularly has been extensively used to study electron transfer in biological systems.

Methods

The synthetic route in Scheme 1 was followed to synthesize bimetallic complex **1.11**. A number of well established reactions such as the Suzuki Miyaura Cross-Coupling reaction, Dess-Martin Oxidation, and Horner-Wadsworth-Emmons Olefination are utilized in the route. All reactions were carried out under an inert atmosphere. Products were purified by flash chromatography and characterized by NMR.

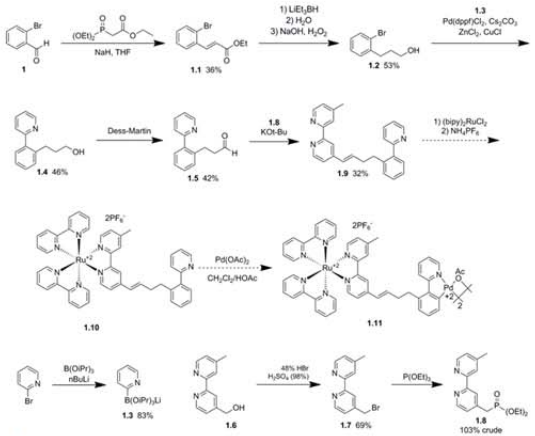

Scheme 1. Synthesis of Ru-Pd Complex

Results

Problems with the original synthetic scheme prevented us from completing the synthesis of complex **1.11**. We were only able to get as far as synthesizing **1.9**. The first problem was with the Suzuki Miyaura Cross-Coupling. Initial attempts using $Pd_2(dba)_3$ and diphenylphosphine oxide as the catalyst resulted in no reaction. Upon switching to the catalyst system composed of $Pd(dppf)Cl_2$, $ZnCl_2$, and CuCl, we were able to obtain **1.4** in 38% yield on the first attempt, and 53% on the second attempt. Oxidation of **1.4** to aldehyde **1.5** also presented problems, as the Swern Oxidation yielded only 32%. Dess-Martin Oxidation yielded an improved 42%. Synthesis of **1.8** worked well, with an overall yield of 72%. Problems again arose with the Horner-Wadsworth-Emmons Olefination as original attempts using KHMDS as a base yielded mostly one of the starting materials, phosphonate **1.8** while the other starting material, aldehyde **1.5** decomposed. When KO^tBu was used instead, we were able to synthesize **1.9**, but attempts to purify from starting material **1.8** using flash chromatography were unsuccessful, as Figure 2 demonstrates.

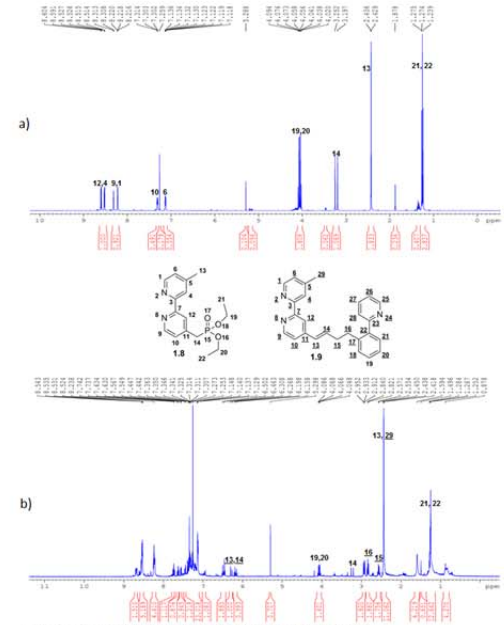

Figure 2. a) ^1H NMR of **1.8** b) ^1H NMR of **1.9** with leftover starting material **1.8**

Conclusion

The synthesis of **1.9** following Scheme 1 was successful. In order to allow easy purification of **1.9** we suggest using a slight excess of aldehyde **1.5** in the Horner-Wadsworth-Emmons Olefination. Based on polarity, **1.9** and **1.5** will be easily separated using flash chromatography.

Acknowledgments

We thank the University of Arkansas REU program and the NSF REU/CHE-0851505 for their support, and Mack Clements, Soumitra Maity, and Spencer Shinabery for their guidance in the lab.

Expression and Purification of Cdc42 and PBD46, a Cancer-Causing Combination

Edward Evans Jr. and Dr. Paul D. Adams
Department of Chemistry and Biochemistry, University of Arkansas, Fayetteville, AR 72701

Abstract

The Ras superfamily consists of low molecular weight G-proteins that are heavily involved in cellular signaling, leading to various downstream responses. Like other Ras proteins, Cdc42 (cell division cycle 42) acts as a molecular switch interchanging from its active (GTP-bound) and inactive (GDP-bound) state through the utilization of GAP (GTPase-activating proteins) and GEF (guanine nucleotide exchange factor) effectors (See Figure 1). It has been shown that Cdc42 signaling pathways play a major role in cell proliferation and differentiation leading to tumor growth. PBD46 is an effector of Cdc42 proven to inhibit GTP hydrolysis, stabilizing the Ras protein in its active state. PBD46, as well as many other effectors, bind to the Switch I region (amino acids 28-40) of Cdc42. By site-directed mutagenesis, threonine of position 35 was replaced with alanine forming a Cdc42 mutant (See Figure 5). With the use of affinity column chromatography, Cdc42(wild type), Cdc42(T35A), and PBD46 were expressed and purified for future tests of the Switch I binding interface.

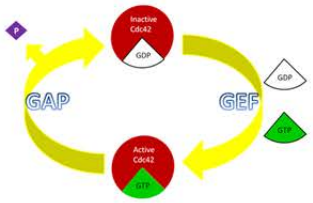

Figure 1. The Cdc42 cycle. Cdc42 interchanges from active and inactive states. Other proteins of the Ras superfamily behave similarly.

Methods

Expression

Cdc42(WT) and T35A

- Grow to an OD_{600} of 0.4-0.6.
- Induce with 1 mM IPTG.
- Allow to express for 3.5 hours and centrifuge.

PBD46

- Grow to an OD_{600} of 0.8-1.0.
- Induce with 1 mM IPTG.
- Allow to express for 4 hours and centrifuge.

Purification

Cdc42(WT) and T35A

- Resuspend in lysis buffer (30mL Tris binding buffer, 30mg lysozyme, 300 µL Halt Protease Inhibitor, 3.5 mg PMSF, 1 mM GDP per 1 liter of pellet).
- Sonicate for 20 seconds 5 times with 1-minute rest intervals.
- Incubate on ice for 30 minutes and add DNAse.
- Incubate at room temperature for 15 minutes and centrifuge, separating the lysate and pellet.
- Run lysate over Ni^{2+} affinity column, allowing the hexahistidine tag to bind to nickel ions.
- Elute Cdc42 with a higher concentration of imidazole.
- Dialyze overnight in Tris buffer (0.1 M NaCl, 0.05 M Tris-base pH 8.0, 0.01 M $MgCl_2 \times 6H_2O$).
- Use spectrophotometer to determine protein concentration.

PBD46

- Resuspend in lysis buffer (30mL PBS buffer, 30mg lysozyme, 300 µL Halt Protease Inhibitor, 3.5 mg PMSF per 1 liter of pellet).
- Sonicate for 20 seconds 5 times with 1-minute rest intervals.
- Incubate on ice for 30 minutes and add DNAse.
- Incubate at room temperature for 15 minutes and centrifuge, separating the lysate and pellet.
- Run lysate over pre-packed gluthathione column, immobilizing the protein.
- Elute PBD46-GST with a higher concentration of glutathione.
- Dialyze PBD46-GST in PBS buffer (0.14 M NaCl, 0.0030 M KCl, 0.01 M $Na_2HPO_4 \times 7\ H_2O$, 0.0018M KH_2PO_4 at pH 7.3).
- Rerun PBD46-GST over a glutathione column, and add thrombin to cleave the tag.
- Elute PBD46 and thrombin and run over a Heparin column.
- Dialyze purified PBD46 in PBS buffer.
- Use spectrophotometer to determine protein concentration.

Results

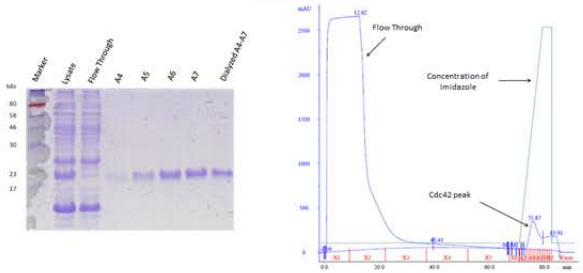

Figure 2: 15% SDS gel for expression of Cdc42(WT) and chromatogram of purification. When the concentration of imidazole is increased, Cdc42 elutes off the nickel column, providing an absorbance peak. A4-A7 are the fragments from this absorbance peak. Gel electrophoresis of the appropriate samples verify that Cdc42 has been purified. It is approximately 21 kDa which is reaffirmed on the gel.

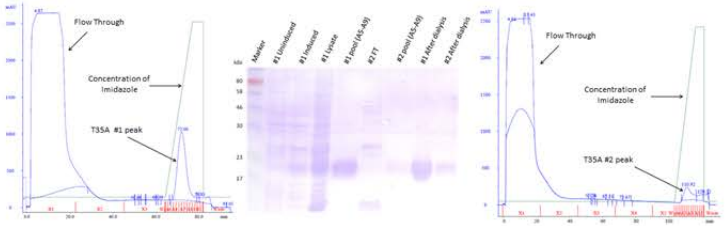

Figure 3: Two lysates of T35A were purified on a nickel column. Similar to the wild type, the mutant is approximately 21 kDa and its expression and purification are verified on the gel.

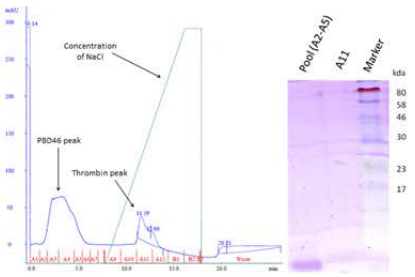

Figure 4: At approximately 5 kDa, PBD46 is shown well below the 17 kDa molecular weight marker. The band in the pool (A2-A5) lane suggests that PBD46 has been purified, but this is not conclusive.

Discussion

After dialysis, the protein concentration of all three proteins was determined by taking the absorbance at 280 nm of diluted samples. Using Beer's law, the protein concentration was extrapolated from the absorbance values. The concentrations for Cdc42(WT), T35A #1, T35A #2, and PBD46 were 10.7 mg/mL, 2.2 mg/mL, 0.5 mg/mL, and 0.1 mg/mL, respectively.
With the use of gel electrophoresis and the chromatograms, it appears that the wild type and the T35A mutant of Cdc42 have been properly expressed and purified. However, such conclusions about PBD46 cannot be made, considering that it is smaller than 17 kDa. After submitting a sample for mass spectroscopy, no traces of PBD46 were found.

Conclusion

With the use of affinity column chromatography, both Cdc42(WT) and T35A have been expressed and purified in sufficient amounts to perform assays in the future. However, there is not enough evidence to conclude that PBD46 has been properly isolated. Even so, 0.1 mg/mL is not sufficient to perform a reasonable number of experiments.

Future Work

Optimization of PBD46 purification is essential. Changes proposed to enhance isolation include using a different buffer for lysis and dialysis. Also, using gel beads instead of a pre-packed column when purifying may provide a better yield.
With sufficient protein on hand, fluorescence and isothermal titration calorimetry tests may be performed to determine the thermodynamics of the binding affinity of PBD46 to the wild type and mutant. Comparison of the binding differences between Cdc42(WT) and T35A is the gateway to altering cellular signaling of Ras proteins.

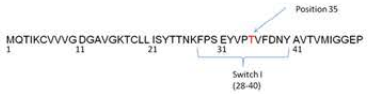

Figure 5: The first 50 amino acids of Cdc42. The Switch I region is where PBD46 and other effectors bind to Cdc42. At position 35, the threonine has been changed to alanine, producing T35A.

Acknowledgements

A great level of appreciation goes to Dr. Adams, the Adams lab group, Dr. Willyerd Collier, NSF-REU CHE-0851505 for funding, and NIH-ABI for grants to Dr. Adams.

Redox-Magnetohydrodynamic Microfluidics Using Multiple Electrode Pairs and Sweep-Step Potential Waveforms

Elaine M. Haas, Christena Nash, and Ingrid Fritsch

REU Program, Department of Chemistry and Biochemistry, University of Arkansas, Fayetteville, AR 72701

Purpose:

- **Background**
  - Microfluidics are important to automating lab-on-a-chip devices
  - Redox-magnetohydrodynamics (MHD) offers unique fluid control, not possible with existing microfluidic pump[1] (e.g. an MHD array setup eliminates the need for channels that induce fluid flow,[2] thus decreasing the complexity of the detection system)
  - Complication with redox-MHD: the need for redox species in the solution
  - Possible solution: tether redox species to electrodes (keep them out of solution and minimize contact with sample)
- **Anticipated challenges with tethered redox species:**
  - Identify appropriate redox-species/tethering chemistries
  - Thin layer of tethered redox species will deplete in a short time period (estimated 220 ms for a 500 nm Nafion film)
  - Switching or a potential waveform that allows recovery of redox species is needed
- **This project focuses on:**
  - Initial investigation of tethering redox species at electrode surfaces (results shown here for the sulfonated fluoropolymer Nafion in conjunction with the redox species ruthenium hexaamine chloride ($Ru(NH_3)_6Cl_3$ and $Ru(NH_3)_6Cl_2$)).[3]
  - Exploration of potential waveforms to allow recovery of redox species. Initial studies (shown here) with unmodified electrodes and redox species in solution for the same time period and approximate concentrations as expected for modified electrodes, varying electrode configuration, timing, potential waveform, and switching.

Microelectrode Array Chip

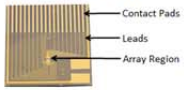

Characterization of Array Chip

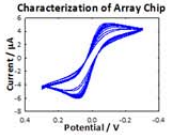

Overlay of CV responses for individual electrodes showing similar behavior for each in 0.1 M $K_4Fe(CN)_6$ and $K_3Fe(CN)_6$ in 0.1 M KCl. E^0 = 0.0 V vs. on-chip gold pseudo-reference electrode

Experimental Methods:

- **Cyclic Voltammetry (CV) characterization (to check activity of electrodes):**
  - Solution: 0.1 M ferrocyanide and ferricyanide in 0.1 M KCl
  - Swept potential of each electrode from -0.3 V to 0.3 V and back at 0.05 V/s.
  - On-chip gold counter and on-chip gold pseudo-reference electrodes were used, distant from array region
- **Modified Electrodes (to tether a redox species to electrode surface through ion exchange into a thin-film polymer):**
  - Spin-coated Nafion on gold macrochips (not arrays) at varying RPMs
  - Thicknesses ranging from 183 to 557 nm measured with Dektak 3030.

Nafion-Coated Gold Macroelectrode

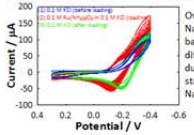

Overlay of CV responses showing expected behavior of a Nafion film in three sequential experiments:-(1) Expected background current in electrolyte alone before loading, (2) diffusion-limited current from redox species in solution during loading, and (3) expected shift in $E_{1/2}$ due to stabilization of oxidized form loaded in negatively-charged Nafion.

- **Sweep-Step Redox-MHD studies:**
  - *Permanent NdFeB magnet (1.5" diameter and 0.5" height) below chip generated field of 0.34 T*
  - *Application of potential waveform and monitoring current:*
    - CH Instruments 1030A multipotentiostat controlled up to two sets of working electrodes simultaneously, using opposing paired electrode across the array as the combined counter-pseudoreference electrode.
    - Sweep-step at Working 1 (W1): swept from +0.3 V to 0 V and back at 1.36 V/s (short sweep, 0.220 s) or 0.45 V/s (long sweep, 0.660 s) and then held 0.3 V for 0.220 s.
    - Constant potential at Working 2 (W2): held at +0.3 V for entirety of experiment
  - *Tracking fluid flow:*
    - 10-µm diameter latex polystyrene microspheres were used to visualize fluid movement in the manner of Anderson et al.[4]
    - Nikon Eclipse ME600P microscope, interfaced to a Sony Handycam digital camera
    - Particle imaging velocimetry (PIV) software (DynamicStudio v.3.00 software, Dantec Dynamics) used to process bead velocities.

Setup for Redox-MHD Studies:

Setup Schematic[4]

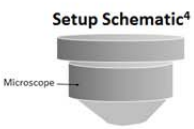

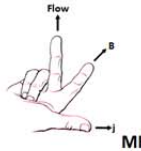

MHD Theory:[5]

Right Hand Rule

j = Ion Flux

B = Magnetic Field

Fluid flow is in the direction of the resulting force.

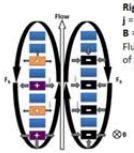

Sweep-Step Studies on Unmodified Electrodes:

Short Sweep Studies

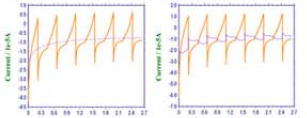

Overlay of raw current responses over 6 cycles W1: Sweep-step (W2 off) W2: Step (W1 off)

Overlay of raw current responses of two electrode pairs over 6 cycles W1: Sweep-step (W2 step) W2: Step (W1 sweep-step)

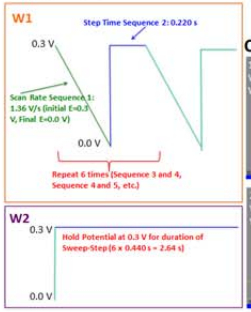

Particle Imaging Velocimetry

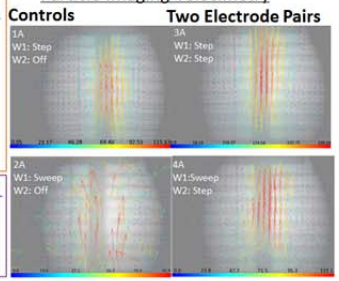

Controls:

Step part of cycle causes flow between active electrodes in a fairly flat flow profile. Sweep part of cycle slows beads to a stop when going from +0.3 V to 0.0 V.

Two Electrode Pairs:

Combined step produces ~2x velocity of control (with 2x the electrodes and current with reinforcing flow enhancement). During sweep of one electrode set the fluid continues to flow, but at half the speed, as expected.

Summary:

Fluid continues to flow while alternating electrodes are swept to recover redox species.

Longer sweep time will allow more electrode sets to be included with sweep-step functions that are out of phase with each other to ensure continuous fluid flow over long times.

Long Sweep Studies

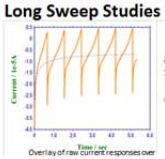

Overlay of raw current responses over 6 cycles W1: Sweep-step (W2 off) W2: Step (W1 off)

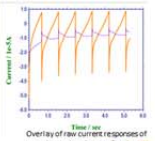

Overlay of raw current responses of two electrode pairs over 6 cycles W1: Sweep-step (W2 step) W2: Step (W1 sweep-step)

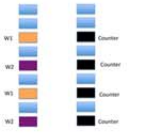

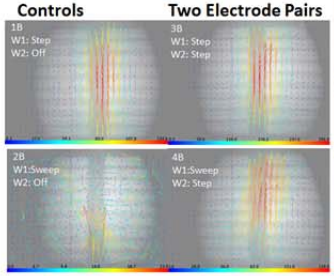

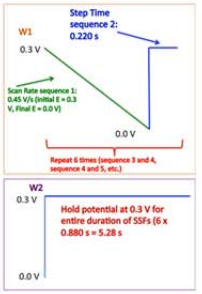

Bead Speed During Sweep-Step Studies

Experiment	*Speed* / µm·s⁻¹*
1A	113.1 ± 19.8
2A	41.3 ± 20.0
3A	232.3 ± 19.9
4A	105.3 ± 21.5
1B	120.6 ± 1.6
2B	14.3 ± 7.1
3B	234.0 ± 18.7
4B	108.8 ± 20.8

The bead velocities occurred as predicted. Fluid flow was greater during sweep-step experiments with the second working electrode held at a potential than during sweep-step experiments with a second electrode at open circuit.

*Speeds are averages calculated from three experimental trials, each from Cycle 1.

Conclusions:

- The Sweep-Step studies here show that fluid flow is increased by twofold as the number of electrode pairs are doubled. This suggests that the maximum velocity can be tuned to a specific application by increasing or decreasing the number of electrode pairs that are activated simultaneously.
- The current during a sweep decreases with time, and likewise beads slow to a stop. Thus, electrodes that are sweeping decrease their contribution to the overall fluid flow. As long as other electrode pairs are activated with a step, fluid continues to flow, but at a lower velocity.

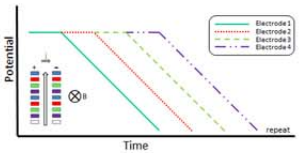

- If new electrode pairs are stepped to oxidizing potentials only when old electrode pairs begin their sweep-recovery cycle, then the fluid should achieve a fairly constant velocity with small pulses at the switching times. But, this kind of switching will require modification and reprogramming of existing instrumentation.
- In the future, we hope to be able to create waveforms such as the one pictured above, where cycles are performed on multiple pairs of electrodes, out of phase with one another, allowing for continued pumping of fluid at some electrodes while replenishment of redox species occurs at others. The cycles will be repeated, such that fluid flow is sustained over long periods of time.
- Also in the future, more work needs to be done to tether redox species to electrodes. There was not enough time to investigate the Nafion/$Ru(NH_3)_6^{3+/2+}$ system, thoroughly. Many other possible systems are reported in the literature. However, the most optimized conditions will be those where redox species are covalently attached to avoid loss into surrounding fluid, films are as thin as possible to maximize electron transfer and diffusion rates (e.g. monolayer), and redox concentrations are high to minimize frequency of recovery cycles.

Acknowledgements:

The National Science Foundation is acknowledged for financial support through grant CHE-0719097 and a REU for E.H. through grant NSF CHE-0851505/REU. Support has also been provided in part by the Arkansas Biosciences Institute, the major research component of the Arkansas Tobacco Settlement Proceeds Act of 2000. Special thanks also go to the Fritsch Group.

References:

1. M. C. Weston; M. D. Gerner; I. Fritsch. *Anal. Chem.* **2010**, *82*, 3411-3418.
2. M. C. Weston; C. K. Nash; I. Fritsch. *Anal. Chem.* **2010**, *82* (17), 7068-7072.
3. D. A. Buttry; F. C. Anson. J. Amer. Chem. Society. **1983**, *105* (4), 685-689.
4. E. C. Anderson; M. C. Weston; I. Fritsch. *Anal. Chem.* **2010**, *82* (7), 2643-2651.
5. (a) N. Leventis; X. Gao. *Anal. Chem.* **2001**, *73*, 3981–3992. (b) J. Lee; S. R. Ragsdale; X. Gao; H. S. White. *J. Electroanal. Chem.* **1997**, *422*, 169–177. (c) N. Leventis; M. Chen; X. Gao; M. Canalas; P. Zhang. *J. Phys. Chem. B* **1998**, *102*, 3512–3522.

Chemical Synthesis of Pd_xFe_y-Pt Core-Shell Electrocatalysts

Jonathan Janzen, Shutang Chen, and Jingyi Chen
Department of Chemistry and Biochemistry, University of Arkansas, Fayetteville, AR 72701

Introduction

The fuel cell has become the object of much interest due to its ability to convert chemical energy directly into electricity. In the fuel cell, the fuel is separated from oxygen by an electrolyte membrane. At the anode, fuel undergoes a reaction as it comes in contact with a catalyst ($H_2 \rightarrow 2H^+ + 2e^-$). The protons travel across the electrolyte membrane. On the cathode side, the oxygen reduction reaction (ORR) takes place. Oxygen reacts with the electrons and protons, forming water ($½O_2 + 2e^- + 2H^+ \rightarrow H_2O$). Catalysts are generally made from Platinum (Pt), Pt-based alloys, or carbon-supported catalysts (Pt/C). The catalyst at the anode can have low Pt amounts without performance loss. The catalyst at the cathode requires the use of much more platinum (about 8 times) . This is an issue because of the rarity and the price of Pt ($55+/ gram).

The problem is that OH tends to adsorb strongly to the catalyst, blocking the oxygen from reaching it. To get around this, different facets of the Pt-alloy crystal can be exposed. For example, (111) facets of Pt are much better at ORR than (100) facets[1]. Alloying Pt with other 3d transition metals (i.e.. Co, Fe, Ni) significantly improves catalytic ability. Noble metals, such as Palladium (Pd, less than $30/gram) are also expected to improve catalytic ability when alloyed with Pt[2]. The other metal changes the electronic structure of the catalyst to balance the adsorption of the oxygen and the OH (interfering species).

My research project dealt with making a core-shell structure catalyst. The core is to be made of iron and palladium (both expected to enhance catalytic ability and use less expensive, wasted platinum in the core of the nanocrystal) and the shell is to consist of Pt.

Figure 1. Reaction scheme for Pd_xFe_y nanocrystals. This was taken during the synthesis of Sample 1 prepared with Iron (II) Chloride tetrahydrate and Palladium (II) acetylacetonate. The left picture was taken at room temperature and the inset shows the $W(CO)_6$ solution. The middle was the injection and the right picture was taken at the end of the reaction at 240 °C.

Experimental

Pd_xFe_y nanocrystals were synthesized in an organic solution of oleic acid (OA) and oleylamine (OLA). In a typical synthesis, 0.05 mmol of Iron precursor [Iron (II) Chloride tetrahydrate, ($FeCl_2{\cdot}4H_2O$), Iron (II) Stearate ($Fe(St)_2$), Iron (III) acetylacetonate, ($Fe(acac)_3$), and Iron (III) Stearate, ($Fe(St)_3$)] and 0.05 mmol of Palladium (II) acetylacetonate ($Pd(acac)_2$) were loaded into a three-neck flask (see Figure 1) with 6.0 mL of OLA. The three-neck flask was degassed to remove oxygen using a flow of argon for 10 minutes at room temperature (RT), and it was stirred vigorously for the remainder of the experiment. The temperature was then set to 130 °C. In a separate vial, 0.05 g of tungsten hexacarbonyl ($W(CO)_6$, ~1.4 mmol) was added to 2.0 mL of OA and 2.0 mL of OLA and degassed under argon. Using heating, shaking and ultrasonication, the $W(CO)_6$ was dissolved in the vial forming a bright lime colored solution. When the three-neck flask reached 130 °C, the solution in the vial was injected into it via glass syringe. The solution in the three-neck flask was then set to 240 °C and allowed to react for 45 minutes. The flask was removed from heat and allowed to cool to RT. The product was then washed twice: using methanol, centrifuging at 4,000 RPM, and removing the supernatant. Then it was washed four more times in a similar way using a small amount of toluene, to disperse the nanoparticles, and more methanol. Final products were put in toluene, but they did not disperse well. The black product was found to drift in solution toward a magnet.

Results and Discussion

The core materials were synthesized using different iron precursors and palladium precursors in the presence of OA and OLA as capping ligands, as well as a trace amount of $W(CO)_6$. Figure 2 shows the transmission electron microscope (TEM) images of the samples. The nanoparticles noticeably aggregated in a toluene solution. The nanocrystals are not very dispersed on the TEM grid either.

Figure 3 is an image of the X-ray diffraction (XRD) pattern of the four samples. The first two samples look virtually the same, exhibiting peaks that are consistent with $Pd_{0.963}Fe_{0.037}$, and the black vertical bars represent the relative position and peaks of that alloy. The last two samples show a few other peaks that are not consistent with an iron-palladium alloyed nanocrystal. The peak showing up around 23 degrees is indicative of an iron oxide, hematite (Fe_2O_3). The peaks around 30, 54, and 63 degrees are from another iron oxide, magnetite (Fe_3O_4).

The nanocrystals form in the organic solution by deposition of supersaturated precursor that grow by ripening[3]. Oleic acid and oleylamine can serve as capping ligands to direct

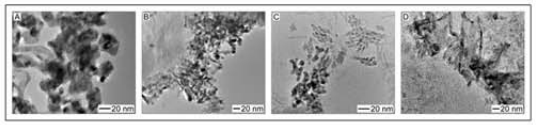

Figure 2. TEM images of Pd_xFe_y nanocrystals as synthesized from different iron precursors: A) Iron (II) Chloride tetrahydrate, B) Iron (II) Stearate, C) Iron (III) acetylacetonate, and D) Iron (III) Stearate.

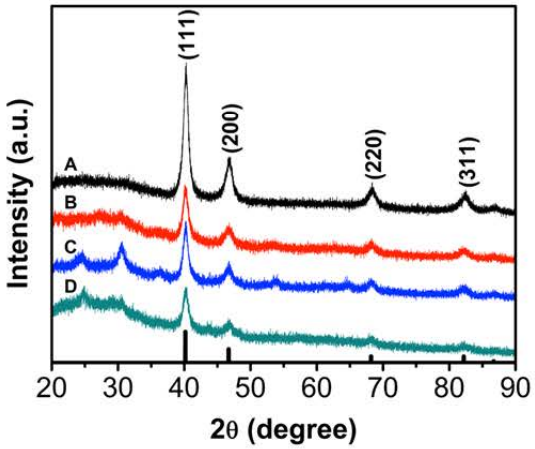

Figure 3. XRD patterns of palladium-iron nanocrystals prepared from different precursors: A) Iron (II) Chloride, B) Iron (II) Stearate, C) Iron (III) acetylacetonate, and D) Iron (III) Stearate . The black vertical lines at the bottom show the relative standard peaks of $Pd_{0.963}Fe_{0.037}$.

crystal growth. Figure 4 shows the infrared (IR) spectra of OA and OLA along with the four samples. The capping agent appears to be OA. The peaks of the IR spectra are assigned in the chart under the graph[4].

Conclusion and Future Work

In conclusion, Pd_xFe_y nanocrystals were synthesized in an organic solution of oleic acid and oleylamine and verified by X-ray diffraction. Oleic acid was determined to be the capping agent that remained on the sample after the synthesis was over. Future work includes adding Platinum on the surface of the nanocrystals and testing its catalytic ability for the oxygen reduction reaction.

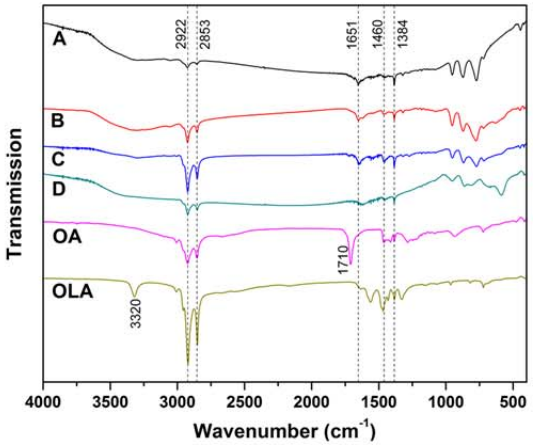

Figure 4. IR spectra of the ligands on the four samples compared with oleic acid (OA) and oleylamine (OLA). Samples were prepared using various iron precursors, A) Iron (II) Chloride, B) Iron (II) Stearate, C) Iron (III) acetylacetonate, and D) Iron (III) Stearate. The chart on the right shows what functional groups are responsible for the different peaks.

Peak (cm^{-1})	Assignment
3320	N–H Stretch
2922	CH_2 Asymmetric Stretch
2853	CH_2 Symmetric Stretch
1710	C=O Stretch
1651	COO^- Metal Asymmetric Stretch
1460	COO^- Symmetric Stretch
1384	COO^- Metal Symmetric Stretch

References

(1) Zhang, J. et al. *Nano Lett.* **2010**, *10*, 638-644.
(2) Ramirez-Caballero, G. E. et all. *Phys. Chem. Chem. Phys.*, **2010**, *12*, 2209-2218.
(3) Chen, Y. et al. *J. Am. Chem. Soc.*, **2007**, *129*, 10937-10947.
(4) Lewis, W. K. et al. *J. Phys. Chem. C* **2010**, *114*, 6377-6380.

Acknowledgments

I would like to thank Dr. Jingyi Chen for her mentorship and Shutang Chen for his help in my research. I would also like to acknowledge NSF CHE/REU 0851505.

Digestive Enzyme Analysis of Rheb (Ras Homolog Enriched Brain)

Ja'Qualane Scales
Philander Smith College

UNIVERSITY OF ARKANSAS

Introduction

Ras homolog enriched brain [Homo Sapiens] is a gene consisting of 183 amino acids and a molecular weight of 20.7 kDa. It is a member of the GTPase superfamily and it encodes proteins that are bound to lipids in the cell membrane. Some of the major functions of this protein are cell proliferation, cell differentiation and regulation of growth due to its interaction with mTOR/S6K1/4E-BP1 signaling transduction pathway.

Many researchers suggest that S6K1 plays a vital role in the S-phase of the cell cycle. On the other hand, 4EBP1/eIF4E does not have a critical role in the cell cycle progression but it is overexpressed in human tumors. S6K1 and eIF4E pathways function separately to increase cell size along mTOR and it promotes mTOR-dependent cell cycle progression coupled with cell growth during cell proliferation.

Digestive enzymes are important because they work together as catalysts to aid in absorption and digestion. Chymotrypsin is an example of a digestive enzyme that slices peptide bonds specifically on the carboxyl-terminal (C-terminal) side of the hydrophobic and aromatic amino acids, such as phenylalanine and methionine. Trypsin is another amino acid that slices peptides on the C-terminal side of lysine and arginine amino acid deposits.

Summer Aim

To perform digestive enzyme assays using trypsin and chymotrypsin to cleave at the aromatic and basic sides of the protein.

Future Research

To analyze protein patterns; view protein interactions and label small fragments of the protein that have been cleaved by the digestion enzymes; and use fluorescent dye as a control to compare the number of fragmentations produced by each enzyme.

Experimental Procedure

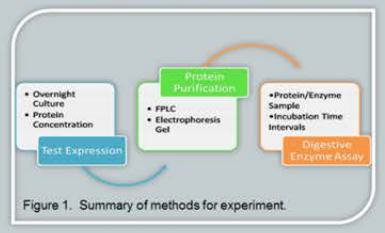

Figure 1. Summary of methods for experiment.

Data Collection

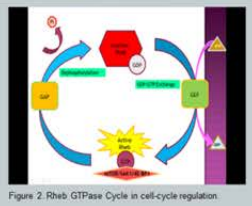

Figure 2. Rheb GTPase Cycle in cell-cycle regulation.

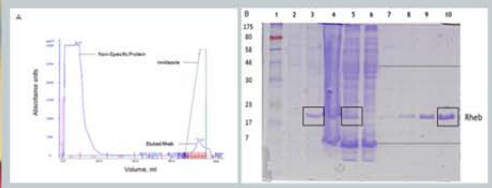

Figure 3. **Purification of Rheb-His6 protein. A**, chromatogram from the purification of Rheb-His6. **B**, 15% SDS-GEL analysis of fractions from the purification of Rheb-His6. Lane 1, molecular weight marker (kDa); lane 2, uninduced Rheb; lane 3, induced Rheb; lane 4, protein pellet; lane 5, supernatant; lane 6, flow-through fraction; lane 7-10 eluted protein.

Figure 4. **Chymotrypsin.** Gel electrophoresis of chymotrypsin assay. Lane 1, molecular weight maker (kDa). Lane 2, Rheb. Lane 3, Chymotrypsin. Lane 4, 0 minutes. Lane 5, 1 minute. Lane 6, 5 minutes. Lane 7, 10 minutes. Lane 8, 20 minutes. Lane 9, 30 minutes. Lane 10, 60 minutes.

Figure 5. **Trypsin.** Gel electrophoresis of trypsin assay. Lane 1, molecular weight maker (kDa). Lane 2, Rheb. Lane 3, Trypsin. Lane 4, 0 minutes. Lane 5, 1 minute. Lane 6, 5 minutes. Lane 7, 10 minutes. Lane 8, 20 minutes. Lane 9, 30 minutes. Lane 10, 60 minutes.

Results

Four digestive enzyme assays were performed. Of the four assays, two produced results. According to the chymotrypsin SDS-Gel, Rheb was completely sliced immediately. According to the trypsin SDS-Gel, there is evidence of fragmentation. However, the intensities of the Rheb bands were not significantly different.

Conclusion

Further research must be done on chymotrypsin and trypsin to analyze its affects on Rheb. There is a possibility that the ratio of Chymotrypsin to Rheb (1:10) was too low. Also, Rheb would probably have to be in the presence of trypsin longer than 60 minutes to produce more fragments.

Acknowledgements

NSF REU Program (CHE-0851505)
NIH & ABI Grant to P.D.A.
I would like to thank my mentor, Dr. Paul Adams, research assistants, Christian Hundshammer and Dr. Reena Chandrashekar, Kyla Morris, Seth Haynes, and Edward Evans.

References

Berg, j., Tymoczko, J., & Stryer, L. (2007). *Biochemistry*. New York City: W.H. Freeman and Company.

Digestive enzymes. (n.d.). *Yourbodycanheal.com*, Retrieved from http://www.yourbodycanheal.com/enzymes.html

F., T., & CL, G. (2001). Protein farnesylation in mammalian cells: effects of farnesyltransferase inhibitors on cancer cells. *PubMed.gov*, Retrieved from http://www.ncbi.nlm.nih.gov/pubmed/11706990

Fingar, D. (2003). mtor controls cell cycle progression through its cell growth effectors s6k1 and 4e-bp1/eukaryotic translation initiation factor 4e. *Molecular and Cellular Biology*, *24*(1),

Lohrey, J. (2010, November 10). *What is protein purification?*. Retrieved from http://www.livestrong.com/article/303147-what-is-protein-purification/

Lu, Zhi. (2010). Mammalian target of rapamycin activator rheb is frequently overexpressed in human carcinomas and is critical and sufficient for skin epithelial carcinogenesis. *Cancer Research*, Retrieved from http://m.cancerres.aacrjournals.org/content/70/8/3287.abstract

Rheb ras homolog enriched in brain [homo sapiens]. (2011). *NCBI*, Retrieved from http://www.ncbi.nlm.nih.gov/gene/6009

Worthington, K. (2009, July 07). *Trypsin*. Retrieved from http://www.worthington-biochem.com/try/default.html

Yu, Y., Li, S., Xu, X., Li, Y., & Guan, K. (2005). Structural basis for the unique biological function of small gtpase rheb. *The Journal of Biological Chemistry*, *280*(17), Retrieved from http://m.jbc.org/content/280/17/17093.full.pdf doi: 10.1074

Tailoring Polymer-Coated Gold Nanocages for Chemical Sampling in a Microdialysis Device

Sweta Shrestha, Julie A. Stenken, and Jingyi Chen
Cameron University, Lawton, OK 73505
University of Arkansas, Fayetteville, AR 72701

INTRODUCTION

Gold (Au) nanocages have extensive biomedical applications such as photothermal effects, contrast agent, and drug delivery. Gold nanocages are synthesized by galvanic replacement reaction between gold salt solution precursor and silver (Ag) nanocube suspension.[1] The polymer poly-*N*-isopropylacrylamide (p-NIPAAm) is thermally responsive polymer that can change its structural conformations with change in temperature with respect to its low critical solution temperature (LCST).[2] Gold nanocages with localized surface plasmon resonance (LSPR) tuned to near IR region are coated with p-NIPAAm and this polymer controls the release of samples from nanocages with the temperature change. P-NIPAAm coated nanocages besides with other biomedical applications such as drug delivery, photoacoustic imaging, and contrast agents, this preliminary study was done to demonstrate if they can be used for chemical sampling through microdialysis device. Microdialysis sampling is a minimally invasive device that collects samples via diffusion from different tissues and organs with aid of semipermeable hollow fiber membrane.[4] The analyte diffuses into the semipermeable membrane and is carried out by perfusion fluid for further chemical analysis. The main objective of our study is to demonstrate if p-NIPAAm coated Au nanocages passed in the perfusion fluid could collect analytes.

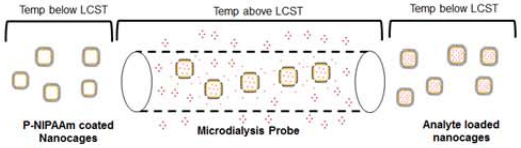

EXPERIMENTAL SECTION

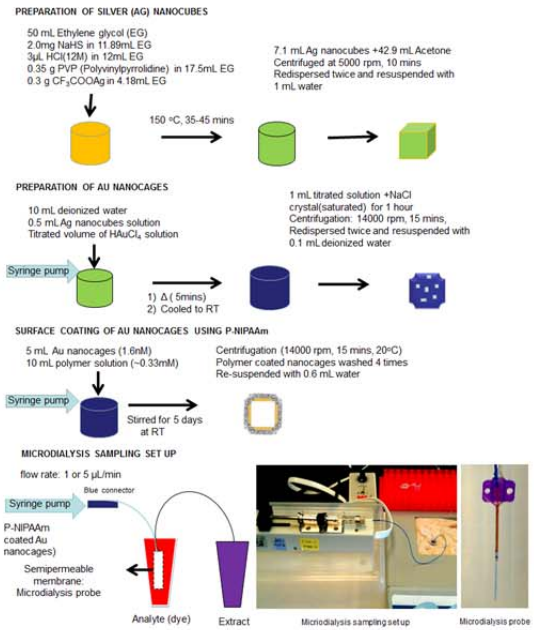

RESULTS/ DISCUSSIONS

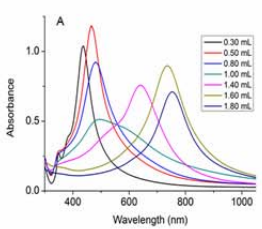

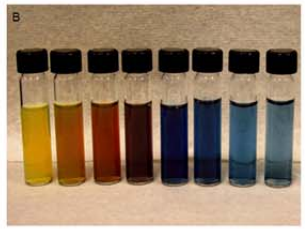

Fig 1 (A): **Tunning of LSPR peak of Au nanocages at different wavelength**. UV-Vis spectra of samples prepared by different titrated volumes of $HAuCl_4$ solution characterized that with the increase of titrated volume of $HAuCl_4$ solution on Ag nanocube suspension, the LSPR peak wavelength red shifts. The titrated volume of $HAuCl_4$ varies depending on the Ag template's LSPR peak and bandwidth. Fig 1 (B): Observation of color change of the solution (going from left to right) with the increase in titrated volume of $HAuCl_4$ solution on Ag nanocubes suspension.

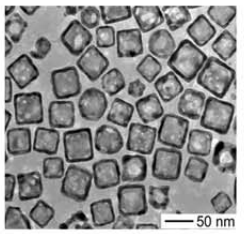

Fig 2: **TEM image of p-NIPAAm coated Au nanocages.** PVP coated nanocages were replaced by the thermally responsive polymer p-NIPAAm. p-NIPAAm attaches on Au nanocages through thiolate linkage. Au nanocages with LSPR peak tuned at near IR region (~800 nm) and size ranging from 40 to 60 nm were used for p-NIPAAm coating.

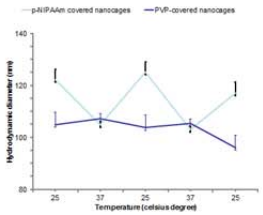

Fig 3: **Change of Hydrodynamic diameter of p-NIPAAm coated nanocages**. p-NIPAAm, thermally responsive polymer, changes its conformation with respect to temperature change. Having Low critical solution temperature (LCST) of p-NIPAAm at 32ºC, temperature above LCST (37ºC) polymer shows shrinkage of its diameter and reversible expansion of diameter upon decreasing temperature below LCST (25ºC) unlike PVP-coated nanocages. The hydrodynamic diameters of PVP-coated nanocages and p-NIPPAm coated nanocages were 105+/-1 nm and 121+/- 4 nm respectively.

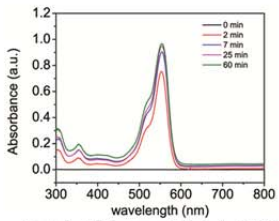

Fig 4: **Controlled release of Rhodamine B (RB) dye from p-NIPAAm coated Au nanocages**. RB dye (~18mM) was loaded on p-NIPAAm coated Au nanocages. Then RB loaded nanocages were conventionally heated at different time intervals, and corresponding absorbance readings were taken. UV-Vis spectra shows that the higher the time of heating, the higher absorbance reading which means the more release of dye. It demonstrated that p-NIPAAm exposes pores of nanocages on heating above its LCST and controls the release of samples from its core of nanocages.

MICRODIALYSIS SAMPLING EXPERIMENTS

Flow rate (µL/min)	Perfusion Fluid	Analyte	Inlet concentration µM	Outlet concentration µM	Extraction Efficiency (EE) %	Recovery of Nanocages %
1	P-NIPAAm nanocages	MO	20.5	4.3	21.1	Not measured
5	P-NIPAAm nanocages	MO	20.3	1.4	6.8	~100

Table 1: Flow rate of perfusion fluid affects the extraction efficiency of microdialysis sampling. The p-(NIPAAm) coated nanocages (16.67µM) was used as perfusion fluid in microdialysis probe. The semipermeable membrane was immersed in the analyte Methyl Orange (MO) stock solution at 40ºC. Extraction efficiency of analyte sampling increased with the decrease in the flow rate of perfusion fluid. Maximum extraction efficiency could be achieved using slow perfusion flow rate because it allows more time for diffused analyte to get entrapped or adsorbed by p-(NIPAAm) coated nanocages.

Perfusion Fluid	Analyte	Inlet concentration µM	Outlet concentration µM	Extraction Efficiency (EE)%	Standard Deviation%	Recovery of Nanocages %
P-NIPAAm nanocages (0.1nM)	MO	16.8	5.6	33.2	0.7	~100
Water	MO	21.9	9.1	41.4	1.3	Not measured

Table 2: Comparison of EE% of chemical sampling between pNIPAAm nanocages and water (Control). Extraction Efficiency of microdialysis sampling using p-NIPAAm nanocages as perfusion fluid was less than using water (Control). The possible reason might be due to not able to detect the dye entrapped inside the nanocages. But the results demonstrated that p-NIPAAm nanocages can be used in microdialysis sampling in order to collect analyte. These nanocages can be applied in microdialysis sampling without probe damage as they are recovered completely through outlet.

CONCLUSIONS

The p-NIPAAm coated nanocages can be used for the collection of samples through microdialysis sampling. There is no damage of microdialysis probe because these nanocages are fully recovered through microdialysis probe. The results of this study showed that the extraction efficiency of analyte using p-NIPAAm nanocages as perfusion fluid increased with the decrease in perfusion flow rate. On the other hand, the extraction efficiency of analyte using perfusion p-NIPAAm nanocages is less compared to water (control). The possible reason might be due to inability of detecting dye entrapped inside the nanocages. As per our objective, p-NIPAAm coated nanocages can be used as perfusion fluid to carry out chemical sampling. The sampling efficiency of microdialysis can be optimized by concentration, porosity, and coating layer of perfusion nanocages.

REFERENCES

1. Skrabalak, S. E., Au, L., X. & Xia, Y. *Nature Protocols* **2,** 2181-2190 (2007).
2. Yavuz, M. S. *et al.Nature Materials* **8**, 935 (2009).
3. Li, W. *et al. Nanoscale* **3**, 1726 (2011).
4. Stenken, J.A. Microdialysis Sampling in *Encyclopedia of Medical Devices and Instrumentation*, Wiley, 2006.
5. Skrabalak, S. E., Chen, J., Sun, Y., Lu, X., Au, L., Cobley, C. M., and Xia, Y. *Accounts of Chemical Research* **41,** 1587-1595 (2008).

ACKNOWLEDGEMENTS

I would like to thank graduate students Leanne Mathurin and Randy Espinal Cabrera who helped me in setting up my experiments. This research was funded by startup funds from University of Arkansas to Jingyi Chen.

Expanding the Scope of the Catalytic Dynamic Resolution of *N*-Boc-2-Lithiopiperidine

Jin Sun Woo[a], Timothy K. Beng[b] and Robert E. Gawley[b]
[a]Department of Chemistry, Mount Holyoke College, South Hadley, MA 01075
[b]Department of Chemistry and Biochemistry, University of Arkansas, Fayetteville, Arkansas, USA
bgawley@uark.edu

Abstract

The scope of the catalytic dynamic resolution (CDR) of *N*-Boc-2-lithiopiperidine **1** has been expanded to the scaled-up synthesis of both enantiomers of pipecolic acid methyl ester. The configurational stability of tertiary benzylic organolithiums has been investigated using enantioenriched *N*-Boc-2-arylpiperidine and pyrrolidines.

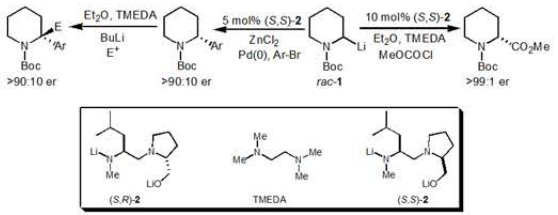

Introduction

Optically active piperidine derivatives are prevalent in natural products and used in thousands of clinical and preclinical researches.[1] Examples include antascomicin B, swainsonine, and conhydrine (Figure 1). Recently, the catalytic dynamic resolution (CDR) of 2-lithiopiperidine **1** using diastereomeric ligands (*S*,*S*)-**2** and (*S*,*R*)-**2** was reported by Beng and Gawley.[2] In small scale reactions (<5 mmol), the authors synthesized both enantiomers of the proline homologue, pipecolic acid as well as the ester and amide derivatives in >97:3 er (Scheme 1).

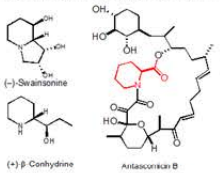

Figure 1. Piperidine alkaloids

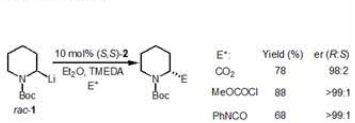

E+:	Yield (%)	er (*R*:*S*)
CO_2	78	98:2
MeOCOCl	88	>99:1
PhNCO	68	>99:1

Scheme 1. Synthesis of (*R*)-pipecolic acid and its derivatives by CDR

- We now report our progress toward a scaled-up synthesis of (*S*)- and (*R*)-pipecolic acid for use in the total synthesis of antascomicin B.[3]
- As part of an investigation into the configurational stability of benzylic organolithiums, we also present rare examples of configurationally stable tertiary benzylic organolithiums in the absence of any chiral influence on piperidine and pyrrolidine heterocycles.
- Such species have been shown to have low barriers to inversion.[4] As such the only configurationally stable benzylic organolithiums reported to date are ones that are either chiral auxiliary mediated[5] or chiral ligand mediated.[6]

Experimental

Synthesis of *N*-Boc-piperidine

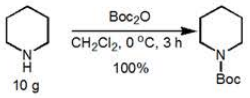

[1]Watson, P. S.; Jiang, B.; Scott, B., *Org. Lett.* **2000**, *2*, 3679-3681.
[2]Beng, T. K.; Gawley, R. E. *J. Am. Chem. Soc.* **2010**, *132*, 12216-12217

Synthesis of conjugate acid of (*S*,*R*)-2

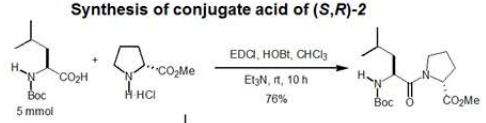

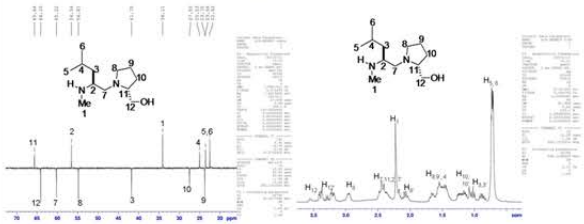

The conjugate acid of diastereomeric ligand (*S*,*S*)-**2** was also synthesized and used to prepare the *R*-enantiomer of pipecolic acid methyl ester.

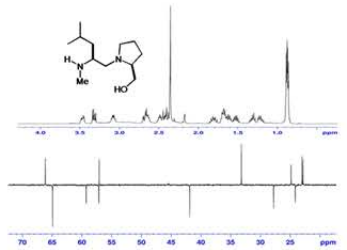

Synthesis of (*R*)-pipecolic acid methyl ester by CDR

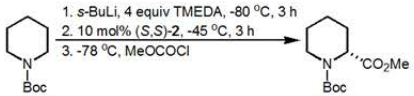

Enantiomer ratio of product determined by CSP-GC
Isolated yield not determined

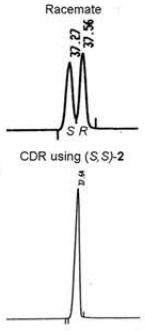

[3]Qi, W.; McIntoch, M. C. *Tetrahedron*, **2008**, *64*, 7021-7025.
[4]Hoell, D.; Schnieders. C.; Muellen, K., *Angew. Chem.* **1983**, *95*(3), 240-1.
[5]Gawley, R. E.; Hart, G.; Goicoechea-Pappas, M.; Smith, A. L., *J. Org. Chem.* **1986**, *51*, 3076-3078.
[6]Beak, P.; Kerrick, S. T.; Gallagher, D. J., *J. Am. Chem. Soc.* **1993**, *115*(23), 10628-36.

Benzylic Lithiations

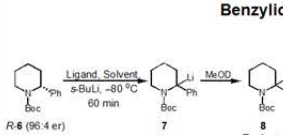

Entry	Solvent	Ligand	er (*R*:*S*)
1	Et_2O	None	91:9
2	Et_2O	1 eq TMEDA	96:4
3	Et_2O	4 eq TMEDA	96:4
4	THF	None	92:8
5	THF	1 eq TMEDA	94:6
6	THF	4 eq TMEDA	96:5
7	Et_2O	4 eq TMEDA*	85:15

*warmed to -55 °C for 1 h

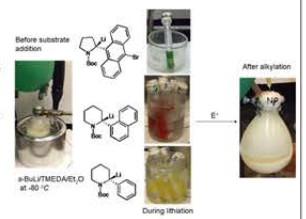

- Quenching with MeOD reveals stereoretentive deuteration
- **7** is less stable in the absence of a ligand (entries 1 & 4)
- **7** maintains configurational stability in the presence of TMEDA in both Et_2O (entries 2 & 3) and THF (entries 5 & 6) at -80 °C
- Configurational integrity is compromised at higher temperatures (entry 7)

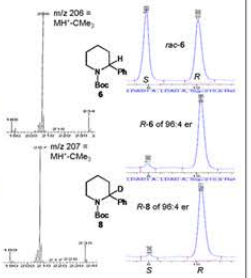

Pyrrolidines work as well

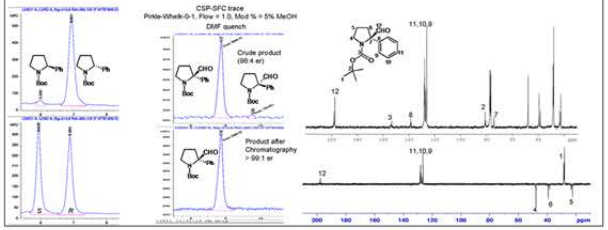

Conclusions

- Reasonable quantities of both enantiomers of pipecolic acid methyl ester have been synthesized in high yields and excellent enantiomer ratios.
- The configurational stability of tertiary benzylic organolithiums have been evaluated on piperidine and pyrrolidine heterocycles.

Acknowledgements and Funding

- Gawley Group
- NSF CHE-1011788
- Arkansas Biosciences Institute

Synthesis of JWH-018 Metabolite

[1]Patience Wright, [2]Beth Emerson, [2]Carrie Snyder, [3]Jennifer Gidden, [3]Jackson O. Lay, Jr, and [2]Bill Durham

[1]Department of Chemistry, Spring Hill College Mobile, AL 36608; [2]Department of Chemistry and Biochemistry, University of Arkansas, Fayetteville, AR 72701; [3]Arkansas Statewide Mass Spectrometry Facility, University of Arkansas, AR 72701

ABSTRACT

Beginning in 2004, herbal mixtures with the name "Spice" or "K2" were sold in "headshops" and on the internet. These mixtures contain 1-pentyl-3-(1-napthoyl)indole, also known as JWH-018. Although JWH-018 and delta-9-tetrahydrocannabinol (Δ9-THC) have different structures, both give cannabis-like effects after consumption. Hallucination, distorted perception, and tachycardia are common effects of usage. Due to this, the Drug Enforcement Agency (DEA) is conducting further studies to determine if these mixtures should be permanently placed on the controlled substances list prohibiting their sale and consumption. For this project, the authors synthesized the JWH-018 metabolite and analyzed the products using gas chromatography-mass spectroscopy (GC/MS). The metabolite was synthesized to mimic the metabolized product found in K2 users' urine after its consumption. Hydroxylation on the alkyl chain is the most common metabolite found in urine; therefore, the authors choose to synthesize it to act as an analytical standard to compare to urine samples of K2 users. Since the carboxylic acid form is the second most common metabolite found, future studies will work toward continuing the synthesis.

OBJECTIVE

- Synthesize JWH-018 metabolite and determine appropriate methodology using GC/MS
- Determine detection limits of hydroxylated metabolite

Astral blast – 1gm ($13)
Space orbit – 1gm ($18)

Figure 1. Different brands of 'Spice' herbal products illustrating differences in packaging and herbal blend appearance. Some packages indicate not intended for human consumption.

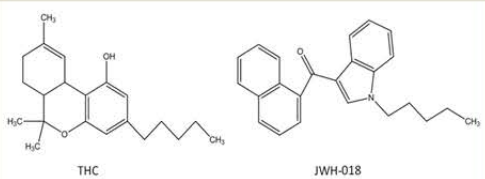

Figure 2. Structural formulas for THC and JWH-018.

ACKNOWLEDGMENTS

- National Science Foundation CHE-0851505/REU
- Durham Group

SYNTHESIS

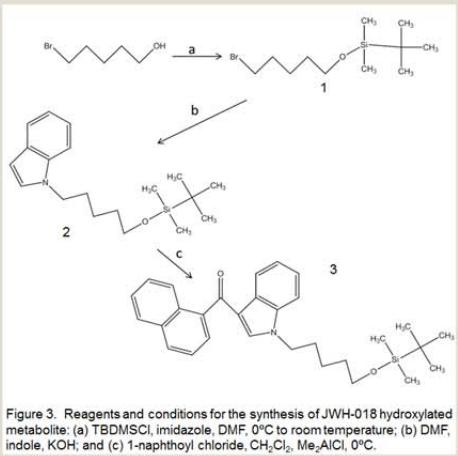

Figure 3. Reagents and conditions for the synthesis of JWH-018 hydroxylated metabolite: (a) TBDMSCl, imidazole, DMF, 0°C to room temperature; (b) DMF, indole, KOH; and (c) 1-naphthoyl chloride, CH_2Cl_2, Me_2AlCl, 0°C.

GC/MS CONDITIONS

Sample Handling
CombiPal, aliquot, 1 µL

GC
Varian 450; Injector- 300°C; Split- 10:1 ratio; Column – Zebron ZB-5HT Inferno 30M x 0.25 ID
Temperature programming-
Step 1, 2: 65°C (2.0 min.) then +25°C/min. to 280°C (2.0 min.)
Step 3: 80°C then +25°C/min. to 310°C (15.0 min.)

MS
Varian 320 MS
Scanning 50-500 amu; 1 sec./scan

RESULTS

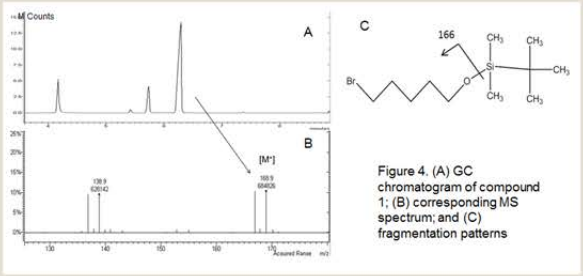

Figure 4. (A) GC chromatogram of compound 1; (B) corresponding MS spectrum; and (C) fragmentation patterns

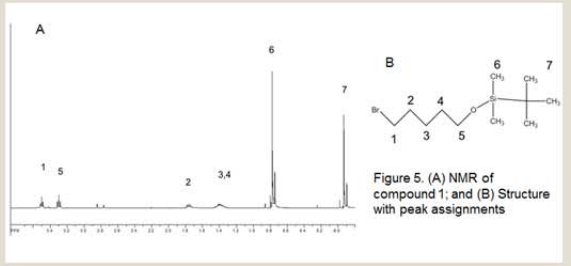

Figure 5. (A) NMR of compound 1; and (B) Structure with peak assignments

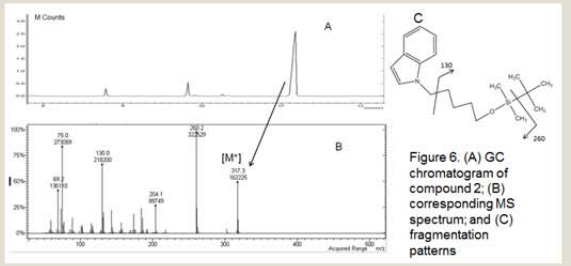

Figure 6. (A) GC chromatogram of compound 2; (B) corresponding MS spectrum; and (C) fragmentation patterns

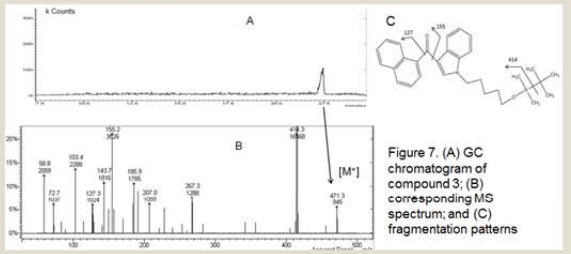

Figure 7. (A) GC chromatogram of compound 3; (B) corresponding MS spectrum; and (C) fragmentation patterns

CONCLUSIONS

- JWH-018 metabolite was synthesized to compound 3 and analyzed with GC/MS
- Better detection limits are obtained with compound 3

FUTURE WORK

- Continue synthesis to form hydroxylated metabolite to oxidize into a carboxylic acid, the second most common metabolite
- Compare synthesized metabolite to the metabolites found in K2 users' urine
- Determine detection limits of JWH-018 hydroxylated metabolite

REFERENCES

- (1) Dehaen, Wim et al. J. Org Chem. 56(2), (1991), 896-900.
- (2) Huffman, John et al. Bioorg. Med. Chem. 13, (2005), 89-112.

National Center for Toxicological Research Trip
Jefferson, Arkansas

Meeting in Miniature

Terry Anderson

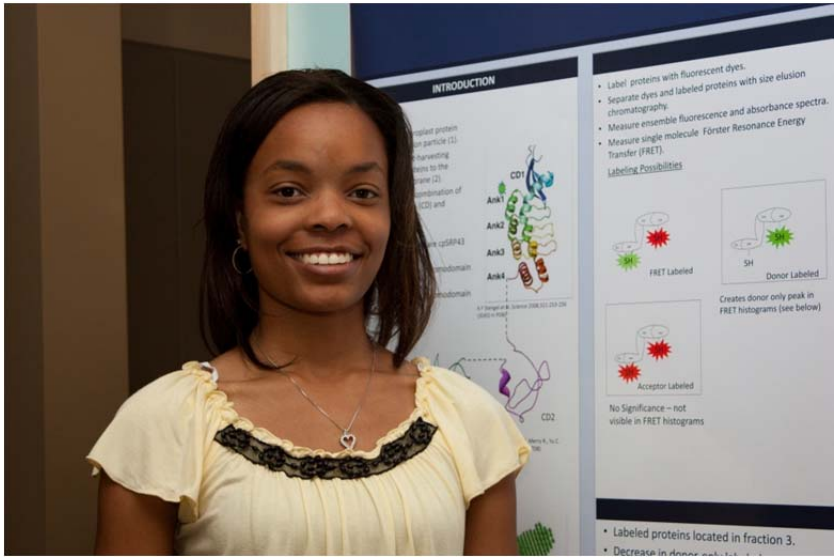

Jasmine Brown

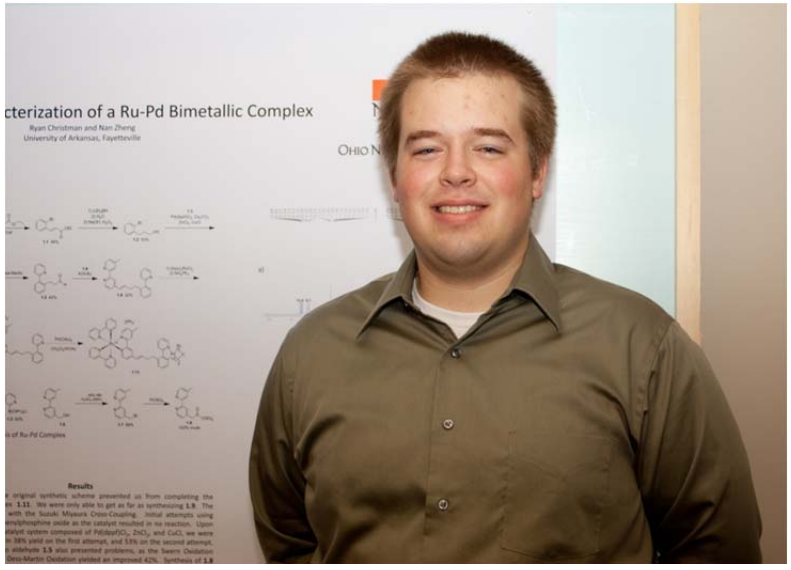

Ryan Christman

Edward Evans, Jr.

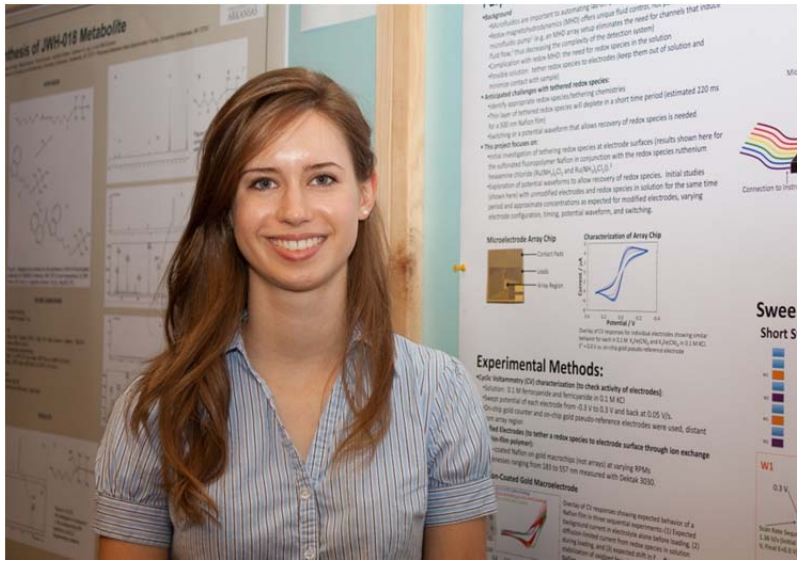

Elaine Haas

Jonathan Janzen

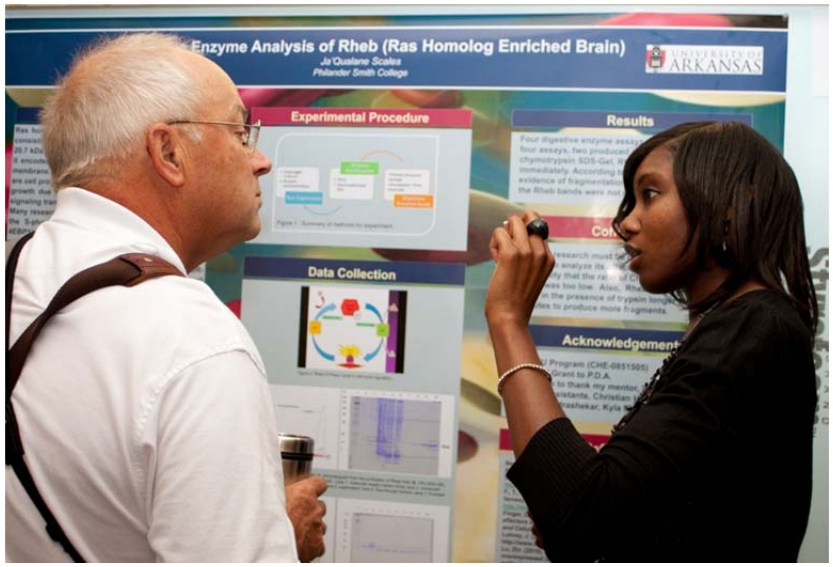

Ja'Qualane Scales

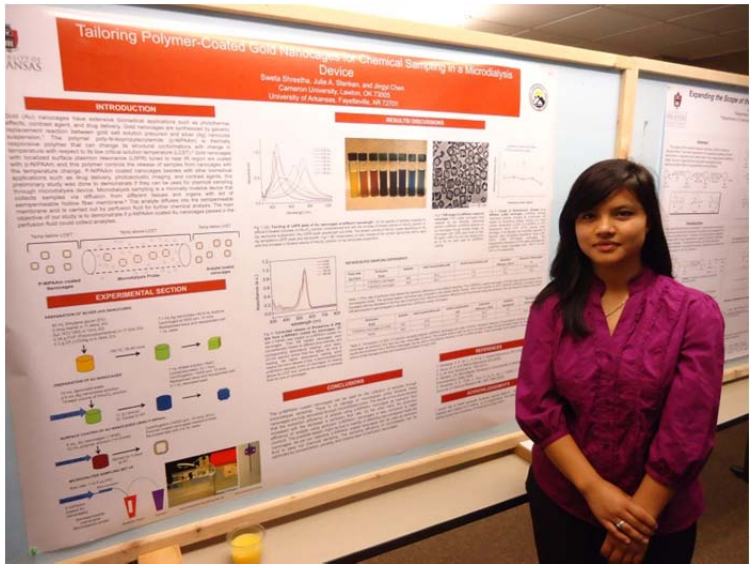

Sweta Shrestha

Jin Sun Woo

Patience Wright

Back Row: Sweta Shrestha, Jin Sun Woo, Edward Evans, Jr., Dr. David Paul, Ja'Qualane Scales, Terry Anderson, Jasmine Brown. Front Row: Elaine Haas, Patience Wright, Jonathan Janzen, Ryan Christman